Mitochondrial Antiviral Signaling Protein (MAVS) in Post-MI Cardiac Remodeling

Teagan Haggerty, BHSc

Thesis submitted to the University of Ottawa
in partial fulfilment of the requirements for the
Master of Science Degree in Cellular Molecular Medicine

Cellular Molecular Medicine | University of Ottawa
Faculty of Medicine
University of Ottawa

ABSTRACT

Background: Mitochondrial Antiviral Signaling Protein (MAVS) is an innate immune effector protein uniquely residing on mitochondrial surfaces. Previously, we identified MAVS as a key regulator of cardiac remodeling, inflammation, and metabolism in murine models of pressure-induced heart failure. This current study investigates MAVS in myocardial infarction (MI), hypothesizing a key role in cardiac stress responses. **Methods:** Utilizing left anterior descending artery (LAD) ligation, we induced MI in *Mavs*$^{-/-}$ and WT mice to assess remodeling, function, and molecular changes. **Results:** Male *Mavs*$^{-/-}$ mice exhibited reduced MI-induced hypertrophy, preserved ejection fraction, and diminished heart failure markers compared to WT controls. Several notable sex-based variations indicate MAVS functions in a sex-specific context. **Impact:** Our findings indicate that MAVS may be a critical regulator of cardiac hypertrophy and remodelling post-MI. This research underscores the potential for targeting mitochondrial activity-based pathways to improve post-MI cardiac remodeling, with MAVS as a possible candidate.

DEDICATION

To my Grandma and Grandpa Proven,
who instilled in me optimism, tenacity, and a love of medicine
&
Réjean Lefebvre, qui restera toujours dans nos cœurs
et continue toujours à nous inspirer

ACKNOWLEDGMENTS

To my incredible supervisor, Dr. Peter Liu, your devotion to medicine and research is one of my biggest inspirations. Your kind encouragement, drive for academic excellence and ingenuity have helped shape my achievements and further solidified my passion for generating positive impact.

I would like to express my appreciation to senior scientist Dr. Liyong Zhang. Despite your many responsibilities, you always make training the next generation of scientists a priority. Your patience, dedication to scientific excellence and mentorship always helped me feel motivated, capable and supported.

A most heartfelt thank you to my thesis committee members, Dr. Ruth Slack and Dr. Erin Mulvihill. I found so much comfort and support from your kindness, expertise, and scientific passions – this helped make my MSc so enjoyable.

A special thank you to my family, friends and fellow trainees, your support and encouragement have been invaluable to me.

FUNDING SOURCES

This research was supported by the Canadian Institute of Health Research, Canada Graduate Scholarship - Master's (CIHR CGS-M), along with our lab's funding sources, Genome Canada, Canadian Institute of Health Research (CIHR), Brain-Heart Interconnectome Canada First Research Excellence Fund (CFREF), Brain-Heart Research Integrative Innovation Team Endeavor (BHRIITE) Grant from Heart & Stroke Foundation.

TABLE OF CONTENTS

ABSTRACT ..... *ii*

ACKNOWLEDGMENTS ..... *iv*

FUNDING SOURCES ..... *iv*

LIST OF ABBREVIATIONS ..... *viii*

LIST OF TABLES ..... *xii*

LIST OF FIGURES ..... *xii*

1 INTRODUCTION *1*

1.1 Cardiovascular System and Cardiovascular Disease **1**

1.1.1 Myocardial Infarction 2

1.1.1.1 Clinical Diagnosis and Treatment of MI 3

1.1.1.2 Myocardial Infarction Pathophysiology and Cardiac Repair 4

1.1.2 Heart Failure 8

1.2 Mitochondrial Mechanisms in Cardiovascular Disease **9**

1.2.1 Energy Production and Fatty Acid Oxidation 10

1.2.2 Reactive Oxygen Species Management 10

1.2.3 Calcium Mishandling and mPTP dysregulation 11

1.2.4 Mitochondrial Biogenesis and Degradation Dynamics 14

1.2.5 Angiogenesis and Lymphangiogenic Pathways 16

1.2.6 Mitochondria-Associated Endoplasmic Reticulum Membranes 16

1.3 Mitochondrial Antiviral Signalling Molecule **19**

1.3.1 Canonical MAVS Signalling 19

1.3.1.1 RIG-I-like receptor (RLR) signalling 19

1.3.1.2 NLR family pyrin domain containing 3 (NLRP3) Inflammasome Activation 20

1.3.2 MAVS Signalling in CVD 22

1.4 Mouse Models of Myocardial Infarction **26**

1.5 Metabolic-Based Therapeutic Translation **28**

1.6 Rationale, Objective, Hypothesis, Aims **28**

***1.7* Impact and Outcome** **30**

2 MATERIALS AND METHODS *31*

2.1 Mice strains and LAD ligation model of Myocardial Infarction **31**

2.2 Measurement of Cardiac Function in Mice **32**

2.3 Histology and Immunocytochemistry **32**

2.4 qRT-PCR 33
2.5 Statistics and Reproducibility 34
3 RESULTS 35
3.1 4-WEEK POST MI: REMODELLING OUTCOMES 35
3.1.1 Male Mavs$^{-/-}$ mice display preserved heart and lung weight 4-weeks post MI .35
3.1.2 Left Ventricular Ejection fraction is preserved in Male Mavs$^{-/-}$ mice 4-weeks post MI 38
3.1.3 Mavs$^{-/-}$ heart sizes were significantly smaller compared to their WT controls .40
3.1.4 Mavs deficiency protects male and female mice from cardiomyocyte hypertrophy 43
3.1.5 Increased fibrosis is observed in Male Mavs deficient mice 4-weeks post MI 46
3.1.6 Mavs deficient male mice show reduced heart failure biomarkers 49
3.2 3-DAYS POST MI: INFLAMMATORY OUTCOMES 52
3.2.1 No notable gross heart structure differences 3 days post MI 52
3.2.2 H&E staining shows LV wall thinning and loss of papillary muscle 3 days post MI in male Mavs$^{-/-}$ mice 54
4 DISCUSSION AND FUTURE DIRECTIONS 56
4.1 DISCUSSION 56
4.1.1 Mavs deficiency may protect against MI-induced heart failure 56
4.1.1.1 Mavs deficiency is protective against MI-induced myocyte hypertrophic remodeling 56
4.1.1.2 Mavs deficiency preserves LVEF, reduces lung congestion and heart failure biomarkers 57
4.1.2 Mavs$^{-/-}$ mice display sex-specific phenotypic differences 59
4.1.3 MAVS may function as a key modulator of the fibrometabolic switch 61
4.1.4 MAVS likely functions together with other mitochondrial control mechanisms 63
4.1.4.1 MAVS and metabolic substrate switching 63
4.1.4.2 MAVS and mitophagy 63
4.1.4.3 MAVS and cGAS-STING 65
4.1.4.4 MAVS and Sirt3 65
4.1.4.5 MAVS and NLRP3 66
4.2 FUTURE DIRECTIONS 67
4.2.1 Cell culture modelling of MAVS activation 67
4.2.2 Cardiac Specific Mavs$^{-/-}$ 67
4.2.3 Identifying negative regulators of MAVS 67
4.2.4 Temporal and spatial mapping of MAVS activation post-MI 68
4.2.5 Metabolic Profiling 68
4.3 LIMITATIONS 69

5 CONCLUSION 70

6 REFERENCES 71

7 APPENDIX A: SUPPLEMENTAL DATA 92

7.1.1 Two Angiotensin II treatment regimens induce MAVS activation in AC16 cells 92

7.1.2 24-hour treatment with 200nm Angiotensin II induces MAVS activation in AC16 cells 94

7.1.3 MAVS antibody is most effective in detecting MAVS in mitochondrial isolates from human AC16 cells 96

7.1.4 Verification of $Mavs^{-/-}$ mouse by PCR genotyping and q-RT-PCR 99

7.1.5 No significant differences in body weight between mouse cohorts 101

7.1.6 Summary of all cardiac function measures acquired from echocardiography 103

7.1.7 RT-qPCR Primer Sequences 106

LIST OF ABBREVIATIONS

AAR	Area at risk
AC16	AC16 Human Cardiomyocyte Cell Line
Ang II	Angiotensin II
ANOVA	Analysis of Variance
Anp	Atrial Natriuretic Peptide
ATP	Adenosine Triphosphate
Bnp	Brain Natriuretic Peptide
BPM	Beats per Minute
BW	Body weight
CARD	Caspase Recruitment Domain
cGAS-STING	Cyclic GMP-AMP synthase - Stimulator of Interferon Genes
CSA	Cross-sectional Area
CTL	Control
CVD	Cardiovascular Disease
ECG	Echocardiography
ECM	Extracellular Matrix
EF	Ejection Fraction
ER	Endoplasmic Reticulum
ETC	Electron Transport Chain

H&E	Hematoxylin and Eosin
HF	Heart Failure
HFpEF	Heart Failure with Preserved Ejection Fraction
HFrEF	Heart Failure with Reduced Ejection Fraction
HW	Heart weight
Igfbp7	Insulin Growth Factor Binding Protein 7
IR	Ischemia Reperfusion
LAD	Left Anterior Descending Artery
LV	Left ventricle
LVEF	Left Ventricular Ejection Fraction
LW	Lung weight
MAVS	Mitochondrial Antiviral Signaling Molecule
Mavs$^{-/-}$	Genetic *Mavs* Knockout
MDA5	Melanoma Differentiation-Associated Gene 5
MI	Myocardial Infarction
mRNA	Messenger ribonucleic acid
mtDNA	Mitochondrial Deoxyribonucleic acid
NLRP3	NLR family pyrin domain containing 3
NOD1	Nucleotide-binding oligomerization domain-containing protein 1
PBS	Phosphate Buffered Saline

PINK1	PTEN-Induced Kinase 1
PL	Permanent Ligation
PPP	Pentose Phosphate Pathway
PRKN	Parkin E3 Ubiquitin Protein Ligase
PRR	Pattern Recognition Receptor
PSR	Picrosirius Red
PTEN	Phosphatase and tensin homolog
PTP	Protein Tyrosine Phosphatase
qRT-PCR	Quantitative Reverse Transcription Polymerase Chain Reaction
RAGE	Receptor for Advanced Glycation Endproducts
RIG-I	Retinoic Acid-Inducible Gene I
RIP2	Receptor-interacting serine/threonine-protein kinase 2
RLR	RIG-I-like receptors
RNA	Ribonucleic acid
ROS	Reactive Oxygen Species
SIRT1	Sirtuin 1
SIRT3	Sirtuin 3
SW	Spleen weight
TAC	Transverse Aortic Constriction
TBK1	TANK-binding kinase 1

TLR	Toll-like receptor
TRAF	Tumor Necrosis Factor Receptor-Associated Factor
VEGF	Vascular Endothelial Growth Factor
VEGFR	Vascular Endothelial Growth Factor Receptor
WGA	Wheat Germ Assay
WT	Wildtype

LIST OF TABLES

Table 1. DAMPs, their receptors and downstream inflammatory signalling pathways in myocardial infarction 6

Table 2 Comparison of technical outcomes and clinical relevance of murine permanent ligation and ischemia reperfusion models of myocardial infarction 27

LIST OF FIGURES

Figure 1.1 Summary of mitochondrial-based mechanisms that influence major metabolic function pathways in CVD. 13

Figure 1.2 Summary of mitochondrial-based mechanisms that influence mitochondrial dynamic pathways in CVD. 15

Figure 1.3 Summary of mitochondrial-based mechanisms that influence cell regulation and network pathways in CVD. 18

Figure 1.4 Canonical MAVS activation and signalling pathway. 21

Figure 1.5 *MAVS* mRNA expression is enriched in human cardiac tissue. 24

Figure 1.6 MAVS/NOD1/RIP2 signalling in Cardiac Hypertrophy. 25

Figure 3.1 Male *Mavs*$^{-/-}$ mice display no change in normalized heart weight or lung weight 4 weeks post-MI compared to WT mice who display increases. 37

Figure 3.2 Male *Mavs*$^{-/-}$ mice are protected from reductions in left ventricular ejection fraction (%) 4 weeks post MI, compared to WT controls. Females display an opposite trend. 39

Figure 3.3 Male and female *Mavs*$^{-/-}$ mice have smaller hearts and display reduced wall thickness 4-weeks post MI compared to their WT controls. 42

Figure 3.4 Both male and female *Mavs*$^{-/-}$ mice exhibit less cellular hypertrophy 4-weeks post-MI. (A) 45

Figure 3.5 Male *Mavs*$^{-/-}$ mice exhibit increased scar/whole heart area (%) 4-weeks post-MI. Females do not display this same difference. 48

Figure 3.6 Gene expression profiles of male WT and *Mavs*$^{-/-}$ cardiac tissue 4-week post MI or Sham operations. 51
Figure 3.7 No notable structural differences observed within male and female cohorts 3 days post-MI. 53
Figure 3.8 Male and female *Mavs*$^{-/-}$ mice display reduced wall thickness 3 days post MI compared to their WT controls. 55
Figure 7.7.1 Two Angiotensin II treatment regimens induce MAVS activation in AC16 cells. (A,C) 93
Figure 7.2 200nm 24hrs Ang II treatment induces MAVS activation in AC16 cells. 95
Figure 7.3 MAVS antibody is most effective in detecting MAVS in mitochondrial isolates from human AC16 cells. 98
Figure 7.4 Mavs knockout model validation. 100
Figure 7.5 No significant differences in body weights between groups pre and 4 weeks post MI. 102
Figure 7.6 Cardiac measure calculated from echocardiography, males and female mice 4-week post MI. 105

1 INTRODUCTION

1.1 Cardiovascular System and Cardiovascular Disease

The cardiovascular system consists of the heart, blood and an intricate network of blood vessels (veins, venules, capillaries, arterioles, and arteries)[1]. Pulmonary circulation facilitates the oxygenation of the blood, whereas systemic circulation supplies the body's cells and organs with blood rich in oxygen, nutrients, hormones, and other key components[1]. Both the parasympathetic and sympathetic nervous systems, in response to various stimuli (changing blood volume/flow, hormonal/inflammatory signals, and inter-organ-cross-talk signalling), contribute to regulating cardiovascular system activity[1]. Dysregulation of or pathophysiological insults involving the cardiovascular system can lead to cardiovascular disease (CVD). CVDs are non-communicable diseases involving one or more components of the cardiovascular system and remain a leading cause of death worldwide[2].

In Canada, CVD prevalence has increased by 156.4% between the years 1990 and 2019, with a small decrease of 20.7% in age-standardized rates[3]. Ischemic heart disease (IHD), peripheral artery disease (PAD), and non-rheumatic valvular disease are the most prevalent[3]. Furthermore, CVD death increased from 74,467 to 82,644 - an 11.0% increase[3]. Additionally, Canadian HF patients present with an average of 3.9 comorbidities, commonly chronic IHD, atrial fibrillation and flutter, diabetes, and renal failure[4]. The rise in comorbid patients emphasizes the changing landscape of cardiovascular disease, highlighting the need for holistic, diagnostic, prevention, and treatment strategies that target underlying disease causes and multi-organ systems[3,5].

1.1.1 Myocardial Infarction

Myocardial infarction (MI) is heart muscle necrosis secondary to the acute reduction or complete cessation of blood supply, and thus oxygen, to a region of the myocardium[6]. Acute MI involves a rapid reduction or arrest of coronary blood flow, typically due to an occlusion following an atherothrombotic plaque rupture or erosion[7]. Comparatively, chronic myocardial ischemia is associated with various causes of prolonged reductions in coronary blood flow[7].

Coronary artery disease and atherosclerosis, hypertension, coronary artery spasms, cardiac hypertrophy, and haematological diseases such as anemia can all function as precursors for MI[7]. In patients with coronary artery atherosclerosis, increased low-density lipoproteins (LDL), reactive oxygen species (ROS), and foamy macrophages sustain inflammation and the formation of atherosclerotic plaques[8]. Plaque accumulation contributes to the narrowing of the arteries, which significantly reduces and disturbs laminar blood flow and can contribute to chronic myocardial ischemia[8]. However, in the event of a plaque rupture or erosion, thrombogenic material is released into the bloodstream, which may result in the formation of a thrombus, causing a partial or complete vascular occlusion[7,8]. Hypertensive patients, due to mechanical stress caused to the heart and blood vessels, are far more likely to develop endothelial dysfunction, left ventricular hypertrophy, and accelerated atherosclerosis - predisposing them to myocardial ischemia[9]. In the case of coronary artery spasms, intense vasoconstriction of the epicardial coronaries can cause partial or complete vascular occlusions, which ultimately result in moments of cardiac ischemia[10]. These spasms can be triggered by endothelial dysfunction, smooth muscle cell hyperactivity, and impaired calcium handling, among others[10]. Finally, cardiac hypertrophy, adverse cardiac remodelling, and

haematological diseases are all associated with higher likelihoods of oxygen supply and demand mismatch and propensity towards heart failure[7].

As early as 10-15 minutes after the onset of ischemia, depleted cellular glycogen, mitochondrial abnormalities, myofibril relaxation, and sarcolemma disruption are observed[11,12]. Within hours, prolonged ischemia ultimately results in necrosis, which progressively spreads from the subendocardium to the subepicardium. Where applicable, timely reperfusion therapy significantly reduces the area at risk of ischemic injury[12].

1.1.1.1 Clinical Diagnosis and Treatment of MI

Clinical diagnosis of MI involves a combination of tests, including clinical assessment/differential, electrocardiography, cardiac biomarkers, and cardiac imaging[12]. Cardiac troponin I (cTnI) and T (cTnT) are components of the cardiac contractile system and are expressed almost exclusively in myocardial cells – making them sensitive and specific biomarkers of cardiac injury[13]. By definition, a cTnT value increased above the 99th percentile upper reference limit indicates myocardial injury[12,13]. However, elevated cTnT values are not useful in distinguishing the underlying pathophysiological mechanism of disease, and increases can be induced by any mechanical or physiological stresses in otherwise healthy hearts[12]. As such, a multifactorial contribution to myocardial injury should be described in patient records[12]. Other biomarkers, such as creatine kinase-MB (CK-MB), are less sensitive and specific[12]. MI is also detected in patients using 12-lead electrocardiography (ECG), biomarker detection, and cardiac imaging[12]. An abnormal ECG would indicate any or a combination of the following: ST segment elevation, ST segment depressions, T-wave changes, and pathological Q waves[12]. Finally, cardiac imaging techniques such as

echocardiography, cardiac magnetic resonance imaging, radionuclide imaging (SPECT, PET), myocardial perfusion scintigraphy, and possibly computed tomography can be used to indicate myocardial viability, perfusion, and function[12].

The mainstay of treatment consists of reperfusion therapy, most commonly percutaneous coronary intervention (PCI) with balloon angioplasty/stents, or less frequently coronary artery bypass grafting (CABG) surgery, followed by long-term management strategies[12]. Although essential to prevent further tissue necrosis and save lives, coronary reperfusion therapies can initiate myocardial stunning (reperfusion injury) - pathological consequences mediated by oxygen free radicals, neutrophil-endothelium interaction, apoptosis, and intracellular calcium overload[14]. Due to the complexity and multifarious nature of reperfusion pathology, an effective treatment would include an antagonist(s) that is equally multifaceted[14], but currently does not exist.

1.1.1.2 Myocardial Infarction Pathophysiology and Cardiac Repair

MI pathophysiology and cardiac repair can be separated into 3 phases: inflammatory, reparative/proliferative, and remodelling/maturation[15]. The initial intense inflammatory response, occurring approximately day 0-3 post MI, is essential as it serves to degrade and clear damaged cells and the extracellular matrix (ECM) that is deposed following injury[15]. The reparative/proliferative phase, occurring approximately day 3-7 post MI, includes granulation tissue formation with reprogrammed myofibroblasts, angiogenesis, and collagen deposition to initiate scar tissue formation[16]. Finally, the remodelling/maturation, occurring approximately day 7 post MI and onwards, involves ECM maturation, some cellular reprogramming, and functional remodelling[15,16].

1.1.1.2.1 Inflammatory Phase

Immediately following an occlusion, cellular contents released from cardiomyocytes dying via necrosis act as damage-associated molecular patterns (DAMPs) to initiate an intense inflammatory response and activate innate immune signalling mechanisms[16]. Furthermore, ROS are generated in large quantities and overwhelm the intrinsic antioxidant system, further exacerbating inflammatory signalling while simultaneously inhibiting myocardial function[16]. Broadly speaking, DAMPs bind to pattern recognition receptors (PRRs) on parenchymal and infiltrating leukocytes, and all cardiovascular cells found in the viable tissue surrounding the infarct – termed the border or peri-infarct zone and elicit downstream intracellular inflammatory response mechanisms[16]. Key DAMPs and their receptors that are activated in response to MI are summarized in **Table 1**. Most notably, toll-like receptor/interleukin 1 receptors (TLR/IL-1Rs), complement system receptors, receptor for advanced glycation end-products (RAGE), and nucleotide-binding oligomerization domain–like receptors (NLRs) are all activated[15,17,18]. The resulting downstream signal transduction includes activation of nuclear factor (NF)-kB and mitogen-activated protein kinases (MAPKs). The former drives production of inflammatory cytokine and chemokines such as tumor necrosis factor-α (TNF) and Interleukins (IL)-1b/6/18), as well as cell adhesion molecules, and complement factor B[19,20]. These factors trigger the recruitment of leukocytes (neutrophils, monocytes, and T-lymphocytes) and encourage macrophage proliferation, further propagating inflammation, DAMP production, efferocytosis, tissue digestion, and proteolysis[15,21].

Table 1. DAMPs, their receptors and downstream inflammatory signalling pathways in myocardial infarction

Class	Endogenous Ligand	Receptor(s)	Reference(s)
Proteins	HMGB1	TLR2, TLR4, TLR9, RAGE	18,22–27
	IL-1a	IL-1R	28,29
	HSP-60/70	TLR2, TLR4, TLR6	26,30–34
	S100A8/S100A9/S100A1	TLR4, NLRP3, RAGE	18,26,35,36
	Fibronectin-EDA	TLR2, TLR4	17,37
Matricellular Proteins	CCN1	TLR2*, TLR4*	38
	Osteopontin (OPN or Eta-1)	TLR9 (MyD88)	39
	Galectins	Various/unknown	40,41
	Tenascin-C (TN-C)	TLR4	18,26,42
Purine Metabolites	ATP	P2X7/NLRP3	43,44
	Uric Acid	TLR2, TLR4, NLRP3	45,46
Nucleic Acids	Mitochondrial DNA (mtDNA)	TLR9, AIM2 NLRP3	47–51
	mRNA	TLR3	52
Proteoglycan	LMW HA	TLR2, TLR4, NLRP3	53,54

*Expected mechanism – i.e., interaction established outside of an MI context

1.1.1.2.2 Inflammation Resolution and Regenerative/Proliferative Phase

After approximately 7 days, the cardiac microenvironment transitions from an inflammatory environment to a reparative one. This repair is largely driven by: reparative monocytes, macrophages switching from a pro-inflammatory (M1) to an anti-inflammatory (M2) phenotype, and increased gene expression of anti-inflammatory, profibrotic, and angiogenic factors, including IL-10, transforming growth factor β (TGF-β), vascular endothelial growth factor (VEGF), respectively[55,56]. A pro-resolving phenotype, and pro-fibrotic and anti-inflammatory cytokines are released in response to neutrophils being phagocytosed by macrophages, ultimately reducing inflammation and promoting tissue repair. Due to the hearts' insufficient rate of myocyte regeneration, the infarcted area is repaired by scar formation, driven by the proliferation of fibroblasts and myofibroblasts and their deposition of collagen[57]. The temporary cardiac matrix, comprised of fibrin and fibronectin, is replaced by ECM in time[54]. To offset contractile functional loss, the remaining viable cardiac muscle tissue undergoes dilation and segmental hypertrophy, setting the stage for possible heart failure in the future[58].

1.1.1.2.3 Maturation Phase

Following the proliferative phase, during the maturation phase, the ECM becomes cross-linked and stabilized[59]. Quiescence and occasionally apoptosis deactivates reparative cells such as infarct myofibroblasts, through mechanisms that remain largely unelucidated[60]. Inactivation of fibrogenic growth factor TGF-β, cessation of angiotensin II signalling, and clearance of matricellular proteins are proposed mechanisms that may suppress proliferation

and reduce the fibroblast activity[59]. Despite post-MI cardiac repair being a fine-tuned process, excessive fibrosis and maladaptive remodelling establish a structural basis for the development of heart failure[58]. Therefore, a balance between efficient repair and pathological fibrosis is essential for optimal long-term cardiac function[57].

1.1.2 Heart Failure

In many instances, CVDs, including myocardial infarction, act as precursors of heart failure (HF)[61]. HF occurs when the heart muscle is unable to supply adequate blood to the critical organs to maintain function[62,63]. HF can be anatomically classified into three types according to primary location: left-ventricular, right-ventricular, and biventricular, affecting the left, right, and both ventricles, respectively[61]. Left-ventricular HF can be further sub-categorized as either heart failure with reduced ejection fraction (HFrEF) or heart failure with preserved ejection fraction (HFpEF)[64,65]. HFrEF, also known as systolic dysfunction, occurs when the heart is unable to contract effectively, resulting in inadequate oxygenated blood circulating to the organs of the body[66]. HFrEF is often caused by the loss of cardiac muscle due to ischemia, infarction, genetic mutations, myocarditis, or valvular diseases[65]. Conversely, HFpEF occurs when the cardiac muscle becomes thick, stiff, the chambers reduce in size, and is unable to effectively fill and circulate sufficient blood volumes[65]. HFpEF is frequently preceded by cardiovascular comorbidities such as high blood pressure, metabolic syndromes such as obesity and diabetes, and kidney diseases[65].

Heart failure treatment largely consists of lifestyle changes and natural history-altering medications such as beta blockers, angiotensin receptor-neprilysin inhibitors (ARNIs), sodium-glucose transport protein 2 (SGLT2) inhibitors, and aldosterone blockers[61].

Unfortunately, once developed, HF is difficult to reverse, emphasizing the importance of adopting preventative and/or early-stage interventions that delay, or inhibit entirely, heart failure progression[61]. The treatments for HFpEF are much fewer, including SGLT2 inhibitors, aldosterone antagonists, and glucagon-like peptide-1 receptor agonist (GLP-1ra) for obese patients[67].

1.2 Mitochondrial Mechanisms in Cardiovascular Disease

Given their plasticity and highly dynamic nature, mitochondria are invaluable to metabolism, homeostatic maintenance, and stress. Since myocardium is a highly oxidative tissue, mitochondria are highly involved in the maintenance of cardiovascular performance as well as the development and progression of pathological remodeling[68]. Additionally, since the myocardium is comprised of non-dividing cells, the dynamic nature of mitochondria is indispensable for compensating for dead/diseased tissue and optimizing remaining cardiac function. However, in the failing heart, mitochondrial dysfunction and metabolic abnormalities such as energetic deficits, ineffective substrate utilization, oxidative stress, etc., directly contribute to cardiomyocyte injury and thus disease progression[69].

Optimizing mitochondrial dynamic processes has the potential to optimize cardiac remodeling effectiveness and maximize heart function[68,70,71]. Thus, understanding the intricate network of proteins that modulate changes in cardiac metabolism, during and after stress exposure, is critical for informing the development and validating the potential of mitochondrial/metabolic-specific CVD therapeutics. Based on a rigorous literature search, **Figures 1.1, 1.2, and 1.3** were designed to summarize the known existing molecular

mechanisms in which mitochondria contribute to pathophysiological changes in cardiac immunology and metabolism. These summaries will undoubtedly help streamline future mechanistic studies – enabling our lab's future research to focus on MAVS' role in metabolic control.

1.2.1 Energy Production and Fatty Acid Oxidation

Under normal physiological states, to match the heart's high energy demand, mitochondrial fatty acid oxidation contributes to 60-80% of cardiac ATP production as well as providing several metabolic intermediates which are key for biosynthesis, protein modification, and signal transductions[72–74]. In a failing heart, pathological remodeling results in unfavorable cardiac geometry, impaired calcium handling, and increased neurohormonal stimulation - all of which demand increased energy expenditure[75–79]. Additionally, in a failing heart, mitochondrial oxidative capacity is diminished, and the heart shifts to glycolytic pathways[76,79,80]. This metabolic switch results in a further decrease in energy and metabolic intermediate supply, which in turn exacerbates pathologic mechanisms[76].

1.2.2 Reactive Oxygen Species Management

Oxidative phosphorylation can result in the production of ROS such as hydroperoxides (RO_2H), superoxide (O_2^-), hydroxyl radical (OH), and singlet oxygen[81]. In healthy mitochondria, ROS levels remain low, and these species are effectively cleared by both intracellular and intramitochondrial scavenging systems as well as brief openings of mitochondrial permeability transition pores (mPTP)[82,83]. However, in pathologic states such as HF, ROS accumulate much quicker, which impairs mitochondrial function, damages cellular membrane proteins and lipids, and triggers inflammation and cell-death cascades[81].

1.2.3 Calcium Mishandling and mPTP dysregulation

Calcium is indispensable for cardiomyocyte contraction and mitochondrial function as it serves to activate many metabolic enzymes such as pyruvate dehydrogenases, isocitrate dehydrogenase, and a-ketoglutarate dehydrogenase[84–86]. In healthy cardiomyocytes, mitochondrial calcium homeostasis is maintained via active calcium transport systems, but under pathological conditions, calcium accumulates and forces mPTP opening[87,88]. Prolonged mPTP opening leads to 1) the loss of membrane potential, which impairs complex activity and ATP production, and 2) leak of mitochondrial contents, such as cytochrome c or mtDNA, which have been shown to trigger inflammatory processes and subsequently induce apoptosis and necroptosis[89–93].

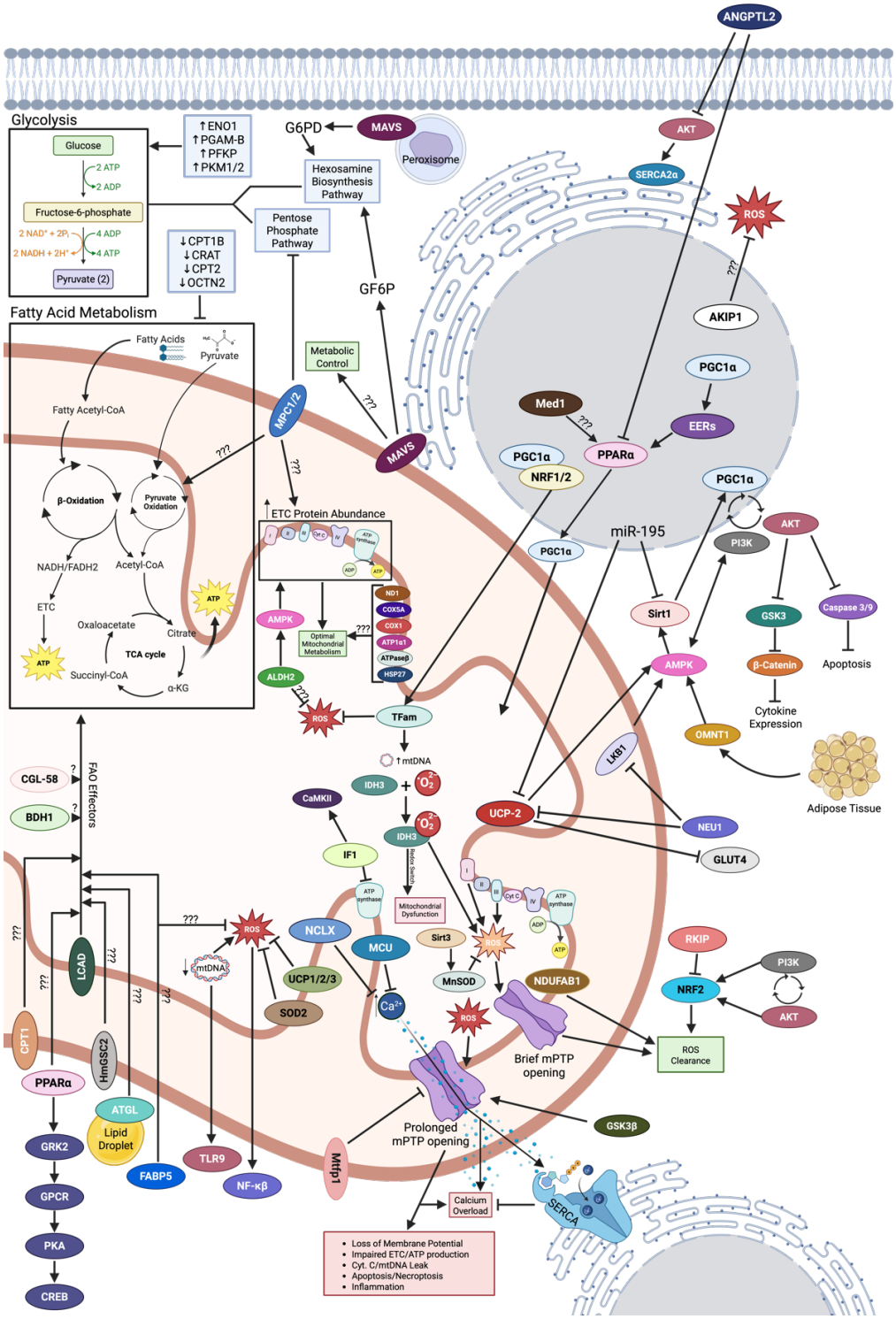
ANGPTL2
Glycolysis
Glucose
2 ATP
2 ADP
Fructose-6-phosphate
2 NAD+ + 2Pi
4 ADP
2 NADH + 2H+
4 ATP
Pyruvate (2)
↑ENO1
↑PGAM-B
↑PFKP
↑PKM1/2
G6PD
MAVS
Peroxisome
AKT
SERCA2α
ROS
Hexosamine Biosynthesis Pathway
Pentose Phosphate Pathway
GF6P
↓CPT1B
↓CRAT
↓CPT2
↓OCTN2
AKIP1
Fatty Acid Metabolism
Fatty Acids
Pyruvate
Metabolic Control
PGC1α
Med1
EERs
PPARα
NRF1/2
Fatty Acetyl-CoA
MPC1/2
β-Oxidation
Pyruvate Oxidation
ETC Protein Abundance
miR-195
PI3K
NADH/FADH2
Acetyl-CoA
ETC
ATP
Oxaloacetate
Citrate
TCA cycle
Succinyl-CoA
α-KG
AMPK
Optimal Mitochondrial Metabolism
ND1
COX5A
COX1
ATP1α1
ATPaseβ
HSP27
Sirt1
GSK3
Caspase 3/9
β-Catenin
Apoptosis
Cytokine Expression
ALDH2
TFam
↑mtDNA
OMNT1
LKB1
Adipose Tissue
CGL-58
BDH1
FAO Effectors
CaMKII
IDH3
UCP-2
NEU1
GLUT4
IF1
Mitochondrial Dysfunction
NCLX
MCU
Sirt3
MnSOD
NDUFAB1
RKIP
NRF2
ROS Clearance
UCP1/2/3
SOD2
Ca2+
Brief mPTP opening
Prolonged mPTP opening
GSK3β
LCAD
CPT1
HmGSC2
PPARα
ATGL
Lipid Droplet
FABP5
GRK2
GPCR
PKA
CREB
TLR9
NF-κβ
Mfp1
Calcium Overload
SERCA
Loss of Membrane Potential
Impaired ETC/ATP production
Cyt. C/mtDNA Leak
Apoptosis/Necroptosis
Inflammation

Figure 1.1 Summary of mitochondrial-based mechanisms that influence major metabolic function pathways in CVD. Including a magnified mitochondrial double membrane with signaling moieties (*items not drawn to scale for illustrative purposes only*).

1.2.4 Mitochondrial Biogenesis and Degradation Dynamics

In a healthy heart, regulating mitochondrial dynamics (mitochondrial biogenesis, fission/fusion, and mitophagy) is central to maintaining healthy heart function. Abnormal changes in these regulatory processes contribute to heart failure progression[94]. Decreased levels of key fusion factors, mitofusin 1/2 (MFN1/2) and optic atrophy protein (OPA1), and increased levels of key fission factors mitochondrial dynamin-related protein 1 (Drp1)/fission protein (Fis1) dampen mitochondrial fusion and promote mitochondrial fragmentation, respectively[95–97]. As a result, cardiomyocytes in the failing heart are largely equipped with fewer numbers of small mitochondria that, as a compensatory remodeling mechanism, aggregate together[97,98]. Not only are these mitochondrial aggregates less metabolically efficient, but they are also largely comprised of damaged mitochondria that are prone to releasing vast amounts of ROS, which can modify cellular DNA, proteins, and lipids[95,99–101]. Severe impairment of mitochondrial biogenesis in HF is indicated by a large reduction of mtDNA content, mtDNA-encoding proteins, and a key biogenesis regulator, peroxisome proliferator-activated receptor gamma co-activator (PGC-1a)[102–104]. The activity and abundance of key mitophagy effector molecules such as PTEN-induced kinase 1 (PINK1) and Parkin (PRKN) are also reduced in HF patients, leading to severely impaired mitophagy[105,106]. The mechanisms of decreased biogenesis and impaired mitophagy limit mitochondria replenishment/clearance, allowing damaged mitochondria to accumulate and ultimately exacerbate cardiac injury[94].

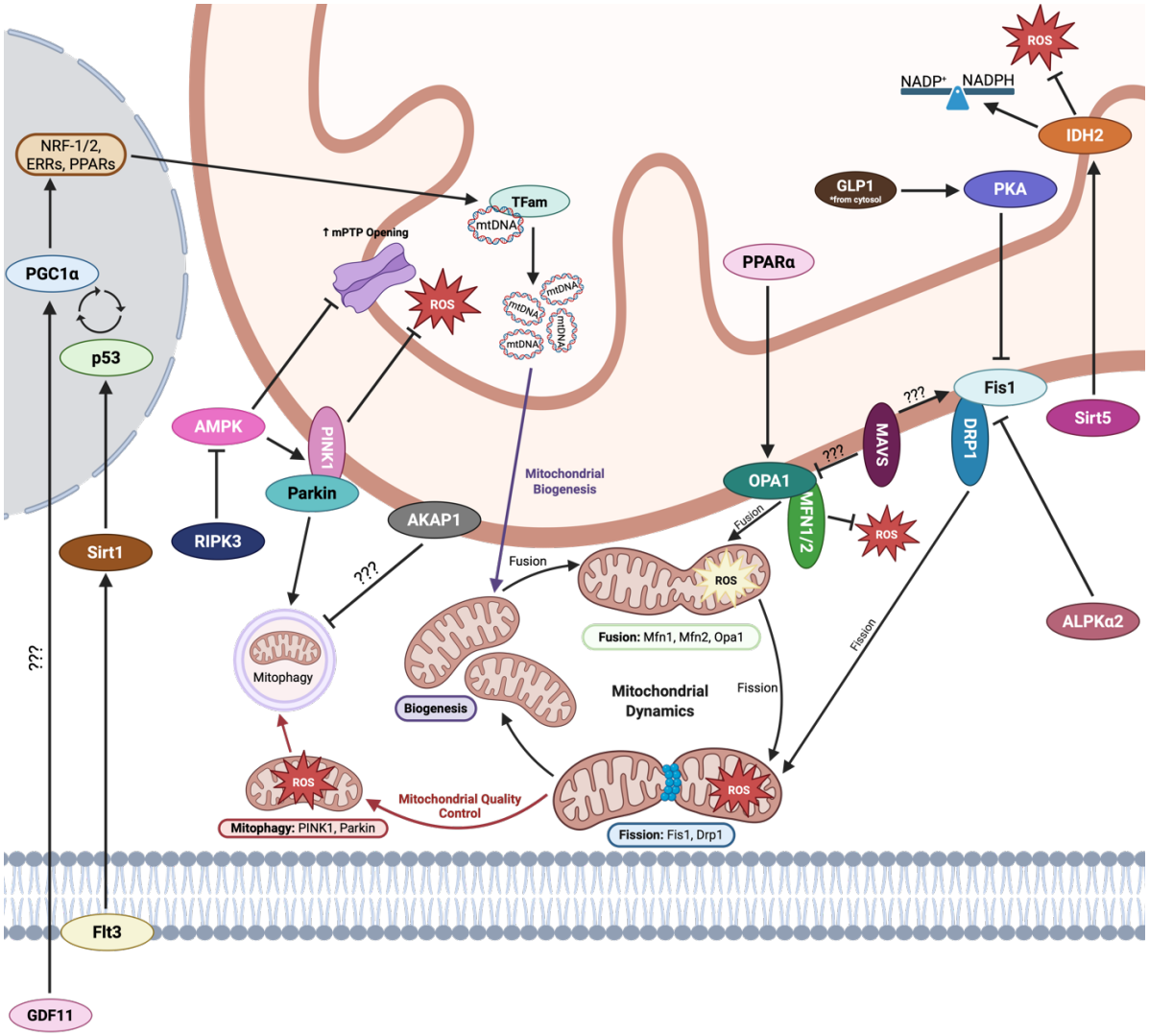

Figure 1.2 Summary of mitochondrial-based mechanisms that influence mitochondrial dynamic pathways in CVD. Including a magnified mitochondrial double membrane with signaling moieties (*items not drawn to scale for illustrative purposes only*).

1.2.5 Angiogenesis and Lymphangiogenic Pathways

A large body of evidence supports that increased angiogenesis is associated with increased blood flow and improved cardiac function and remodeling outcomes in ischemic and hypertensive heart diseases[107–110]. Vascular endothelial growth factors (VEGFs) and their receptors (VEGFRs) are formidable angiogenesis promoters and are essential for vascular endothelial cell proliferation[111]. VEGF-A and its receptors VEGFR-1/2 play major roles in physiology and pathological angiogenesis, whereas VEGF-C/D and their receptor VEGFR-3 mostly function as a lymphangiogenesis regulator[111]. In fact, recent research suggests that upregulating a mitochondrial SIRT3 activates the VEGFC-VEGFR3 axis, promotes migration and proliferation of lymphatic endothelial cells (LECs) and cardiac lymphangiogenosis, which ultimately attenuates hypertension-induced cardiac injury[112]. However, it is important to note that in atherosclerosis research, various studies suggest that promoting angiogenesis contributes to the growth of atherosclerotic lesions and plaque instability[113]. Thus, when considering the development of angiogenesis-promoting therapeutic agents, it is important to consider the context and patient comorbidities[5].

1.2.6 Mitochondria-Associated Endoplasmic Reticulum Membranes

The ER-mitochondrial interaction (ie, mitochondria-associated endoplasmic reticulum membranes (MAM)) remains the best described to date[114]. This interaction allows for transfer of Ca^{2+} stores from the ER to the mitochondria, which can then increase the Krebs cycle and ETC activity to produce ATP[88,115–117]. However, in the failing heart, aberrant formation of MAMs and calcium mishandling exacerbate HF progression via mitochondrial dysfunction and calcium overload, ETC overactivity, and thus excessive ROS production, ER stress, and

apoptosis[118–121]. Additionally, in HF, Ca^{2+} transfer of MAM affects local cytosolic Ca^{2+} concentrations, which can induce pro-hypertrophic Ca^{2+} signalling and contractile dysfunction[69,122]. By extension, the MAM functions as a site for inflammasome formation and mitochondrial fission[49,123–125].

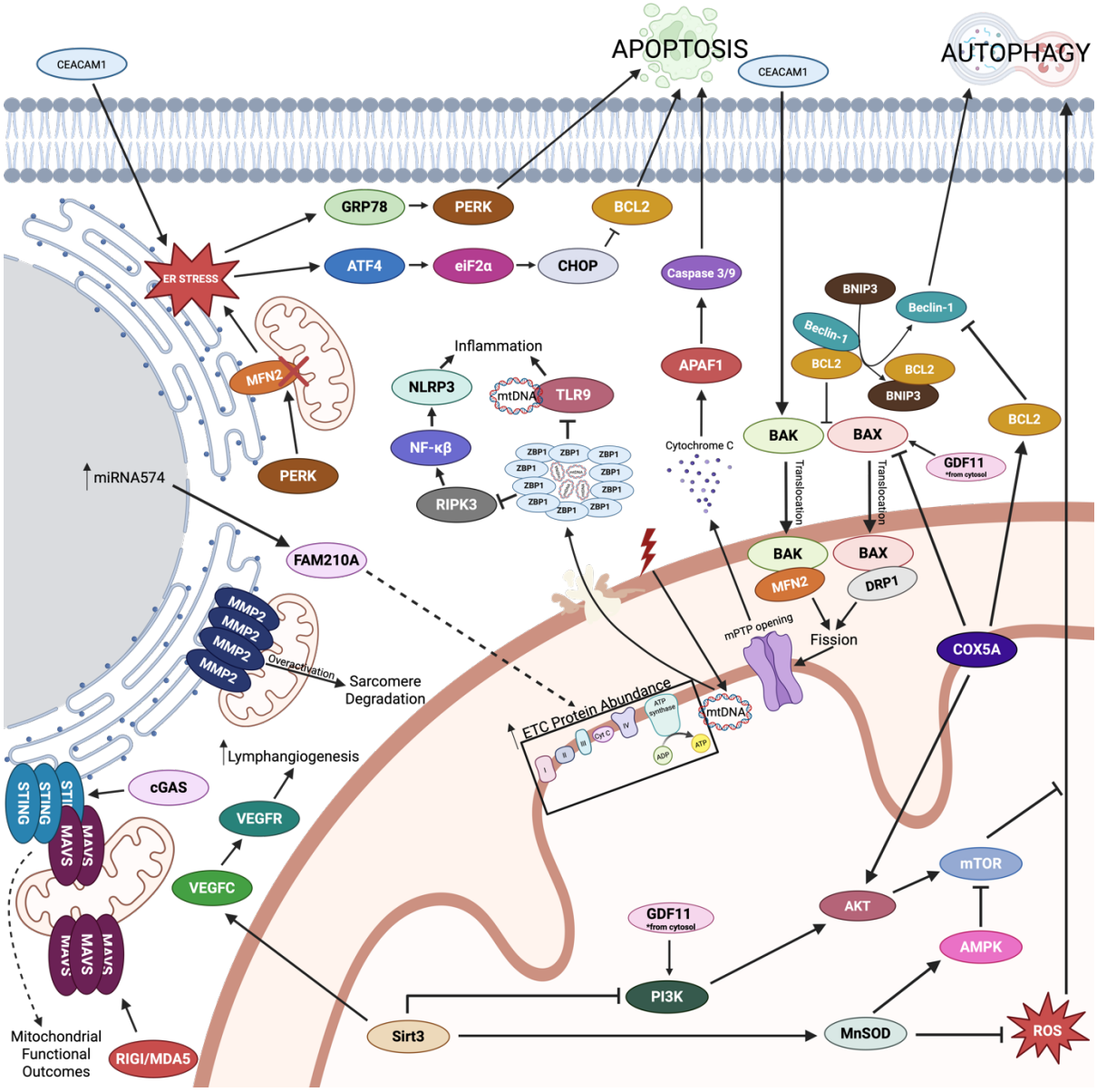

Figure 1.3 Summary of mitochondrial-based mechanisms that influence cell regulation and network pathways in CVD. Including a magnified mitochondrial double membrane with signaling moieties (*items not drawn to scale for illustrative purposes only*).

1.3 Mitochondrial Antiviral Signalling Molecule

The Mitochondrial Antiviral Signalling Protein (MAVS; also known as IPS-1/VISA/CARDIF) is the key caspase recruitment domain (CARD)-containing innate immune molecule that mainly resides on the outer mitochondrial membrane, although it has also been recognized on peroxisomes and mitochondrial-associated endoplasmic reticulum membranes[126–128]. MAVS is 540 amino acids in size and contains three key domains: a caspase recruitment domain (CARD) located at the N-terminal, a proline-rich region (PRR) found in the center, and the transmembrane (TM) domain that functions to anchor the protein to the outer mitochondrial membrane[129](**Figure 1.4A**).

1.3.1 Canonical MAVS Signalling

1.3.1.1 RIG-I-like receptor (RLR) signalling

The CARD domain of MAVS is classically known to contribute to RLR signalling pathways, as a downstream adaptor of retinoic acid-inducible gene I (RIG-I)[129] (**Figure 1.4B**). In response to microbial RNA in the cytosol, the CARD domain of MAVS interacts with the similar CARDs of two RIG-I-like receptors (RLRs) - retinoic acid-inducible gene I (RIG-I)/melanoma differentiation-associated protein 5 (MDA5)[130–132]. This intracellular signalling pathway triggers the formation of MAVS prion-like aggregates – an essential step to the biological function of MAVS[133]. MAVS-aggregation facilitates binding with TRAF2, TRAF3, TRAF5, or TRAF6 through its PRR domain[134]. MAVS CARD domains bound to TRAF2/5/6, an IKK-complex (containing IKKa/b and NEMO) is formed, which activates NF-kB to promote proinflammatory cytokine transcription. Simultaneously, MAVS CARD domains bound to TRAF2/3/5/6 promote TBK1 complex (containing TBK1, IKKi/e, and NEMO)

formation, subsequent IRF3 and/or IRF7 phosphorylation, and thus the initiation of type I interferon (IFN) transcription, downstream signalling, and other antiviral signalling cascades[135–137].

1.3.1.2 NLR family pyrin domain containing 3 (NLRP3) Inflammasome Activation

During viral infection or cellular stress, MAVS recruits NLR family pyrin domain-containing 3 (NLRP3) to the outer mitochondrial membrane (OMM)[138]. NLRP3 then assembles with apoptosis-associated speck-like protein containing a CARD (ASC), and pro-caspase 1 to form functional NLRP3 inflammasomes[138,139]. This ultimately results in the inflammasome-dependent generation of inflammatory cytokines IL-6 and IL-1β[131] (**Figure 1.4B**). NLRP3 inflammasome activation has been associated with mitochondrial dysfunction - reductions in mitochondrial membrane potential, increased ROS production, and mtDNA release - which can further exacerbate NLRP3 inflammasome-mediated inflammation[140,141].

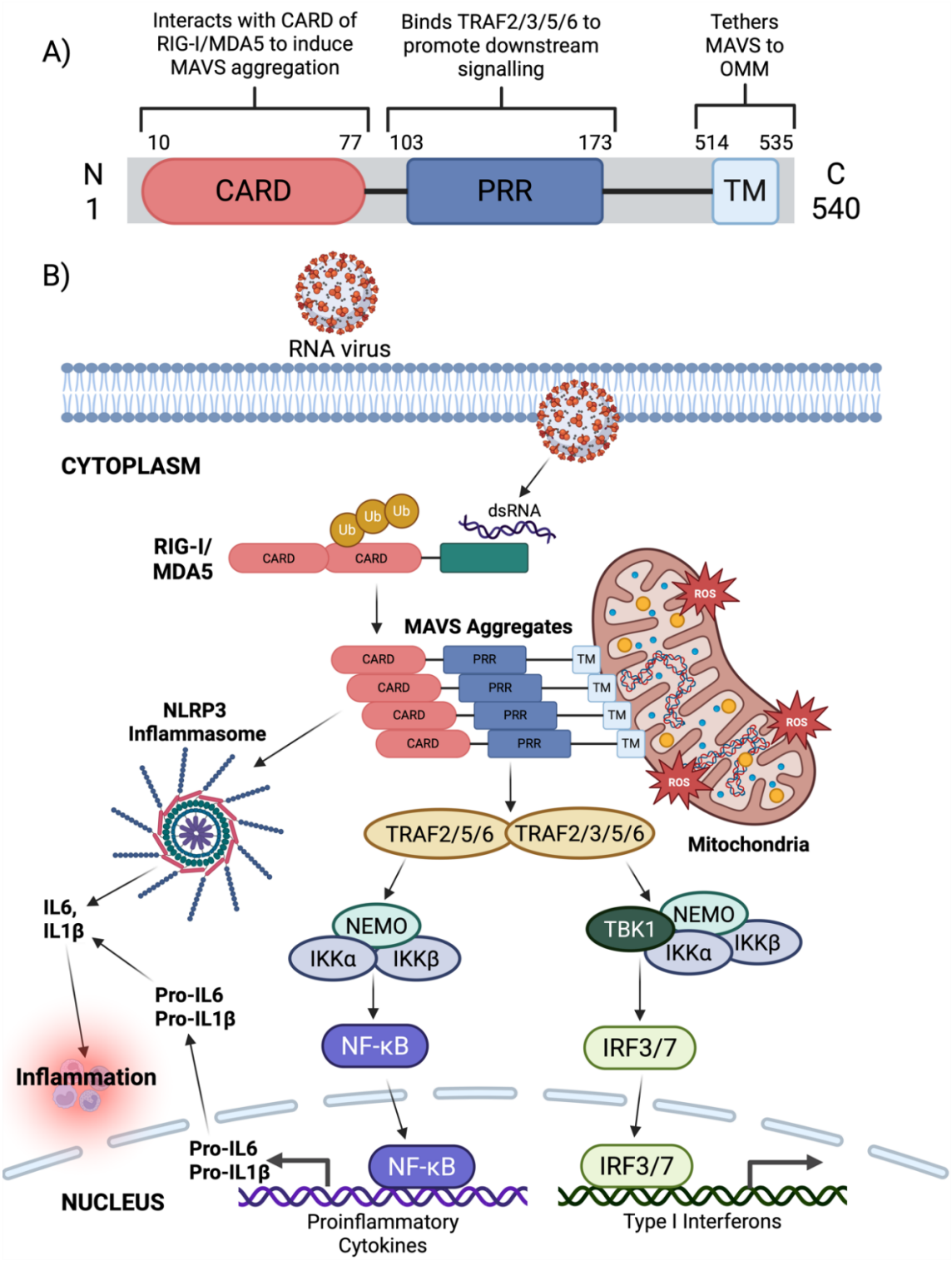

Figure 1.4 Canonical MAVS activation and signalling pathway.

1.3.2 MAVS Signalling in CVD

The human *MAVS* gene is comprised of 2912 base pairs, located on chromosome 20, and the human MAVS protein shares 51.8% amino acid homology with the mouse equivalent[142]. An RNAseq analysis, as per the protein atlas (http://www.protein-atlas.org/), revealed that *MAVS* mRNA is most abundantly expressed in skeletal, tongue, and heart muscles[143]. By extension, cardiac-specific RNA expression is most enriched in cardiomyocytes but also present in fibroblasts, endothelial, and smooth muscle cell UMAP clusters (http://www.protein-atlas.org/), making MAVS ideally positioned to play a major role in cardiac-related immunity[143] (**Figure 1.5**).

Recently, our lab has recognized MAVS for its non-canonical role in coordinating cardiac remodelling, inflammatory response, and altering mitochondrial energy metabolism in stressed hypertrophic cardiomyocytes[144]. In this pathway, the CARD domains of RIP2/NOD1 interact with the MAVS CARD domain and induce MAVS aggregation on mitochondrial surfaces[144] (**Figure 1.6**). Excess MAVS activation was found to contribute to adverse cardiac remodelling, inflammation activation, and impaired metabolic response in an *in vivo* murine transverse aortic constriction (TAC) model of pressure overload[144]. Additional research suggests that downregulation of MAVS in non-hypertrophic conditions contributes to declined cardiac function, indicated by left ventricular dilation, decreased systolic function, energy metabolism disorders by disruption of lipid metabolism, aggravated mitochondrial dysfunction by inducing mitochondrial oxidative stress, and impaired mitophagy[145]. The role of MAVS in MI-induced ischemic HF remains elusive.

In the context of myocardial ischemia-reperfusion injury (MIRI), global MAVS knockdown showed beneficial effects[146]. Mechanistically, MIRI causes release of dsRNA from the affected myocardium, which activates intracellular RIG-I and subsequently MAVS aggregation and signalling[146]. Ultimately, MAVS aggregation triggers the transforming growth factor-β-activated kinase 1 (TAK1) TAK1/(tumor necrosis factor-associated factor family 6) TRAF6 complex and subsequent (mitogen-activated protein kinase) MAPK/(c-jun-NH2 terminal kinase) JNK signaling cascade[146]. *Mavs*$^{-/-}$ reduced JNK phosphorylation and apoptosis, offering cardio protection, whereas JNK agonist abolished the protective nature of *Mavs*$^{-/-}$ [146].

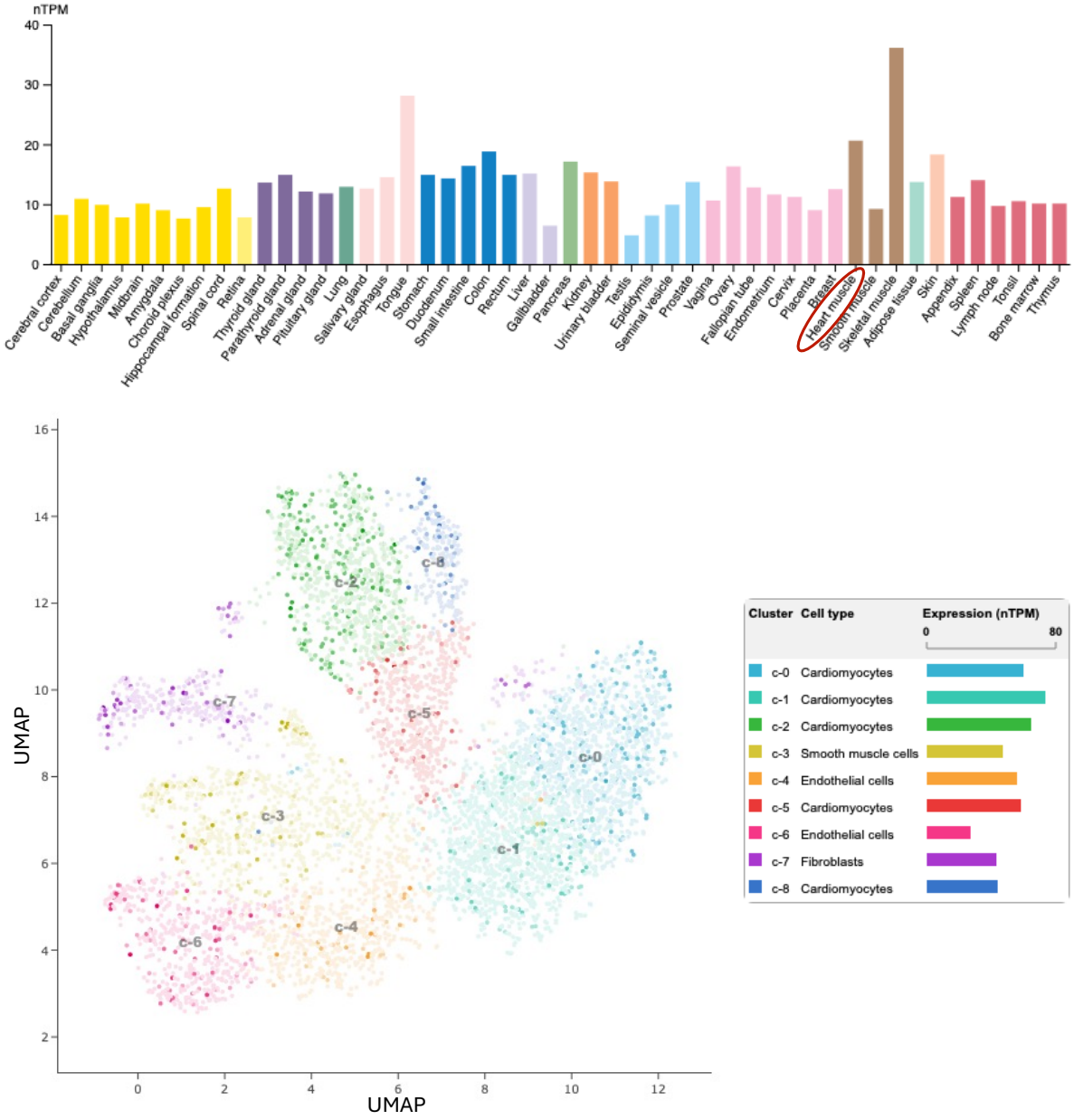

Figure 1.5 *MAVS* mRNA expression is enriched in human cardiac tissue. (A) Relative *MAVS* mRNA expression (nTPM) in various human tissues, with heart muscle highlighted (B) *MAVS* mRNA expression in the single cell type UMAP clusters of cardiac tissues. Image Credits: Human Protein Atlas

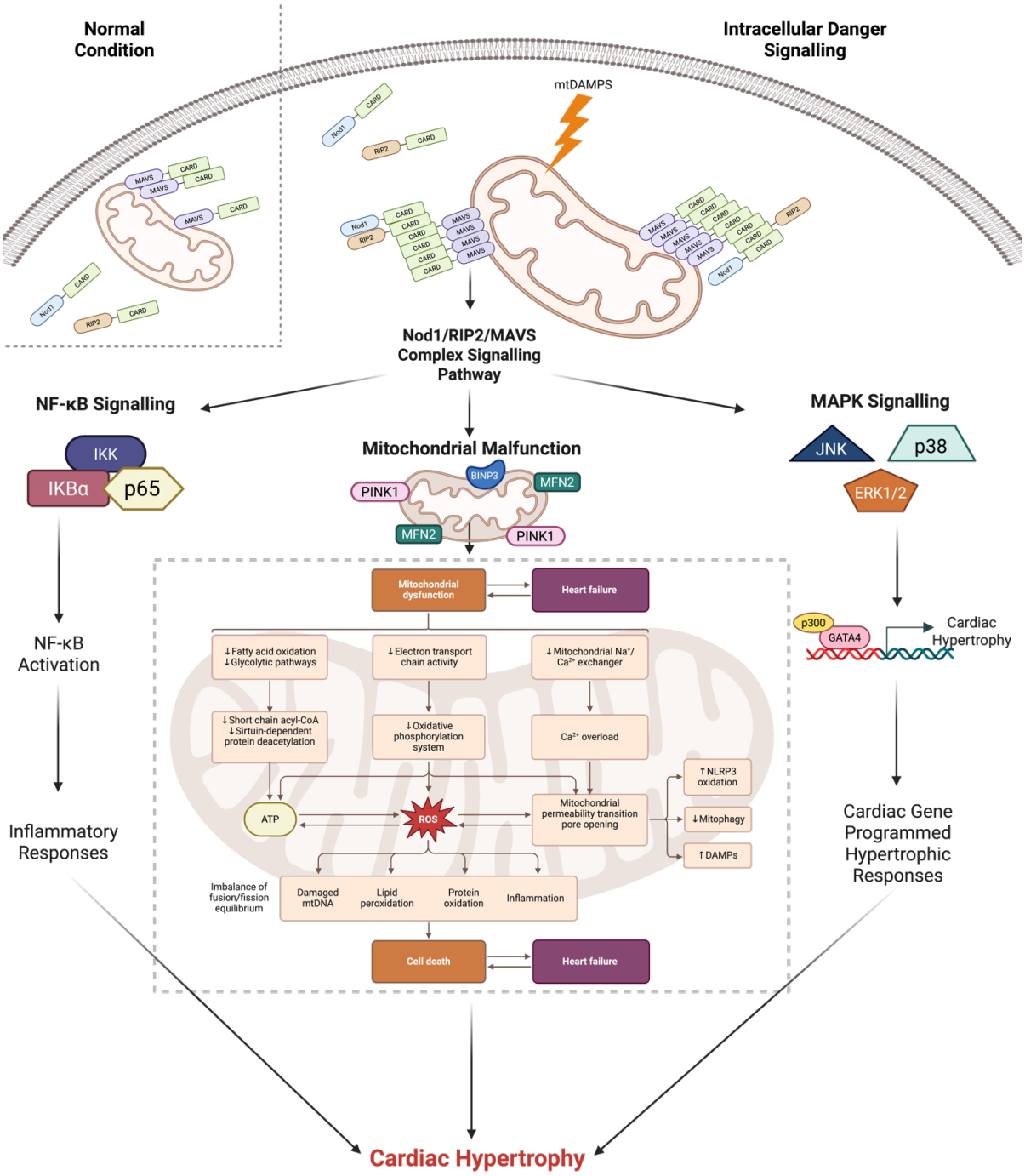

Figure 1.6 MAVS/NOD1/RIP2 signalling in Cardiac Hypertrophy.

1.4 Mouse Models of Myocardial Infarction

Animals have been a longstanding biomedical research tool for modelling human disease and have assisted significantly in elucidating disease mechanisms[147]. Mice specifically are cost-effective, easy to handle, breed, house, and are easily genetically manipulated to study gene function and/or mimic human disease[148]. However, due to their species-specific genetics, environmental and lifestyle variations, murine models are unable to fully recapitulate human disease[147]. As such, careful model selection is essential for appropriately addressing research questions and optimizing potential translatability.

The two most common animal models for studying myocardial infarction are permanent ligation (PL) and ischemia-reperfusion (IR). The former has been used in mice for over 70 years, whereas the latter was developed in dogs in 1988[149,150]. In both procedures, a ligation is made to occlude the left anterior descending coronary artery (LAD), thus inhibiting blood supply to the left ventricle[150]. In PL, the ligation remains, resulting in the majority of the area at risk (AAR) becoming infarcted, and remodelling as scar[151]. Conversely, IR ligation is temporary, mediated by a small tube that is removable for reperfusion (typically after 15min to 2hrs, with 30min being the most common)[149]. IR salvages some AAR and introduces myocardial stunning[152]. A comparison of technical outcomes and clinical relevance for both models is described in **Table 2**[153]. For this experimental series, PL was used to achieve large and reproducible infarct sizes – thus enabling a more robust phenotypic profile of *Mavs*$^{-/-}$ mice cardiac remodelling, as a more appropriate precursor to the development of heart failure[153].

Table 2 Comparison of technical outcomes and clinical relevance of murine permanent ligation and ischemia reperfusion models of myocardial infarction

	Permanent Ligation	**Ischemia Reperfusion**
Technical outcomes	Reproducible, requiring smaller cohort sizes	Some variability, requiring larger cohort sizes
	Large infarct sizes >30% (high level remodelling)	Small infarct sizes <30% (low-level remodelling)
	Postoperative complications result in higher death rates	Low death rates
Model Application/ Clinical Relevance	Represents the human patient population for which reperfusion therapy is unavailable or ineffective	Represents the human patient population for which timely reperfusion therapy is performed
	Model to test regenerative therapies	~30min reperfusion timepoint is not representative of clinical timepoints
	Model for studying long-term ischemia and remodelling	Model for studying cardiac reperfusion injury pathology
	Model of heart failure progression	Mice are unlikely to develop heart failure

1.5 Metabolic-Based Therapeutic Translation

Currently, there are few known mitochondrial protein targets and a limited understanding of their respective relevant molecular mechanisms[154]. As a direct result, there are very few metabolism-based therapeutics available for CVD[155]. Most of the currently approved drugs that have shown potential to improve mitochondrial function are being repurposed in efforts to improve metabolic efficiency as a rehabilitation strategy[156]. For example, implementing mitochondrial-based treatments to improve mitochondrial function in skeletal muscles for physical therapy purposes[156]. As of current, no therapeutics specifically target cardiac mitochondrial function and serve to treat active pathological states exist[154,156]. This underscores the clinical need for identifying novel, cardiac-specific, mitochondrial therapeutic targets. In general, if one aspect of mitochondrial function improves, most other aspects of mitochondrial function also improve[154,157]. Most mechanistic understanding to date is incomplete – nuances regarding whether the currently identified proteins are direct or indirect modifiers of mitochondrial function mediators are unclear[155]. Thus, establishing holistic mechanisms will be essential for understanding the intricacies of how mitochondrial function contributes to heart failure progression, and which mitochondrial proteins would make the most effective/accessible therapeutic targets[156]. Due to its unique location, immune-sensing function/activation, and subsequent ability to dictate downstream metabolic control, MAVS is an intriguing candidate.

1.6 Rationale, Objective, Hypothesis, Aims

Since the myocardium is a highly oxidative tissue, mitochondria are largely involved in the maintenance of cardiovascular performance as well as the development and progression of pathological remodelling[68]. Mitochondrial dynamic processes such as mitochondrial biogenesis, fusion, fission, and mitophagy are largely involved in cardiac remodelling post-MI[68]. Since MAVS is the unique CARD domain interacting with innate immune signalling moiety on the mitochondrial membrane, it may contribute a potential pivotal regulatory role(s) in stress response of the myocardium to danger signals. Thus, *targeting mitochondrial function has the potential to subsequently optimize remodelling effectiveness to maximize preservation of heart function post-MI and ultimately improve patient prognosis*[68,70,71].

Although we recognize the importance and likelihood of MAVS coordinating metabolic control, the purpose of this thesis is to set the stage for more in-depth mechanistic studies. More specifically, this series of experiments seeks to investigate the role of MAVS in cardiac pathology by distinguishing the phenotypic remodeling differences that *Mavs*$^{-/-}$ mice exhibit following MI stress response. Achieving this purpose will be obtained through the following: Overall Aim: determine the nature of *Mavs* deficiency as protective or detrimental in post-MI stress response and cardiac remodelling. We hypothesize that MAVS plays a key role in modifying cardiac remodelling following MI stress response.

Aim 1: Assess remodelling differences, 4 weeks post-MI, between WT and Mavs$^{-/-}$

Aim 1a: Assess pathological differences between WT and *Mavs*$^{-/-}$ mice

Aim 1b: Assess hypertrophic remodelling differences between WT and *Mavs*$^{-/-}$ mice

Aim 1c: Assess cardiac functional outcome between WT and *Mavs*$^{-/-}$

Aim 1d: Assess fibrosis differences between WT and *Mavs*$^{-/-}$

Aim 2: Assess short-term remodelling differences, 3 days post-MI, between WT and Mavs$^{-/-}$

Aim 2a: Assess pathological differences between WT and *Mavs*$^{-/-}$ mice

Aim 2b: Assess morphological and immune cell infiltration changes

Aim 3: Develop an in vitro modelling system for MAVS activation – supplemental data

Aim 3a: Assess the effectiveness of hypertrophic stimuli, AngII, induction of MAVS

Aim 3b: Assess the effectiveness of mitochondrial isolation techniques

1.7 Impact and Outcome

Most of the current MI treatments do not address mitochondria-specific pathways and/or metabolic-specific mechanisms in cardiomyocytes post-injury. This can potentially have short-term benefits, such as relief of stunning, and long-term benefits of better-preserved cardiac function. This project will introduce preliminary evidence and provide novel insight into the potential use of mitochondrial-based interventions as cardiovascular therapeutic targets. Additionally, this research will confer further understanding of the noncanonical roles of MAVS in myocardial infarction.

2 MATERIALS AND METHODS

2.1 Mice strains and LAD ligation model of Myocardial Infarction

Mavs-deficient (*Mavs*$^{-/-}$) with a B6129S52/J genetic background and wild-type (WT) control B6129SF2/J littermates were purchased from Jackson Laboratory. *Mavs*$^{-/-}$ and WT mice were verified following ear notch and subsequent DNA analysis by polymerase chain reaction analysis. Animals were housed in identical conditions, with food and water provided, at the Animal Resource Centre of the University of Ottawa Heart Institute. Experimental protocol HIe#3727 was approved by the Animal Care and Use Committee of the University of Ottawa Heart Institute and performed in accordance with the institutional guidelines.

Male *Mavs*$^{-/-}$ and WT mice (18-20 weeks old) with a body weight of approximately 31g were randomly assigned to either control (sham operation) or myocardial infarction (permanent LAD ligation). Female *Mavs*$^{-/-}$ and WT cohorts (18-20 week-old) with body weight of approximately 25g were similarly randomized. In brief, mice were anesthetized with an appropriate amount of isoflurane, relative to their body weight (~2%) using an induction chamber. A left-sided thoracotomy was performed between the 3rd and 4th rib to open the thorax and locate the heart. Using an 8-0 Prolene suture, the LAD, located between the pulmonary artery and the left auricle, was permanently ligated proximally. Cardiac blanching served as a preliminary indicator of a successful ligation. The thoracic incisions and skin were closed in layers, and the mice were kept on heating pads to recover until responsive to stimuli. Sham-operated mice underwent an identical procedure, except that the LAD ligation was not placed. At the end point, mice were anesthetized using CO2 inhalation, and tissues were

collected at 3 days to assess molecular and inflammatory dynamics and 4 weeks to assess cardiac function and remodelling.

2.2 Measurement of Cardiac Function in Mice

Transthoracic echocardiography was used to assess cardiac function at baseline and 4 weeks post-MI. Specifically, parasternal long axis (PLAX), electrocardiogram-gated kilohertz visualization (EkV), and motion mode (M-mode) images were acquired using the Vevo 3100 imaging system (FUJIFILM VisualSonics). A 40-MHz transducer was used for imaging. Vevo LAB analytic software (FUJIFILM VisualSonics) was used for all qualitative and quantitative measurements. Mice were anesthetized with 1–2% (per liter of O_2) isoflurane during recording acquisition. Systolic function (Left Ventricular Ejection Fraction (LVEF) and stroke volume (SV)) was estimated by two-dimensional area measurements of the endocardial wall at systole and diastole using long-axial electrocardiogram-gated kilohertz visualization (EKV) image analysis. LVEF was calculated as a measure of systolic function.

2.3 Histology and Immunocytochemistry

For morphometry, after arrest in diastole with a 10% potassium chloride solution, heart tissues were fixed with 4% paraformaldehyde solution in PBS (Thermo Fisher Scientific, AAJ19943K2), embedded in paraffin, and sectioned to a thickness of 5μm. Alexa Fluor 488-conjugated WGA-stained (1 μg ml^{-1}; Thermo Fisher Scientific, W11261) sections were used for measurement of heart morphology, and cardiomyocyte cross-sectional areas were measured using FV10-ASW4.2 Viewer software (Olympus). Nuclei were stained with Hoechst 33342 (1 μg ml^{-1}; Thermo Fisher Scientific, WH21492). After calibrating images to

convert pixels to micrometers, CSA was measured using trace and area measurement tools in Image J. Sections were also stained with either hematoxylin-eosin (HE) for histopathology or picrosirius red (PSR) for the collagen deposition. Infarct and border zone fibrosis were quantified using colour deconvolution and "analyze particles" functions in Image J. All histology was performed for a minimum of 3 technical replicates and 3 biological replicates. All section images were acquired using either a Leica Aperio VERSA 8 pathology slide scanner for both brightfield and fluorescent applications or a Zeiss Elyra S.1 LSM 880 Airyscan for confocal microscope.

For immunofluorescent staining, AC16 cells were incubated in MitoTracker Red CMSRos (Thermo Fisher Scientific, M7512) as per manufacturer recommendations, fixed with 4% paraformaldehyde in PBS (Thermo Fisher Scientific, AAJ19943K2), and permeabilized with 0.1% Triton X-100 (Thermo Fisher Scientific, BP151-100) in PBS. After blocking with 10% fetal bovine serum (Thermo Fisher Scientific, 12483020) in PBS for 30 minutes at room temperature, anti-MAVS (Thermo Fisher Scientific, PA5-17256, 1:50) was used for staining. After overnight incubation with primary antibody, the sections were incubated with a matching Alexa Fluor dye-conjugated secondary antibody (Thermo Fisher Scientific, A32731, 1:1,000) at room temperature for 1 hour, followed by nuclear stain with Hoechst 33342 (1 $\mu g\,ml^{-1}$) (Thermo Fisher Scientific, WH21492) at room temperature for 10 minutes and were mounted with ProLong Gold Antifade Mountant (Thermo Fisher Scientific, P36930).

2.4 qRT-PCR

RNA was isolated from mouse heart tissues using TRIzol reagent (Thermo Fisher Scientific, 15596026) and from cultured cells using PureLink RNA Mini Kit (Thermo Fisher Scientific, 12183018A). RNA concentrations were quantified using spectrophotometry, Thermo Scientific NanoDrop 8000 (Thermo Fisher Scientific). cDNA was synthesized from 1 μg of total RNA with either iScript Reverse Transcription Supermix for RT–PCR (Bio-Rad, 170-8841) or 5× All-In-One RT MasterMix with AccuRT (abm, G592). qRT–PCR was carried out using BrightGreen RTqPCR MasterMix (abm, MasterMix-S) or PowerUp SYBR Green Master Mix (Thermo Fisher Scientific, A25918) in Hard-Shell 96-well PCR plates (Bio-Rad, HSR9905K) on a LightCycler 96 System (Roche Life Science, 05815916001). Target gene-specific intro-spanning forward and reverse primers were designed by primer3 and BLAST using the NCBI Primer-BLAST tool (https://www.ncbi.nlm.nih.gov/tools/primer-blast/index.cgi?LINK_LOC=BlastHome). To minimize the effect of genomic DNA contamination, if possible, primer pairs were designed to always be separated by at least one intron on the corresponding genomic DNA. Primer sequences used for qRT–PCR are listed in **Supplementary Table 1**. All reactions were run in triplicate; gene expressions were normalized to HPRT1 (hypoxanthine-guanine phosphoribosyltransferase 1) and/or GAPDH (glyceraldehyde 3-phosphate dehydrogenase) housekeeping genes; and the results are shown as fold change against control.

2.5 Statistics and Reproducibility

Statistical analyses for all data were conducted using GraphPad Prism version 9 (GraphPad Software). For continuous variables, the summary data are presented as mean ±

SEM, and overall *P* values were calculated using ANOVA with Bonferroni correction for multiple comparisons, where applicable. Unpaired two-tailed Student's *t*-tests were used to compare two groups of continuous variables. Details of the statistical tests used are indicated in the respective figure legends. All values are presented as mean ± s.e.m.; *n* refers to the sample size. $P < 0.05$ was considered statistically significant.

3 RESULTS

3.1 4-WEEK POST MI: REMODELLING OUTCOMES

3.1.1 Male Mavs$^{-/-}$ mice display preserved heart and lung weight 4-weeks post MI

As a preliminary indication of organ damage/remodelling, body and organ weights (heart, lung, spleen) were acquired at the time of tissue collection, four weeks post MI, and normalized to tibia length. Four weeks post MI, Male *Mavs*$^{-/-}$ sham body weight was significantly lower compared to their WT controls ($p<0.0188$). No other significant body weight differences were observed among male cohorts (**Figure 3.1A**). WT male mice exhibit increased heart weight normalized to tibia length 4 weeks post-MI ($p<0.0220$). Male *Mavs*$^{-/-}$ mice did not display this increase, with normalized heart weight of the post-MI *Mavs*$^{-/-}$ mice significantly less than their WT MI controls ($p<0.004$) (**Figure 3.1B**). WT male mice exhibit increased lung weight normalized to tibia length 4-weeks post-MI ($p<0.0013$). Male *Mavs*$^{-/-}$ mice did not display this increase, with *Mavs*$^{-/-}$ post-MI lung weight normalized to tibia length significantly less than their WT MI controls ($p<0.0019$) (**Figure 3.1C**). Male spleen weight normalized to tibia length was lower for *Mavs*$^{-/-}$ shams compared to WT sham controls

($p<0.0075$). Additionally, male *Mavs*$^{-/-}$ mice that had undergone MI surgery were associated with significantly reduced spleen weight compared to their sham controls ($p<0.0259$) and WT post-MI controls ($p<0.0001$) (**Figure 3.1D**). No significant differences in body weights or heart weights were noted within female cohorts (**Figure 3.1E/F**). Decreased lung weight was observed in Female *Mavs*$^{-/-}$ sham mice compared to WT shams ($p<0.0061$) (**Figure 3.1G**). Female *Mavs*$^{-/-}$ sham mice displayed decreased spleen weight ($p<0.0008$) compared to WT sham controls. Female *Mavs*$^{-/-}$ MI mice exhibited significantly decreased spleen weight ($p<0.0001$) compared to WT MI controls (**Figure 3.1H**). All male and female cohorts showed no significant differences between baseline body weight and post-sham or MI procedure body weight (**Figure S5**). Overall, these findings indicate preservation of heart and lung weights normalized to tibia length in male *Mavs*$^{-/-}$ mice post MI, suggesting at least partial protection from hypertrophic remodeling and HF-related pulmonary edema, respectively. However, these findings are not replicated in female cohorts – indicating sex-based differences in these models, subject to modest degrees of injury.

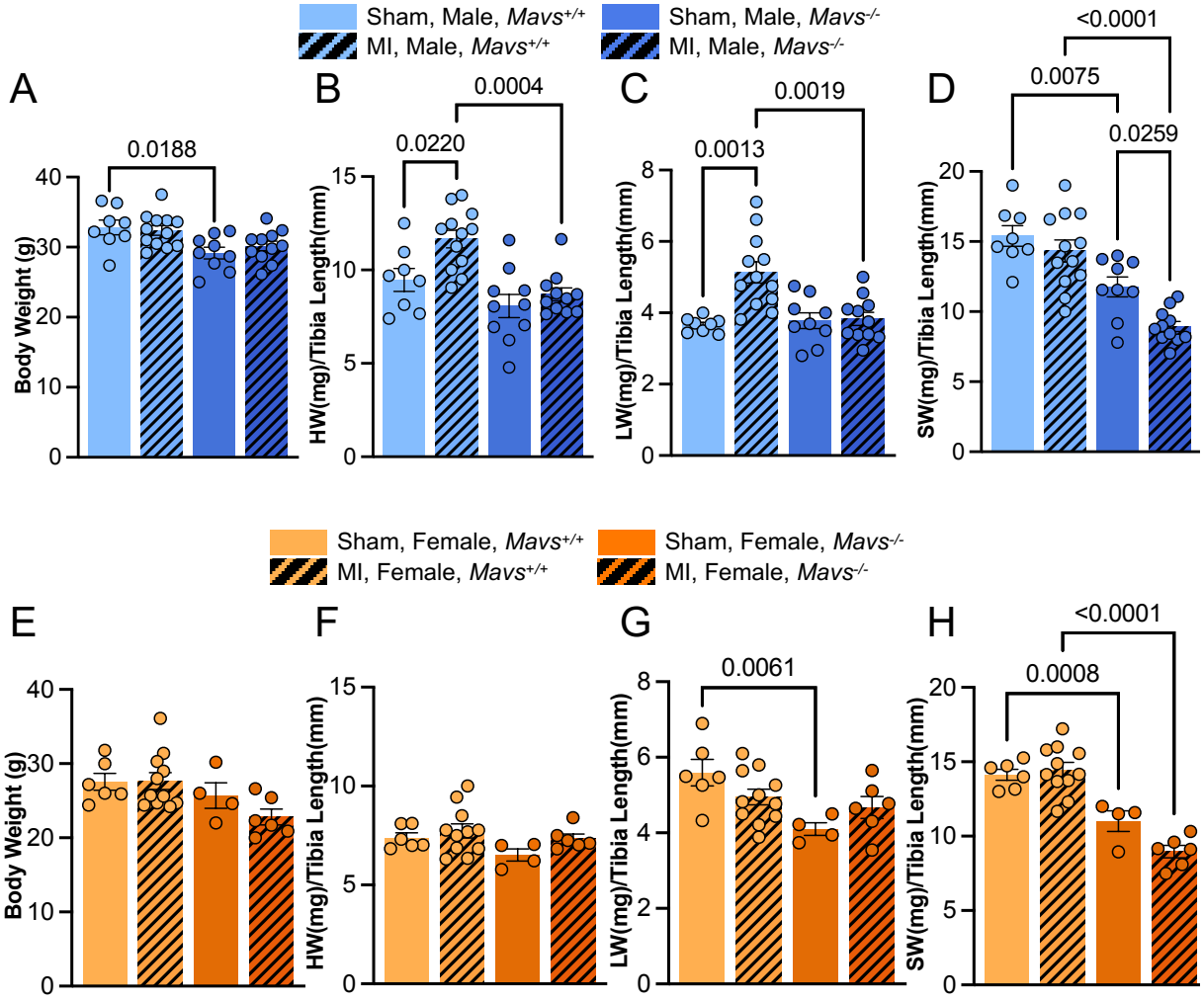

Figure 3.1 Male *Mavs*$^{-/-}$ mice display no change in normalized heart weight or lung weight 4 weeks post-MI compared to WT mice who display increases. Body weight, and organ weights (heart, lung, spleen) normalized to tibia length for males (**A, B, C, D**) and females (**E, F, G, H**), respectively. Male: WT Sham n=8, WT MI n=12, *Mavs*$^{-/-}$ Sham n= 9, *Mavs*$^{-/-}$ MI n=11; Female: WT Sham n=6, WT MI = 11, *Mavs*$^{-/-}$ Sham n=4, *Mavs*$^{-/-}$ MI n=6. All values are presented as mean ± s.e.m.; n refers to the sample size. $P < 0.05$ was considered statistically significant. P values were calculated using ANOVA with Bonferroni correction.

3.1.2 Left Ventricular Ejection fraction is preserved in Male Mavs$^{-/-}$ mice 4-weeks post MI

As a measure of ventricular contractile function, LVEF was used. Male WT mice presented with a mean LVEF reduction of 22.08% 4-weeks post MI compared to their sham controls ($p<0.0182$) (**Figure 3.2A**). Male *Mavs*$^{-/-}$ mice presented with a smaller mean LVEF reduction of 15.06% 4-weeks post MI compared to their sham controls ($p<0.0391$) (**Figure 3.2A**). Female WT mice display no statistically significant LVEF reduction 4-weeks post MI compared to their sham controls (**Figure 3.2B**). However, female *Mavs*$^{-/-}$ mice display a mean LVEF reduction of 24.76% 4-weeks post MI compared to their sham controls ($p<0.0104$) (**Figure 3.2B**). Overall, these results indicate that cardiac function is partially preserved in male *Mavs* deficient mice post-MI compared to WT controls. Interestingly, this result is not observed in female mice, again suggesting that Mavs possibly functions in a sex-dependent manner in the post-MI context.

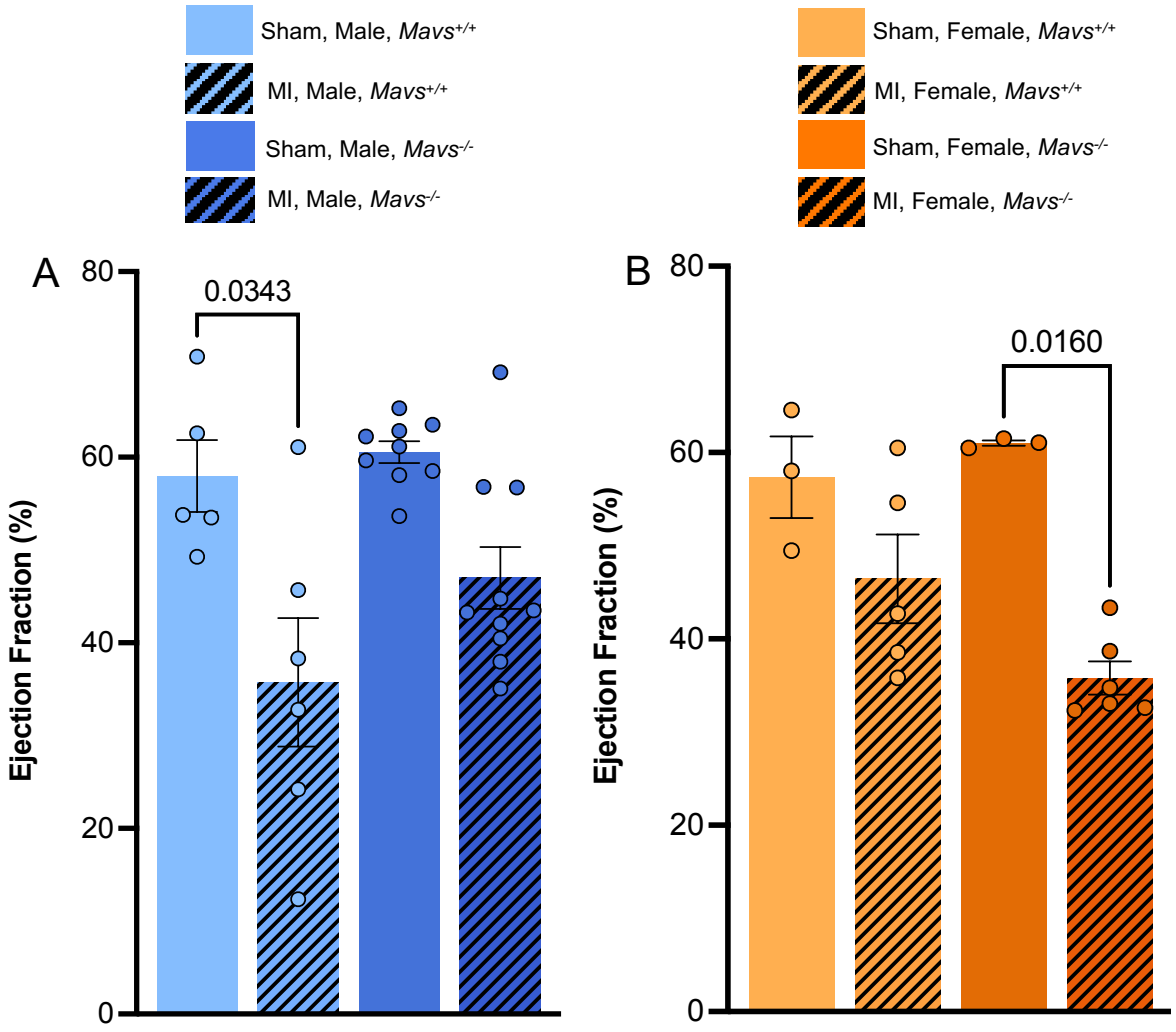

Figure 3.2 Male *Mavs*$^{-/-}$ mice are protected from reductions in left ventricular ejection fraction (%) 4 weeks post MI, compared to WT controls. Females display an opposite trend. (**A**) LVEF calculated using LV trace from echocardiography, for male mice 4 weeks post MI. (**B**) LVEF was calculated from using LV trace from echocardiography, for female mice 4 weeks post MI. Male: WT Sham n=5, WT MI n=6, *Mavs*$^{-/-}$ Sham n= 9, *Mavs*$^{-/-}$ MI n=10; Female: WT Sham n=3, WT MI=5, *Mavs*$^{-/-}$ Sham n=5, *Mavs*$^{-/-}$ MI n=5. All values are presented as mean ± s.e.m.; n refers to the sample size. $P < 0.05$ was considered statistically significant. P values were calculated using ANOVA with Bonferroni correction.

3.1.3 Mavs$^{-/-}$ heart sizes were significantly smaller compared to their WT controls

Male MI and sham *Mavs*$^{-/-}$ mice heart sizes when significantly smaller compared to WT MI and sham controls (**Figure 3.3A**), whereas no significant size differences were noted among female cohorts (**Figure 3.3B**). When comparing like regions, similar degrees of myocyte loss, granulation tissue with formation of microvessels, fibroblast proliferation, and early collagen deposition can be observed in 4-week post-MI tissues compared to their WT MI controls (**Figure 3.3A/B**).

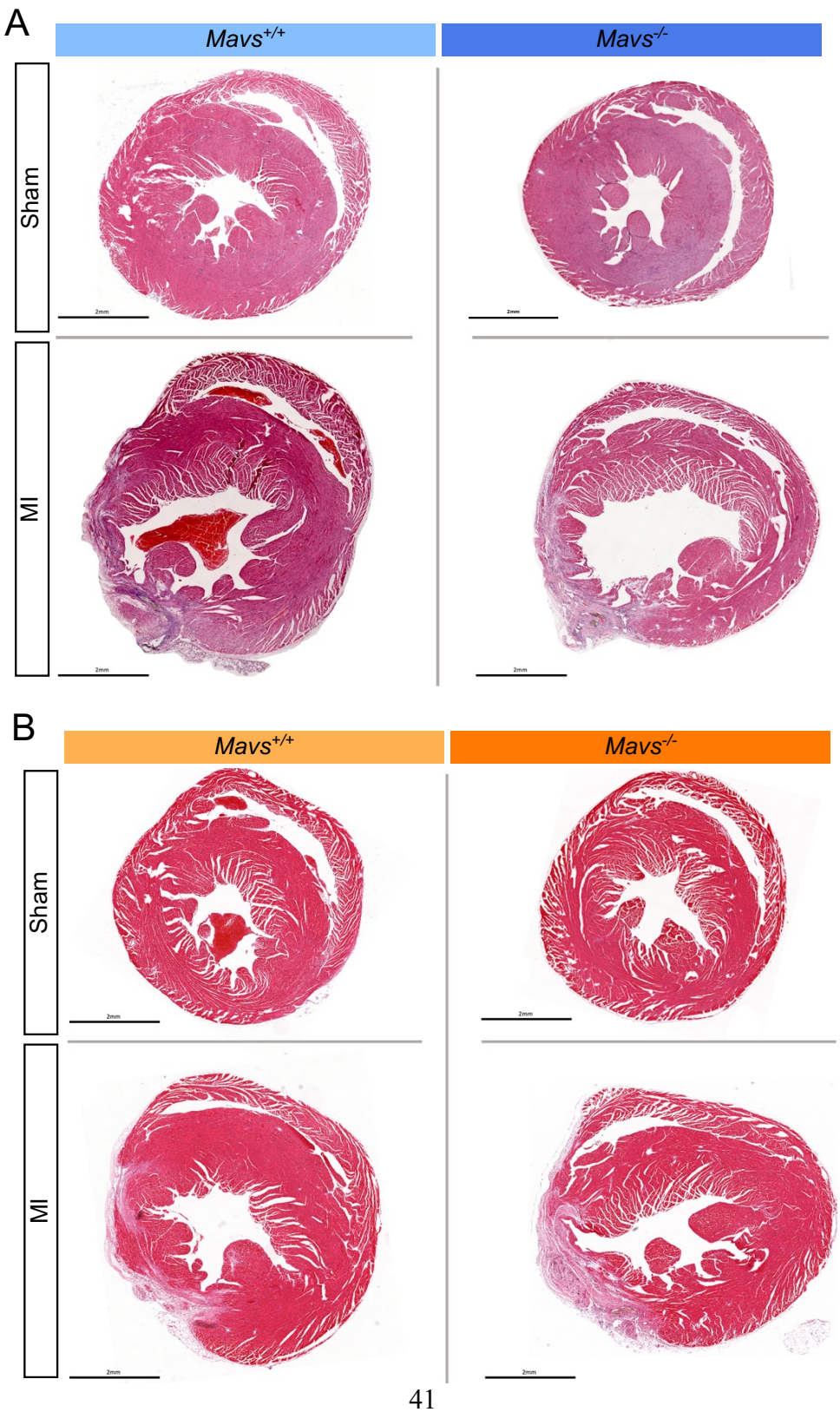
A
Mavs+/+
Mavs-/-
Sham
MI
B
Mavs+/+
Mavs-/-
Sham
MI

Figure 3.3 Male and female *Mavs*$^{-/-}$ mice have smaller hearts and display reduced wall thickness 4-weeks post MI compared to their WT controls. Representative images of hematoxylin and eosin-stained 5μm paraffin cross sections taken from the infarct zone of 4-week post-MI and sham-operated *Mavs*$^{-/-}$ and WT mouse hearts for both sexes (**A**) males (**B**) females. Scale bars, 2mm.

3.1.4 Mavs deficiency protects male and female mice from cardiomyocyte hypertrophy

As a more comprehensive assessment of cellular hypertrophy, cell membrane labeling using wheat germ assay (WGA) confirms that both male and female *Mavs* deficient mice exhibit smaller cardiac myocyte cross-sectional area (CSA) in the area at risk 4-weeks post MI compared to WT mice (**Figure 3.4A/C**). In WT male mice, CSA is significantly larger 4-weeks post MI compared to sham ($p<0.0238$) but not in *Mavs* deficient mice (**Figure 3.4B**). Likewise, CSA is significantly larger 4-weeks post MI compared to sham in WT female mice ($p<0.0270$) but not in *Mavs* deficient mice (**Figure 3.4D**). Overall, WGA staining indicates that both male and female *Mavs*$^{-/-}$ mice are protected from post-MI induced myocyte hypertrophic remodelling.

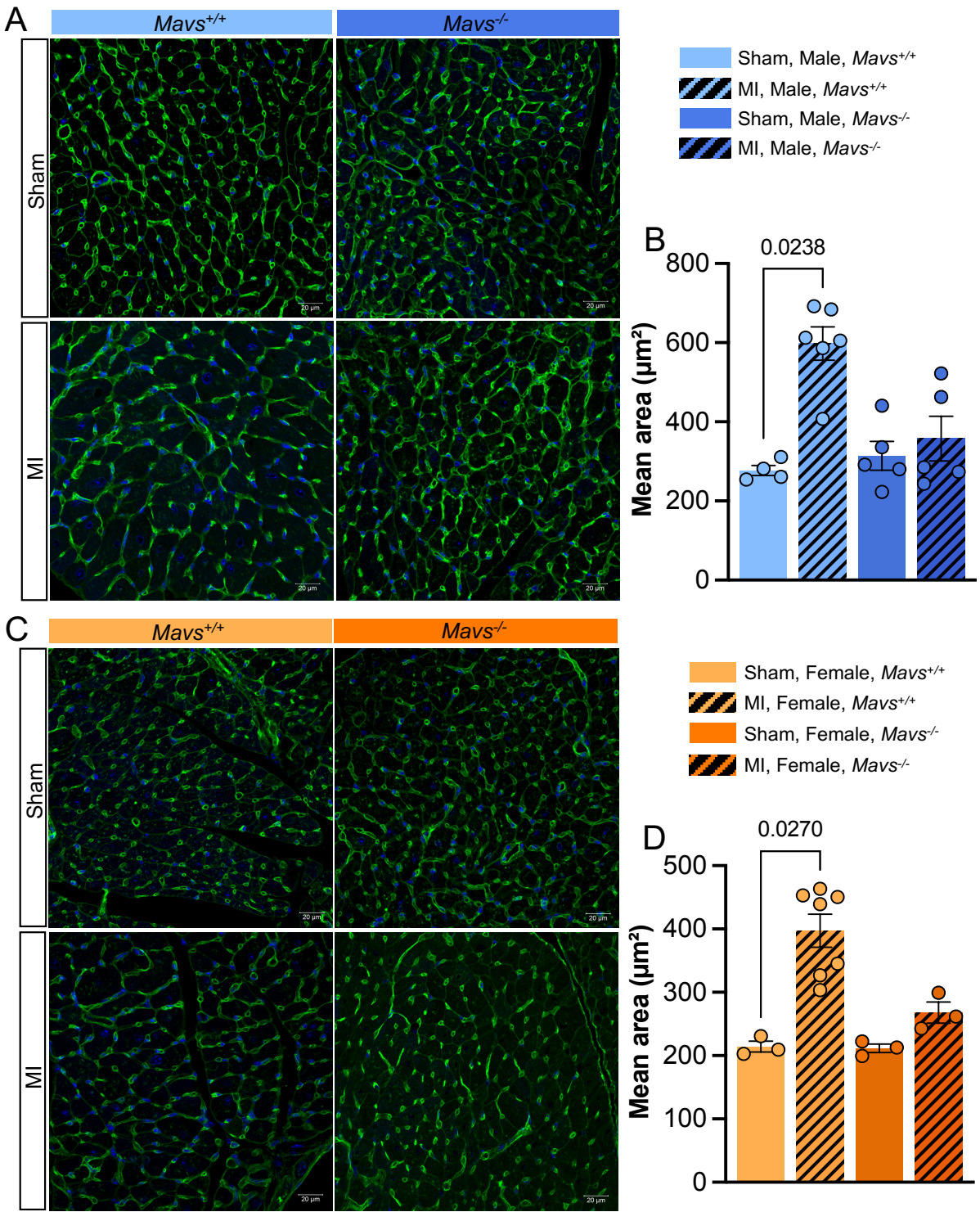
A
Mavs+/+
Mavs-/-
Sham
MI
Sham, Male, Mavs+/+
MI, Male, Mavs+/+
Sham, Male, Mavs-/-
MI, Male, Mavs-/-
B
0.0238
Mean area (µm²)
800
600
400
200
0
C
Mavs+/+
Mavs-/-
Sham
MI
Sham, Female, Mavs+/+
MI, Female, Mavs+/+
Sham, Female, Mavs-/-
MI, Female, Mavs-/-
D
0.0270
Mean area (µm²)
500
400
300
200
100
0

Figure 3.4 Both male and female *Mavs*$^{-/-}$ mice exhibit less cellular hypertrophy 4-weeks post-MI. (A) Wheat Germ Assay staining of 5μm thick paraffin heart cross sections acquired from male WT and *Mavs*$^{-/-}$ mice 4-week post MI and sham with **(B)** calculated mean cell area (μm^2). **(C)** Wheat Germ Assay staining of 5μm thick paraffin heart cross sections acquired from female WT and Mavs-/- mice 4-week post MI and sham with **(D)** calculated mean cell area (μm2). Scale bars, 20μm. Male: WT Sham n=4, WT MI n=6, *Mavs*$^{-/-}$ Sham n= 5, *Mavs*$^{-/-}$ MI n=5; Female: WT Sham n=3, WT MI = 7, *Mavs*$^{-/-}$ Sham n=3, *Mavs*$^{-/-}$ MI n=3. All values are presented as mean ± s.e.m.; n refers to the sample size. $P < 0.05$ was considered statistically significant. P values were calculated using ANOVA with Bonferroni correction.

3.1.5 Increased fibrosis is observed in Male Mavs deficient mice 4-weeks post MI

Male *Mavs*$^{-/-}$ hearts are visually smaller than WTs (**Figure 3.5A**). As indicated by PSR staining and scar area quantification, male *Mavs* deficient mice present with significantly larger scar areas/whole heart area (%) compared to their WT controls 4-weeks post-MI ($p<0.0018$) (**Figure 3.5B**). Female hearts of all cohorts are relatively uniform in size (**Figure 3.5C**) and display no significant differences when comparing scar area between post-MI cohorts (**Figure 3.5D**). Since cardiac hypertrophy is commonly associated with cardiac fibrosis, WGA results (**Figure 3.4**) and PSR results (**Figure 3.5**) are seemingly contradictory. However, fibrometabolism is still an emerging area of research, and since MAVS has been implicated in metabolic control, MAVS may function as a key regulator of this fibrometabolic switch[158]. Further molecular and mitochondrial dynamic studies will be required to validate this hypothesis.

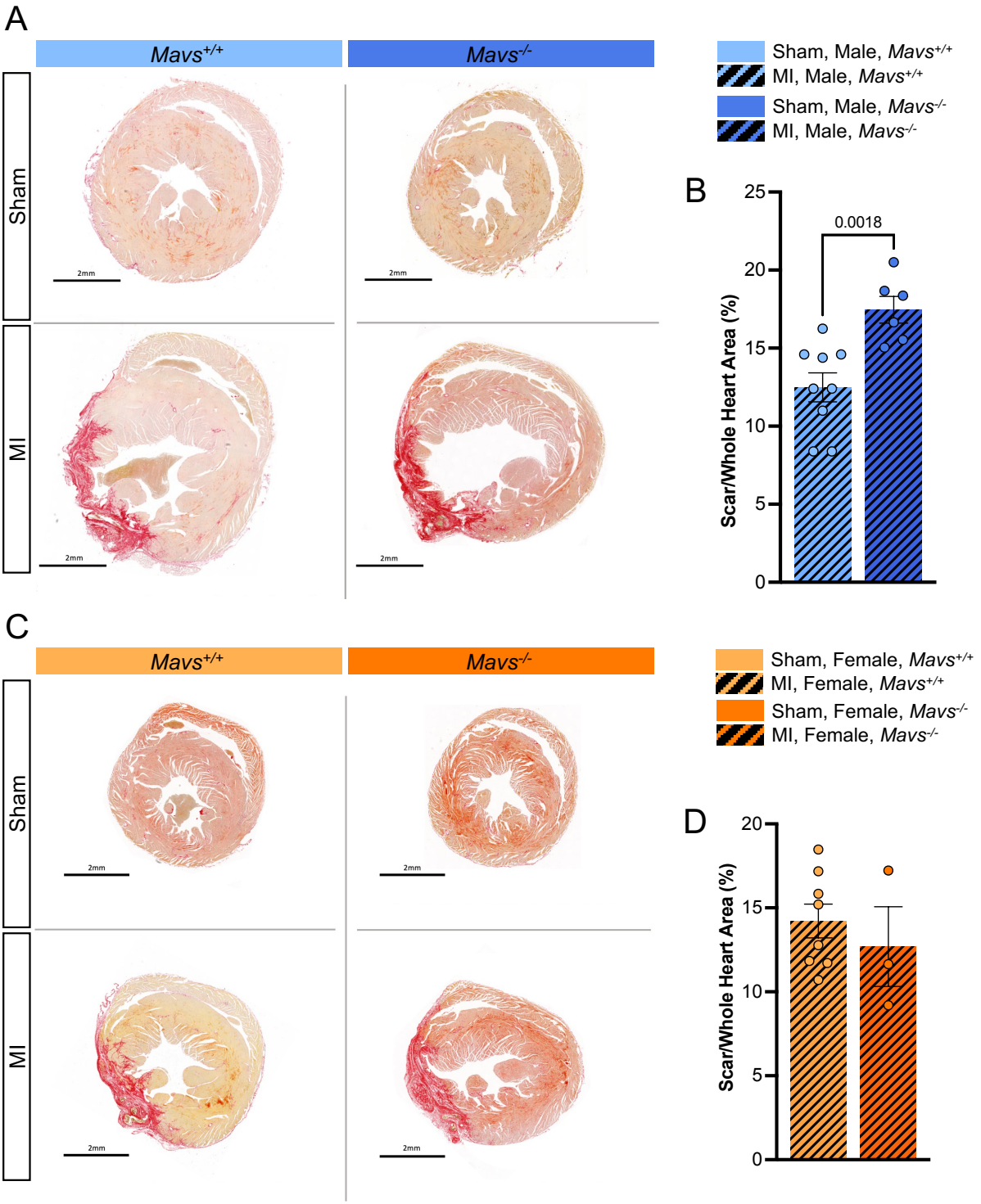
A
Mavs+/+
Mavs-/-
Sham
MI
2mm
Sham, Male, Mavs+/+
MI, Male, Mavs+/+
Sham, Male, Mavs-/-
MI, Male, Mavs-/-
B
0.0018
Scar/Whole Heart Area (%)
25
20
15
10
5
0
C
Mavs+/+
Mavs-/-
Sham
MI
2mm
Sham, Female, Mavs+/+
MI, Female, Mavs+/+
Sham, Female, Mavs-/-
MI, Female, Mavs-/-
D
Scar/Whole Heart Area (%)
20
15
10
5
0

Figure 3.5 Male *Mavs*$^{-/-}$ mice exhibit increased scar/whole heart area (%) 4-weeks post-MI. Females do not display this same difference. (A) Picrosirius red (PSR) staining of 5μm-thick paraffin heart cross sections acquired from male WT and *Mavs*$^{-/-}$ mice 4-week post MI and sham with **(B)** calculated scar/whole heart area (%). **(C)** Picrosirius red (PSR) staining of 5µm thick paraffin heart cross sections acquired from female WT and Mavs-/- mice 4-week post MI and sham with **(D)** calculated scar/whole heart area (%). Scale bars, 50mm. Male: WT Sham n=4, WT MI n=6, *Mavs*$^{-/-}$ Sham n= 5, *Mavs*$^{-/-}$ MI n=5; Female: WT Sham n=3, WT MI = 7, *Mavs*$^{-/-}$ Sham n=3, *Mavs*$^{-/-}$ MI n=3. All values are presented as mean ± s.e.m.; n refers to the sample size. $P < 0.05$ was considered statistically significant. P values were calculated using ANOVA with Bonferroni correction.

3.1.6 Mavs deficient male mice show reduced heart failure biomarkers

RTqPCR was used to assess gene expression changes between male *Mavs*$^{-/-}$ and WT mice. No significant differences in the expression of *Col3α*, *Myh7,* and *Tgfβ* were noted between cohorts (**Figure 3.6A/B/C**). A statistically significant increase in the expression of *Ctgf* is noted in WT ($p<0.0298$) but not in the *Mavs*$^{-/-}$ MI cohorts when compared to their respective sham controls (**Figure 3.6D**). A trending decrease in *Pgc1α* expression is noted in WT MI mice, but not in *Mavs*$^{-/-}$ mice (**Figure 3.6E**). *Mavs* expression is not significantly but notably lower 4 weeks post MI in WT mice (**Figure 3.6F**) and effectively absent in *Mavs*$^{-/-}$ mice (**Figure S4B**). Heart failure markers *Anp* ($p<0.0177$) and *Bnp* ($p<0.0479$) are significantly increased in WT mice 4 weeks post MI but not in *Mavs*$^{-/-}$ mice (**Figure 3.6G/H**). *Mavs*$^{-/-}$ MI mice display significantly lower *Anp* ($p<0.0485$) and *Bnp* ($p<0.0380$) levels when compared to WT MI mice (**Figure 3.6G/H**). WT mice have significantly increased levels of *Igfbp7* expression ($p<0.0317$) 4 weeks post MI, whereas *Mavs*$^{-/-}$ mice do not (**Figure 3.6I**). No notable *IL-6* expression differences were observed between cohorts (**Figure 3.6J**). Most notably, reduced levels of HF biomarkers *Anp*, *Bnp,* and senescence marker *Igfbp7* suggest that male *Mavs*$^{-/-}$ mice are less susceptible to developing MI-induced HF. Additionally, although not significant due to low mouse numbers, a trend towards an increase in IL-6 and Col3a was observed in *Mavs*-/- post MI mice. This, in combination with no increase in CTGF in *Mavs*-/- post MI mice, suggests that there is an imbalance of immune response in the absence of *Mavs* in the post MI setting, driving fibrosis.

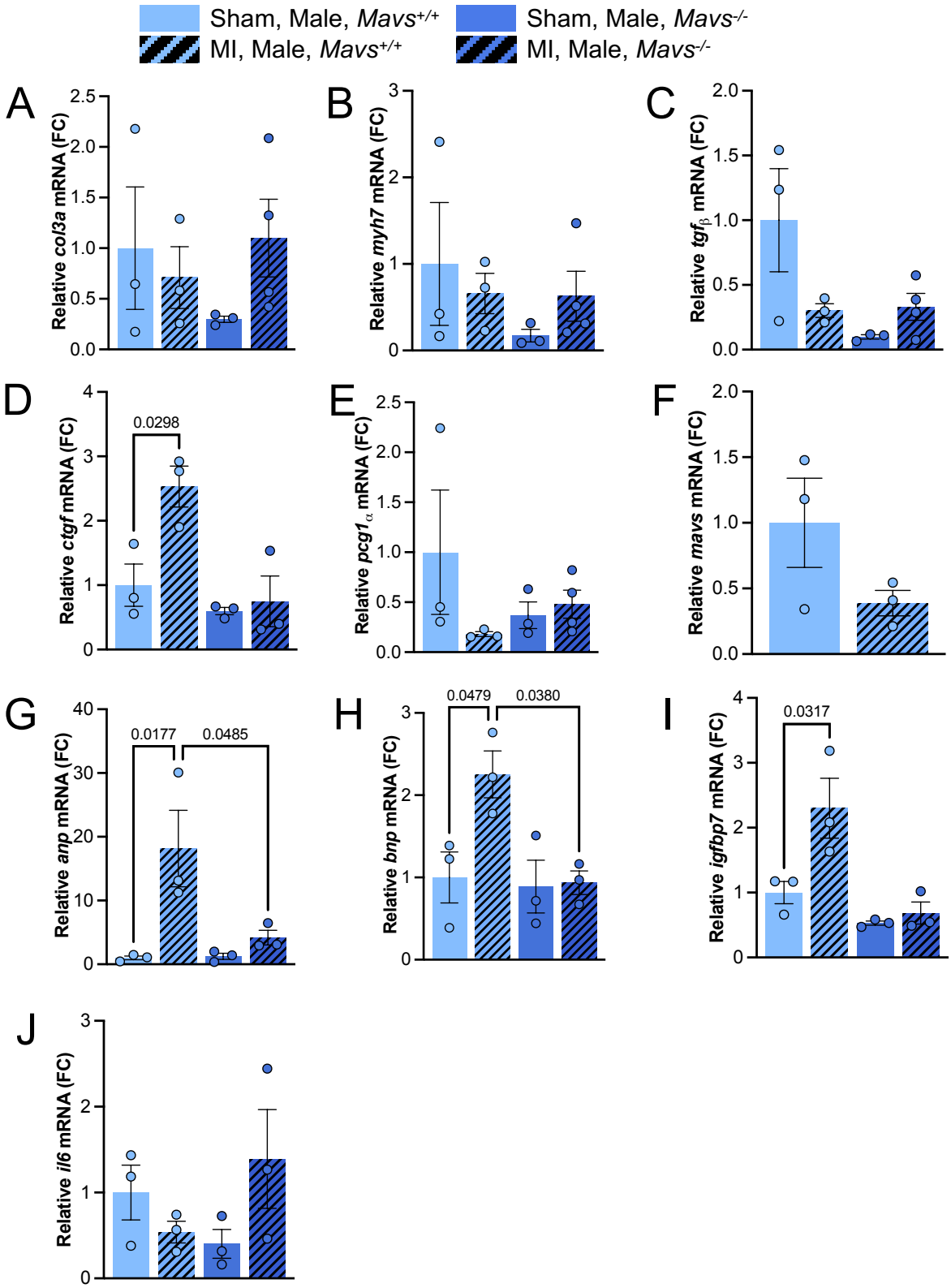
Sham, Male, Mavs+/+
MI, Male, Mavs+/+
Sham, Male, Mavs-/-
MI, Male, Mavs-/-
A
Relative col3a mRNA (FC)
B
Relative myh7 mRNA (FC)
C
Relative tgfβ mRNA (FC)
D
Relative ctgf mRNA (FC)
0.0298
E
Relative pcg1α mRNA (FC)
F
Relative mavs mRNA (FC)
G
Relative anp mRNA (FC)
0.0177
0.0485
H
Relative bnp mRNA (FC)
0.0479
0.0380
I
Relative igfbp7 mRNA (FC)
0.0317
J
Relative il6 mRNA (FC)

Figure 3.6 Gene expression profiles of male WT and *Mavs*$^{-/-}$ cardiac tissue 4-week post MI or Sham operations. mRNA expression levels of cardiac remodeling markers (A) *Col3α,* (B) *Myh7,* (C) *Tgfβ,* (D) *Ctgf*; (E) biogenesis regulator *Pcg1α*; (F) signal transduction molecule *Mavs*, heart failure markers (G) Anp, (H) Bnp; (I) senescence marker *Igfbp7*; (J) inflammatory marker *Il6*. Male: WT Sham n=3, WT MI n=3, *Mavs*$^{-/-}$ Sham n=3, *Mavs*$^{-/-}$ MI n=3. All values are presented as mean ± s.e.m.; n refers to the sample size. $P < 0.05$ was considered statistically significant. P values were calculated using ANOVA with Bonferroni correction.

3.2 3-DAYS POST MI: INFLAMMATORY OUTCOMES

3.2.1 No notable gross heart structure differences 3 days post MI

No notable body weight differences were observed within male or female groups (**Figure 3.7B/G**). No anatomical differences were noted between WT and *Mavs*$^{-/-}$ mouse hearts (**Figure 3.7A/F**). Specifically, no differences in apex shape, ventricle size/shape, atrial size/shape, aorta curvature/anatomical position (**Figure 3.7A/F**). Male *Mavs*$^{-/-}$ sham and MI mice display significantly decreased normalized heart weights compared to WT controls (sham $p<0.0090$; MI $p<0.0208$) 3 days post-surgery (**Figure 3.7C**). Male *Mavs*$^{-/-}$ shams exhibit decreased normalized lung weights ($p<0.0124$) and spleen weights ($p<0.0151$) compared to WT controls (**Figure 3.7D/E**). Female *Mavs*$^{-/-}$ sham mice display decreased lung weight ($p<0.0094$) compared to WT controls (**Figure 3.7I**).

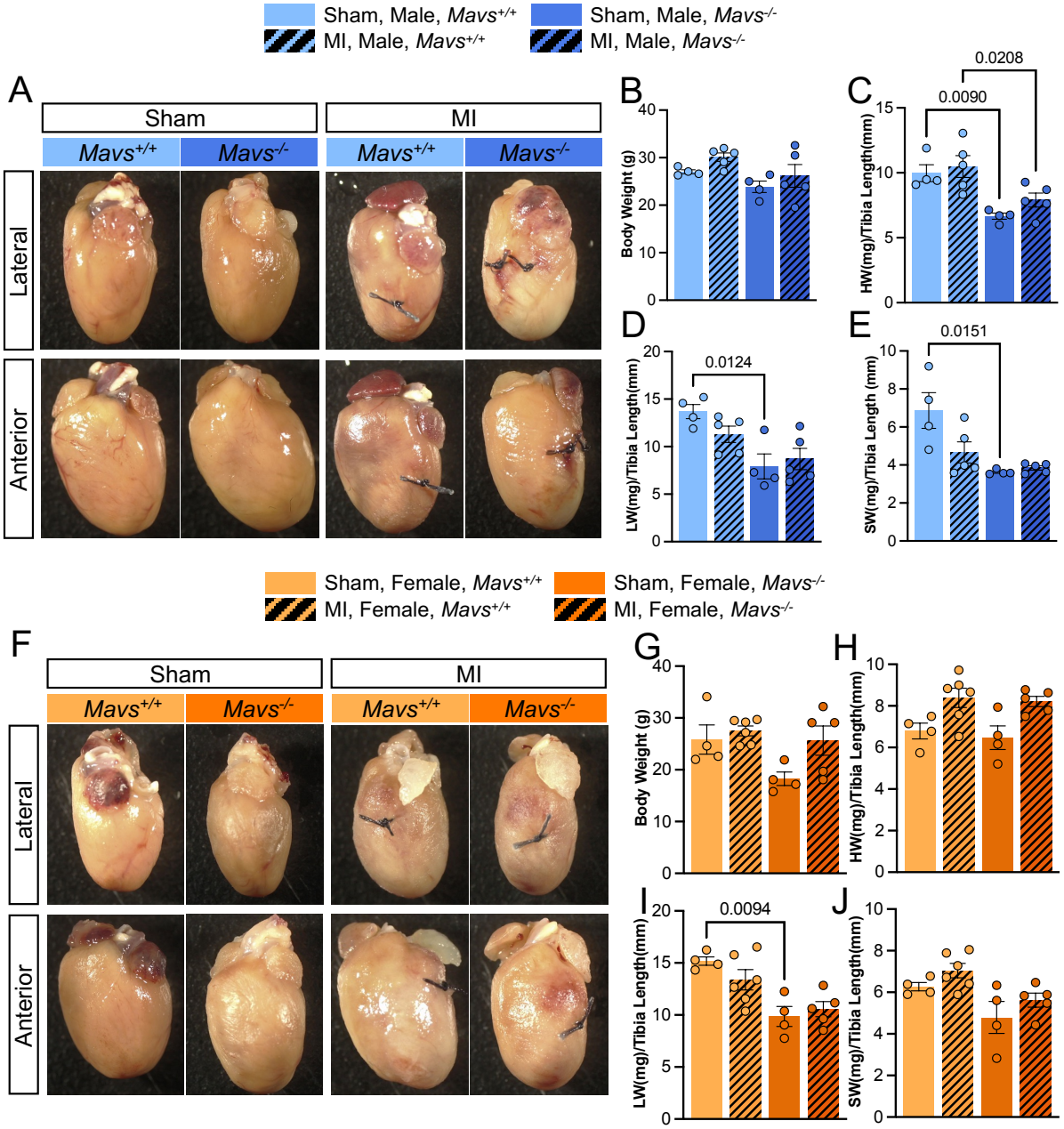

Figure 3.7 No notable structural differences observed within male and female cohorts 3 days post-MI. Representative lateral and anterior images of WT and *Mavs*$^{-/-}$ male (**A**) and female (**F**) mice whole hearts, 3-day post MI or Sham, taken from a dissecting microscope using Zeiss imaging software. Body weight, and organ weights (heart, lung, spleen) normalized to tibia length for males (**B, C, D, E**) and females (**G, H, I, J**), respectively. Male: WT Sham n=4, WT MI n=5, *Mavs*$^{-/-}$ Sham n= 4, *Mavs*$^{-/-}$ MI n=5; Female: WT Sham n=4, WT MI = 6, *Mavs*$^{-/-}$ Sham n=4, *Mavs*$^{-/-}$ MI n=5. All values are presented as mean ± s.e.m.; n refers to the sample size. $P < 0.05$ was considered statistically significant. P values were calculated using ANOVA with Bonferroni correction.

3.2.2 H&E staining shows LV wall thinning and loss of papillary muscle 3 days post MI in male Mavs$^{-/-}$ mice

When comparing whole heart images, *Mavs*$^{-/-}$ MI mice of both sexes, increased wall thinning and loss of papillary muscle in the left ventricle compared to their respective WT controls (**Figure 3.8A/B**). When comparing infarct zone regions, no significant differences are of note - similar degrees of myofibril waviness, diffused neutrophilic infiltration, and necrotic regions are noteworthy in both male and female cohorts (**Figure 3.8A/B**).

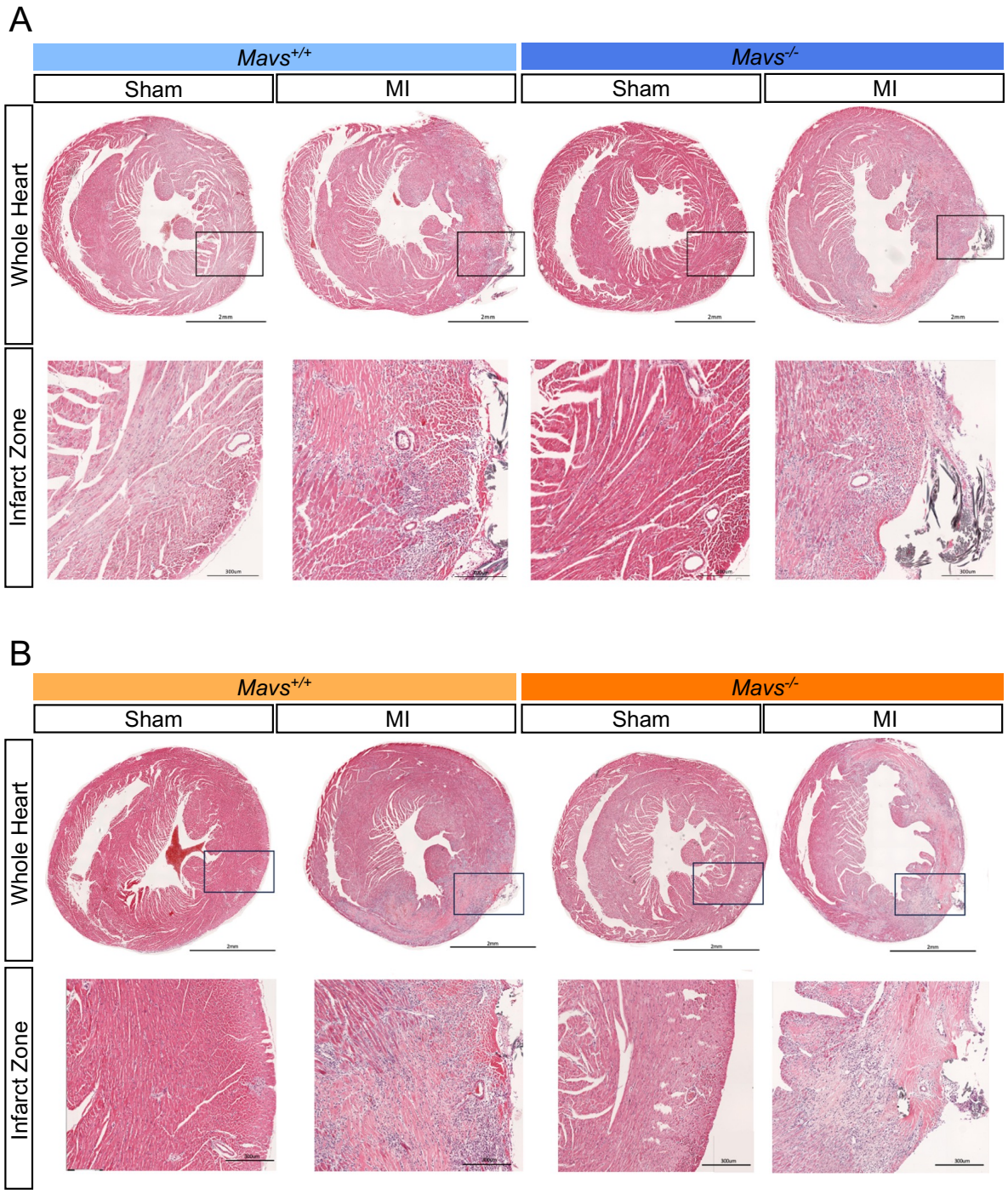

Figure 3.8 Male and female *Mavs*$^{-/-}$ mice display reduced wall thickness 3 days post MI compared to their WT controls. Representative images of Hematoxylin and eosin-stained 5μm paraffin cross sections taken from the infarct zone of 3-day post-MI and sham-operated *Mavs*$^{-/-}$ and WT mouse hearts, for both sexes. (**A**) male (**B**) female. Scale bars: Whole heart, 2mm and Infarct Zone, 300μm.

4 DISCUSSION AND FUTURE DIRECTIONS

4.1 DISCUSSION

4.1.1 Mavs deficiency may protect against MI-induced heart failure

4.1.1.1 Mavs deficiency is protective against MI-induced myocyte hypertrophic remodeling

WT male mice displayed increased, normalized heart weight compared to shams, indicating hypertrophic remodeling (**Figure 3.1B**). By extension, WGA staining and cardiac myocyte cross-sectional area quantification confirmed cellular hypertrophy in both male and female mice (**Figure 3.4A/B**). *Mavs*$^{-/-}$ mice did not display a significant heart weight increase, and WGA confirmed a lesser degree of cellular hypertrophy, suggesting that *Mavs* deficiency is protective against cardiac hypertrophy (**Figures 3.1A and 3.4A/B**)[28]. These results are in keeping with our lab's previous findings, where *Mavs* were recognized as a cardiac hypertrophy promoter, downstream of NOD1/RIP2[144]. The Nod1/Rip2/Mavs complex coordinated cardiac remodeling, inflammatory response, and mitochondrial energy metabolism in various in vitro and in vivo models of hypertrophic stress (TAC-operated mice and phenylephrine-treated cells)[144]. Notably, genetic knockout of *Mavs* protected mice from pressure overload-induced cardiac hypertrophic remodeling[144]. Therefore, the notable decrease in MI-induced cellular hypertrophy observed in this study provides further evidence that Mavs plays an integral role in coordinating hypertrophic remodeling in stressed cardiomyocytes.

To our knowledge, this study is the first to explore hypertrophic remodeling outcomes of *Mavs* deficient mice in a sex-dependent manner. Male mice displayed both global and

cellular reductions in hypertrophy, whereas female mice displayed no significant differences in normalized heart weight but did display similar trends in cellular hypertrophy (**Figures 3.1F and 3.4C/D**). This is in keeping with the sex-specific cardiac hypertrophy differences observed in the clinical setting[160,161]. In humans, women are more likely to develop concentric hypertrophy (increased LV wall thickness with maintenance of chamber size), whereas men are more likely to exhibit eccentric hypertrophy (LV dilation without an increase in LV wall thickness)[161,162]. Further mechanistic and anatomical studies will be required to conclusively confirm this theory; however, our current findings possibly reiterate this compelling sex-based difference. If proven, MAVS may show promise as a sex-specific therapeutic target and personalized treatment[163].

4.1.1.2 Mavs deficiency preserves LVEF, reduces lung congestion and heart failure biomarkers

In WT males, LVEF is significantly reduced after MI but not for *Mavs* deficient mice - indicating preservation of cardiac contractile function (**Figure 3.2A**). Other measures of contractile function, such as fractional shortening (%), showed trending, but insignificant differences that indicate preservation of contractile function in male *Mavs*$^{-/-}$ mice 4 weeks post MI (**Figure S6C**). However, these trends are not observed in females – instead, WT mice display no significant reduction post MI, but *Mavs*$^{-/-}$ mice do (**Figure 3.2B**). The LVEF differences observed in WT mice are in keeping with sex specific differences well characterized in the literature - following acute MI, females tend to have better preservation of systolic function and LVEF compared to males[164,165]. However, the underlying mechanisms that explain whether *Mavs* deficiency produces correlative or causative sex-specific

differences in LVEF (LVEF preservation in males, but reduction in females) require further study.

Pulmonary congestion is a well-known complication post MI, typically due to LV failure, and insufficient cardiac contraction results in a backflow of blood into the pulmonary vein and ultimately the lungs[166,167]. In our study, we used lung weight normalized to tibia length as a proxy measure of congestion and thus an indication of congestive heart failure. Specifically, our results show a significant increase in lung weight and thus potential pulmonary congestion in WT male, but not female mice, 4 weeks post MI (**Figure 3.1C/G**)[168]. Comparatively, no significant differences in lung weight for both male and female *Mavs*$^{-/-}$ mice (**Figure 3.1C/G**) suggest a potentially protective phenotype against cardiogenic pulmonary congestion. Future studies might consider conducting lung ultrasound as a more comprehensive assessment, allowing for a visual assessment of extravascular pulmonary edema[166].

Due to their high diagnostic accuracy, biomarkers Anp and Bnp are considered gold standard biomarkers for HF[169]. By extension, their blood concentrations are uniquely correlated with LV function and HF severity – making them useful for both diagnostic and prognostic purposes[170–172]. Male WT mice displayed significantly increased mRNA expression levels of HF biomarkers *anp* and *bnp* (**Figure 3.6G/H**). Comparatively, male *Mavs*$^{-/-}$ mice do not increase in *anp* or *bnp* mRNA expression (**Figure 3.6G/H**), suggesting that they are protected from developing MI-induced HF.

Taken together, preserved LVEF (**Figure 3.2A**), reduced HF biomarkers *Anp*/*Bnp* (**Figure 3.6G/H**), absence of cellular hypertrophy (**Figure 3.4**), and pulmonary congestion

(**Figure 3.1C/G**), are consistent with the conclusion that male *Mavs*$^{-/-}$ mice are better protected against adverse remodeling and the progression towards HF post MI[173]. Future research should work towards elucidating the molecular players that coordinate this response.

4.1.2 Mavs$^{-/-}$ *mice display sex-specific phenotypic differences*

4.1.2.1.1 Sex Specific Differences in Cardiac Remodeling

Sex-specific variations were to be expected throughout our experimental series, and disaggregating all experimental results by sex was necessary. It is well established that WT male mice show more pronounced maladaptive remodeling via greater ventricular dilation, hypertrophy, and a greater degree of reduction in cardiac function post MI compared to females[174]. In male mice, cardiac hypertrophy is associated with a steady decline in contractile function, whereas it is associated with contractile improvement and delayed decompensated HF in females[174]. This concept is consistent with clinical settings where differences in cardiac remodeling post-stress/injury in women are observed[175,176].

Our results indicate that both WT male and female mice show increased cellular hypertrophy and fibrosis post MI (**Figure 3.4/3.5**). However, unlike WT male mice, WT female mice show no significant reductions in LVEF post MI (**Figure 3.2**) or significant increases in heart and lung weights 4-weeks post MI (**Figure 3.1**). This combination of results is in keeping with the fact that cardiac hypertrophy in WT females is likely to be functionally adaptive and result in improved or lesser reductions in cardiac contractile function. These remodeling outcomes are largely different in *Mavs* deficient mice, in a sex-dependent manner. Most notably, male *Mavs*$^{-/-}$ mice displayed lesser reductions in LVEF, whereas females

displayed increased LVEF reductions post MI (**Figure 3.2**). Additionally, when compared to their WT MI controls, *Mavs*$^{-/-}$ male mice displayed lesser increases in heart and lung weights and increases in fibrosis, whereas females displayed no changes (**Figure 3.1/3.5**). This combination of results indicates that MAVS is essential in cardiac remodeling, but in a sex-dependent manner. Increasing sample sizes and more extensive molecular profiling of female mice will be required to elucidate mechanistic insights.

4.1.2.1.2 Potential Mechanisms of Interest

4.1.2.1.2.1 Sex-specific differences in mtDNA and mitochondrial function

Studies indicate that sex hormones are key determinants of mtDNA content – testosterone increases, and oestrogen decreases mtDNA content[177]. Additionally, males express higher levels of mitochondrial genes, including ETC genes[177]. Since MAVS aggregation can be triggered by the release of ROS and/or mtDNA, higher levels of mtDNA and ETC expression in males could contribute to the heightened MI responses[177].

Additionally, lower numbers of mitochondria, but higher oxidative capacity, are reported in female cardiomyocytes compared to males[178]. Females also display more effective mechanisms for regulating ROS, calcium handling, and mitochondrial membrane potential recovery[179,180]. In HFpEF, female hearts exhibit lower complex II and IV activity, reduced basal and maximal respiration levels[177]. Thus, females are better able to tolerate mitochondrial swelling, high ROS and Ca2+ concentrations, which are characteristic of ischemic conditions[177].

4.1.2.1.2.2 Sex Specific Differences in Mitochondrial Dynamics Proteins

As indicated by LC3B/LC3A ratio, females display significant increases in cardiac autophagy post MI[181]. Additionally, following muscle damage, expression of inner mitochondrial membrane fusion marker OPA1 increases in both sexes; whereas expression of mitophagy markers PINK1 and PRKN increases in females but reduces in males[182]. Taken together, this indicates that females are likely intrinsically predisposed to effectively removing damaged mitochondria, thus contributing to more effective cardiac remodelling post MI. Since PINK1 is indicated as a key regulator of MAVS aggregation, this sex difference may serve as an explanation for the intrinsic sex differences observed between male and female *Mavs*$^{-/-}$ mice.

4.1.3 MAVS may function as a key modulator of the fibrometabolic switch

Mavs$^{-/-}$ *males display a trending increase in cardiac fibrosis, and females show a trending decrease.* No significant differences are of note from H&E (**Figure 3.3A/B**). When comparing like regions, similar degrees of myocyte loss, granulation tissue with formation of microvessels, fibroblast proliferation, and early collagen deposition can be observed in 4-week post-MI tissues. When comparing PSR stains and quantifying scar area, significantly increased fibrosis is noted in *Mavs*$^{-/-}$ males, and a trending decrease in *Mavs*$^{-/-}$ females was noted (**Figure 3.5**). Since cardiac hypertrophy is commonly associated with cardiac fibrosis, male WGA results (**Figure 3.4A/B**) and male PSR results (**Figure 3.5A/B**) are seemingly contradictory. However, observations are consistent with the concept that absence of Mavs can lead to immune imbalance and drive male hearts forward fibrosis[158].

Since fibrosis is the final pathological outcome that follows many common chronic inflammatory, immune-mediated mediated and metabolic diseases such as myocardial infarction, therapies that target fibrotic processes have the potential to largely influence remodelling outcomes[158]. Recent research has identified key metabolic changes that drive fibrotic remodelling and, thus, introduced the concept of fibrometabolism[158,183,184]. Despite recent progress, many key molecular players in this process remain unelucidated. Our results show that *Mavs*$^{-/-}$ mice display a unique remodelling phenotype (increased fibrosis, decreased hypertrophy), thus providing preliminary evidence that MAVS may serve as a key molecular player in the fibrometabolic switch. By extension, based on complementary RNAseq data (http://www.protein-atlas.org/), MAVS is expressed in cardiac fibroblasts; thus, it is plausible that during post-MI cardiac remodeling, *Mavs*$^{-/-}$ may influence fibroblast activation/function and ultimately lead to disregulated fibrotic processes[143]. Further tissue/cell-specific, molecular, and mitochondrial dynamic studies will be required to validate this hypothesis.

Completing replicate PCR assays with different tissue samples and/or using different gene primer pairs to flank different target regions will further confirm our results. By extension, testing additional PCR markers can be used to further analyze autophagy (*PINK1/PRKN* expression and *LC3B II/I type marker protein ratio*[185]), fibrosis (ex., *Periostin, Collagen-1, Osteopontin, TGF-β1,2,3, MMP2,9,12*), inflammation (TNF, IL-1, IL-6, inflammasome components), and hypertrophy. Monitoring these markers will indicate the molecular difference in the long-term remodelling outcomes of *Mavs*$^{-/-}$ and WT mice cohorts. Finally, completing Western blots of these same markers will confirm the consistency of these results at the protein level. All experiments should then be repeated for female cohorts.

4.1.4 MAVS likely functions together with other mitochondrial control mechanisms

4.1.4.1 MAVS and metabolic substrate switching

MAVS has been identified for its involvement in mitochondrial energy metabolism. Knockdown of *Mavs* in neonatal mouse cardiomyocytes, treated with phenylephrine, restores high resting ATP production and spare respiratory capacity[144]. Additionally, *Mavs*$^{-/-}$ mice display higher myocardial glucose uptake after TAC surgery compared to WT mice[144]. Additional research identified that MAVS coordinates glucose metabolism reprogramming by activating the switch from glycolysis to the pentose phosphate pathways (PPP) and the hexosamine biosynthesis pathway (HBP)[186]. Mechanistically, peroxisomal MAVS promotes PPP and type III interferon (IFN) expression by interacting with G6PD to recruit TNF receptor-associated factor 6 (TRAF6) and interferon regulatory factor 1 (IRF1)[186]. Whereas MAM-located MAVS promotes HBP and type I IFN expression by interacting with glutamine-fructose-6-phosphate transaminase to recruit TRAF6 and TRAF2[186].

4.1.4.2 MAVS and mitophagy

MAVS likely plays a key role in regulating mitophagy. In fact, in vitro modelling indicates that in response to excessive RLR signaling, MAVS functions as a mitophagy receptor and can directly interact with LC3 through its LC3-binding motif 'Yxxl'[187]. By extension, *Mavs*$^{-/-}$ TAC mice displayed decreased levels of mitophagy compared to their controls, suggesting that MAVS does, in fact, function as a mitophagy receptor in vivo[144].

Among the most universally known UBS is PRKN-mediated mitophagy, where damaged organelles and protein aggregates are marked for selective autophagy[188,189]. In this pathway, PINK1 is stabilized on the mitochondrial membrane and phosphorylates ubiquitin,

recruiting E3 ubiquitin ligase, PRKN[190,191]. PRKN then constructs ubiquitin chains, flagging the protein aggregate or damaged organelle for degradation[190–192]. Since both MAVS and PINK1 reside on the mitochondrial surface, it is plausible that the PINK1/PRKN ubiquitin-proteasome system plays a key role in regulating both the formation and subsequent clearance of MAVS aggregates.

A recent viral immunology study has highlighted PRKN's ability to directly interact with/catalyse the K48-linked polyubiquitination and subsequent degradation of two RLRs (RIG-I and MDA5) upstream of MAVS, significantly reducing the amount of time innate antiviral immunity is overactive[193]. This study also notes that PRKN can interact with and construct unanchored linear polyubiquitin chains on MAVS[155]. However, they observed that overexpression or knockdown of PRKN did not affect endogenous levels of MAVS and MAVS aggregates[193]. Taken together, these findings suggest the necessary involvement of a second molecular player for recruiting PRKN, triggering PRKN-mediated mitophagy, and regulating MAVS aggregates.

PINK1 is also indispensable in maintaining mitochondrial quality control by regulating PRKN-mediated mitophagy and protecting against mitochondrial dysfunction[105,194–197]. In fact, PINK1 is crucial for maintaining mitochondrial function and myocardial health. A pivotal study indicated that *Pink1*$^{-/-}$ mice, as early as 2 months old, develop left ventricular dysfunction and pathological cardiac hypertrophy[105]. Further, these *Pink1-deficient* mice display significantly impaired cardiac function - discernible by heightened levels of oxidative stress, impaired mitochondrial function, higher degrees of fibrosis, cardiomyocyte apoptosis, and reciprocal reduction in capillary density[105]. Due to its ability to prevent mitochondrial

dysfunction, overexpression of PINK1 may serve as protective against acute ischemia-reperfusion injury in cardiomyocytes[198]. Additionally, a recent discovery made in pulmonary disease models suggests that during mitochondrial stress, PINK1 dynamically interacts with MAVS to inhibit MAVS-mediated innate immune signalling and regulate multimeric MAVS aggregation[199]. Despite plausibility, it remains unclear if MAVS is a novel substrate of PINK1 - physically blocking MAVS aggregation or if PINK1 must phosphorylate/induce ubiquitination of MAVS to initiate MAVS aggregate clearance[199].

4.1.4.3 MAVS and cGAS-STING

Novel research findings show a crosstalk between the cGAS-STING DNA and RIG-I-MAVS RNA sensing pathways[200]. In fact, several studies indicate that STING can interact with RIG-I and MAVS in a stable complex during viral infection[201,202]. Although both MAVS and STING pathways have been separately implicated as key players in cardiovascular function, it has not yet been confirmed if their crosstalk relationship plays a role in heart disease processes, but highly deserving of exploration[144,203,204].

4.1.4.4 MAVS and Sirt3

Sirtuin 3 is a mitochondrial-specific sirtuin that is abundantly expressed in the heart[205]. Sirtuins are key perpetrators of PGC-1a activity. In fact, NEU1 and miR195 are notably increased in failing myocardium and decrease PGC-1a activity by suppressing Sirt1 and Sirt3, respectively[206,207]. In both cases, adverse cardiac remodeling and mitochondrial metabolism, and oxidative stress are noted. Conversely, administering drugs that stimulate mitochondrial Sirtuins and promote PGC-1a expression show positive effects[208]. For example, activating the PPARa/PGC-1a/Sirt3 axis or, in the case of metformin, directly up-regulating Sirt3[209,210]. Even

exercise has been shown to prolong adaptive activation of SIRT1/PGC1a/PI3K/Akt signaling to promote cell survival, mitochondrial biogenesis, alleviate cardiac dysfunction, and enhance cardio protection[211].

It was recently established that in viral infection response, Sirtuin 3 deacetylates MAVS at lysine residue 7 (K7), which enhances MAVS aggregation/activation, leading to increased type I interferon signaling and enhanced antiviral response[205,212]. Thus, it is likely that in the short term, activation of MAVS provides cardiac protection by contributing to initial inflammatory signalling. However, our findings suggest that *Mavs* deficiency contributes to improved cardiac remodeling. Therefore, it is likely that although MAVS aggregation is initially necessary, overexpression and/or persistent activation contribute to adverse remodeling[213]. Further research is required to confirm this hypothesis.

4.1.4.5 MAVS and NLRP3

Several studies indicate the role of inflammasome activation and apoptosis in ischemic myocardial pathogenesis[44]. NLRP3 is a key component of inflammasome formation, and if inhibited, mice display significant reductions in infarct size and preservation of cardiac function post MI[214–216]. Recently, studies have begun to note that NLRP3 inflammasome activation can be inhibited via various MAVS-dependent mechanisms and produces cardioprotective effects[138]. For instance, TAX1BP exerted cardioprotective effects in acute MI by inhibiting inflammasome activation via an RNF34/MAVS/NLRP3-dependent mechanism[217]. Another study indicates that NLRX1 plays a protective role in acute MI by inhibiting MAVS-dependent NLRP3 inflammasome activation and apoptosis[218]. Finally, increasing levels of E3 ubiquitin ligase membrane-associated RING finger protein 2

(MARCH2) played a protective role in ischemic hearts by reducing cardiomyocyte pyroptosis and myocardial injury via negative regulation of PGAM5/MAVS/NLRP3 pathway[219].

4.2 FUTURE DIRECTIONS

4.2.1 Cell culture modelling of MAVS activation

More detailed mechanistic studies are required to fully elucidate the role of MAVS in MI stress response and remodelling. We were able to acquire promising preliminary data to demonstrate effective cell culture modelling systems of MAVS activation. Two different AC16 cell treatment regimens with Angiotensin II: 1) 200nM AngII for 24hrs (**Figure S1A/C**) and 2) 1μM AngII for 2hrs (**Figure S1B/D**) were able to successfully induce MAVS activation. Although several technical replicates were performed, biological replicates (multiple cell batches) were not, limiting the generalizability and thus inconclusivity of results.

4.2.2 Cardiac Specific Mavs$^{-/-}$

It is well documented that innate immune viral infection response is significantly reduced in MAVS-deficient mice[220]. Thus, it is plausible that in the context of MI, the absence of global MAVS alters initial immune response, and the observed improved cardiac remodeling may occur through a non-cardiac specific mechanism. Therefore, evaluating cardiac-specific MAVS knockout mice could provide more meaningful insight into organ-specific mechanisms.

4.2.3 Identifying negative regulators of MAVS

MAVS aggregation on mitochondrial surfaces is key to MAVS functioning and is necessary for propagating innate immune and remodelling functions in the heart[144,221].

However, to maintain homeostatic physiological states, mechanisms should exist to inhibit the spontaneous over-expression and/or persistent activation of MAVS-mediated signalling and aggregation; otherwise, there would be the risk of chronic, persistent, inflammatory, or autoimmune disease states[213]. Despite understanding the importance of regulating MAVS aggregation, such negative regulatory mechanisms remain poorly characterized; thus, this should remain a primary future research focus.

4.2.4 Temporal and spatial mapping of MAVS activation post-MI

Finally, temporal and spatial mapping could help to visualize MAVS aggregation and clearance post-MI in real time. Acquiring spatial-temporal dynamics could reveal insights into cell type specificity, disease progression, and help elucidate the ideal inhibition time point for optimal remodeling outcomes. Employing techniques such as electron microscopy could provide visual confirmation that MAVS aggregation, and not simply increased expression, is a defining feature of MI-induced immune activation.

In non-diseased human hearts, single-cell RNA sequencing has confirmed that *MAVS* is most abundant in macrophages, cardiomyocytes, smooth muscle cells, plasma cells, undifferentiated cells, endothelial cells, neutrophils, T cells, and fibroblasts[143]. However, additional detailed single-cell *RNASeq mapping* in diseased tissues can provide information regarding cell type-specific gene activity, transcription, and activation/shutdown levels – highlighting if MAVS is most active in non-myocytes (fibroblasts, endothelial cells, immune cells) or cardiomyocytes themselves.

4.2.5 Metabolic Profiling

Our lab's future research will provide comprehensive metabolic profiling of *Mavs*$^{-/-}$ mice post MI. Studies have noted the involvement of MAVS in coordinating the switch from glycolysis to the pentose phosphate pathways (PPP) and the hexosamine biosynthesis pathway (HBP)[186]. Additional studies have noted disrupted energy metabolism, especially lipid metabolism, in *Mavs* deficient mice. However, no studies have specifically profiled MI-induced metabolic changes[144,145]. Employing metabolic stress tests and/or carbon tracing techniques will contribute to an understanding of whether and how MAVS contributes to altered metabolic efficiency, substrate switching, ROS clearance, etc., during MI-induced inflammation and remodeling processes. In addition, performing transmission electron microscopy (TEM) of mouse hearts and/or induced pluripotent stem cells (iPSCs) will provide a fine detail and in-depth visual assessment of mitochondrial morphology, dynamics (fusion/fission), and a temporal/geographical map of Mavs aggregation and clearance[222]. Finally, RNASeq/MitoSeq analyses of myocytes in both Mavs$^{+/+}$ and Mavs$^{-/-}$ hearts will provide high-throughput maps of myocyte and mitochondrial gene expression and activity patterns in the various disease states[223].

4.3 LIMITATIONS

In this series, cell culture experiments were performed using a ventricular-derived cell line, AC16s. Due to their immortalized nature, they are extremely proliferative, non-contractile/conductive, genetically unstable, and resilient to stressors, making them an over-simplified recapitulation of mature cardiomyocytes[224]. This posed challenges when designing and performing mechanistic studies. For instance, since genetic knockdown of *MAVS* using

siRNA is transient, the proliferative nature of these cells results in reduced knockdown sustainability in long-term stress experiments (**Figure S3D/E**)[225]. Alternatively, using iPSC-derived cardiomyocytes could provide a more sophisticated recapitulation of human disease and thus allow for more precise evaluation of disease mechanisms[226].

More thorough mitochondrial functional analysis is required to fully profile the phenotypic differences between WT and *Mavs* deficient mice. Our prior research conducted mitochondrial respiration analysis on isolated mitochondria and cardiomyocytes from pressure overload mouse hearts using Seahorse XF[144]. However, to our knowledge, mitochondrial analyses have not been conducted on MI mouse tissues. By extension, using tools such as Oroboros could provide more high-resolution monitoring of respiratory/metabolic activity in tissue biopsy sections[227].

5 CONCLUSION

Taken together, these results indicate that *Mavs* deficiency is associated with differences in cardiac remodelling post-MI. Preliminary evidence suggests that knockout of *Mavs* may improve cardiac function/remodelling post-MI, in a sex dependent manner - thus, identifying a negative regulator of MAVS over-aggregation may serve as a promising therapeutic approach. Sex-specific phenotypes provide an opportunity for the development of sex-specific, personalized therapies. Molecular studies will be required to supplement/justify these findings.

6 REFERENCES

1. Chaudhry, R., Miao, J. H. & Rehman, A. Physiology, Cardiovascular. in *StatPearls* (StatPearls Publishing, Treasure Island (FL), 2025).
2. Martin, S. S. *et al.* 2025 Heart Disease and Stroke Statistics: A Report of US and Global Data From the American Heart Association. *Circulation* **151**, (2025).
3. Al Akeel, M., Alhuneafat, L., Jabri, A. & Altaani, O. GLOBAL BURDEN OF CARDIOVASCULAR DISEASE IN CANADA. *Journal of the American College of Cardiology* **83**, 2472 (2024).
4. Dai, S. *et al.* Comorbidities and Mortality Associated With Hospitalized Heart Failure in Canada. *Canadian Journal of Cardiology* **28**, 74–79 (2012).
5. Goldfarb, M. J. *et al.* Patient-Centered Adult Cardiovascular Care: A Scientific Statement From the American Heart Association. *Circulation* **149**, (2024).
6. Ojha, N. & Dhamoon, A. S. Myocardial Infarction. in *StatPearls* (StatPearls Publishing, Treasure Island (FL), 2025).
7. Schirone, L. *et al.* An Overview of the Molecular Mechanisms Associated with Myocardial Ischemic Injury: State of the Art and Translational Perspectives. *Cells* **11**, 1165 (2022).
8. Jebari-Benslaiman, S. *et al.* Pathophysiology of Atherosclerosis. *IJMS* **23**, 3346 (2022).
9. Picariello, C. *et al.* The Impact of Hypertension on Patients with Acute Coronary Syndromes. *International Journal of Hypertension* **2011**, 1–7 (2011).
10. Sueda, S. & Sakaue, T. Coronary artery spasm-induced acute myocardial infarction in patients with myocardial infarction with non-obstructive coronary arteries. *Heart Vessels* **36**, 1804–1810 (2021).
11. Jennings, R. B. & Ganote, C. E. Structural Changes in Myocardium During Acute Ischemia. *Circulation Research* **35**, (1974).
12. Thygesen, K. *et al.* Fourth Universal Definition of Myocardial Infarction (2018). *Circulation* **138**, (2018).

13. Van Der Linden, N. *et al.* Combining High-Sensitivity Cardiac Troponin I and Cardiac Troponin T in the Early Diagnosis of Acute Myocardial Infarction. *Circulation* **138**, 989–999 (2018).
14. Hoffman, J. W., Gilbert, T. B., Poston, R. S. & Silldorff, E. P. Myocardial Reperfusion Injury: Etiology, Mechanisms, and Therapies. *J Extra Corpor Technol* **36**, 391–411 (2004).
15. Prabhu, S. D. & Frangogiannis, N. G. The Biological Basis for Cardiac Repair After Myocardial Infarction: From Inflammation to Fibrosis. *Circulation Research* **119**, 91–112 (2016).
16. Frangogiannis, N. G. Regulation of the Inflammatory Response in Cardiac Repair. *Circulation Research* **110**, 159–173 (2012).
17. Arslan, F. *et al.* Myocardial Ischemia/Reperfusion Injury Is Mediated by Leukocytic Toll-Like Receptor-2 and Reduced by Systemic Administration of a Novel Anti–Toll-Like Receptor-2 Antibody. *Circulation* **121**, 80–90 (2010).
18. De Haan, J. J., Smeets, M. B., Pasterkamp, G. & Arslan, F. Danger Signals in the Initiation of the Inflammatory Response after Myocardial Infarction. *Mediators of Inflammation* **2013**, 1–13 (2013).
19. Newton, K. & Dixit, V. M. Signaling in Innate Immunity and Inflammation. *Cold Spring Harbor Perspectives in Biology* **4**, a006049–a006049 (2012).
20. Nian, M., Lee, P., Khaper, N. & Liu, P. Inflammatory Cytokines and Postmyocardial Infarction Remodeling. *Circulation Research* **94**, 1543–1553 (2004).
21. Horckmans, M. *et al.* Neutrophils orchestrate post-myocardial infarction healing by polarizing macrophages towards a reparative phenotype. *Eur Heart J* ehw002 (2016) doi:10.1093/eurheartj/ehw002.
22. Kohno, T. *et al.* Role of high-mobility group box 1 protein in post-infarction healing process and left ventricular remodelling. *Cardiovascular Research* **81**, 565–573 (2008).
23. Park, M. & Sweeney, G. Direct effects of adipokines on the heart: focus on adiponectin. *Heart Fail Rev* **18**, 631–644 (2013).

24. Takahashi, K. *et al.* Modulated Inflammation by Injection of High-Mobility Group Box 1 Recovers Post-Infarction Chronically Failing Heart. *Circulation* **118**, (2008).
25. Tian, J. *et al.* Metformin confers longitudinal cardiac protection by preserving mitochondrial homeostasis following myocardial ischemia/reperfusion injury. *Eur J Nucl Med Mol Imaging* **50**, 825–838 (2023).
26. Turner, N. A. Inflammatory and fibrotic responses of cardiac fibroblasts to myocardial damage associated molecular patterns (DAMPs). *Journal of Molecular and Cellular Cardiology* **94**, 189–200 (2016).
27. Scaffidi, P., Misteli, T. & Bianchi, M. E. Release of chromatin protein HMGB1 by necrotic cells triggers inflammation. *Nature* **418**, 191–195 (2002).
28. Lugrin, J. *et al.* Cutting Edge: IL-1α Is a Crucial Danger Signal Triggering Acute Myocardial Inflammation during Myocardial Infarction. *The Journal of Immunology* **194**, 499–503 (2015).
29. Lugrin, J. *et al.* The systemic deletion of interleukin-1α reduces myocardial inflammation and attenuates ventricular remodeling in murine myocardial infarction. *Sci Rep* **13**, 4006 (2023).
30. Satoh, M. *et al.* Elevated circulating levels of heat shock protein 70 are related to systemic inflammatory reaction through monocyte Toll signal in patients with heart failure after acute myocardial infarction. *European J of Heart Fail* **8**, 810–815 (2006).
31. Tian, J. *et al.* Extracellular HSP60 induces inflammation through activating and up-regulating TLRs in cardiomyocytes. *Cardiovascular Research* **98**, 391–401 (2013).
32. Li, Y. *et al.* Myocardial Ischemia Activates an Injurious Innate Immune Signaling via Cardiac Heat Shock Protein 60 and Toll-like Receptor 4. *Journal of Biological Chemistry* **286**, 31308–31319 (2011).
33. Vabulas, R. M. *et al.* Endocytosed HSP60s Use Toll-like Receptor 2 (TLR2) and TLR4 to Activate the Toll/Interleukin-1 Receptor Signaling Pathway in Innate Immune Cells. *Journal of Biological Chemistry* **276**, 31332–31339 (2001).

34. Ohashi, K., Burkart, V., Flohé, S. & Kolb, H. Cutting Edge: Heat Shock Protein 60 Is a Putative Endogenous Ligand of the Toll-Like Receptor-4 Complex. *The Journal of Immunology* **164**, 558–561 (2000).

35. Simard, J.-C., Noël, C., Tessier, P. A. & Girard, D. Human S100A9 potentiates IL-8 production in response to GM-CSF or fMLP via activation of a different set of transcription factors in neutrophils. *FEBS Letters* **588**, 2141–2146 (2014).

36. Volz, H. C. *et al.* S100A8/A9 aggravates post-ischemic heart failure through activation of RAGE-dependent NF-κB signaling. *Basic Res Cardiol* **107**, 250 (2012).

37. Okamura, Y. *et al.* The Extra Domain A of Fibronectin Activates Toll-like Receptor 4. *Journal of Biological Chemistry* **276**, 10229–10233 (2001).

38. Jun, J.-I. & Lau, L. F. CCN1 is an opsonin for bacterial clearance and a direct activator of Toll-like receptor signaling. *Nat Commun* **11**, 1242 (2020).

39. Shinohara, M. L. *et al.* Osteopontin expression is essential for interferon-α production by plasmacytoid dendritic cells. *Nat Immunol* **7**, 498–506 (2006).

40. Sato, S., St-Pierre, C., Bhaumik, P. & Nieminen, J. Galectins in innate immunity: dual functions of host soluble β-galactoside-binding lectins as damage-associated molecular patterns (DAMPs) and as receptors for pathogen-associated molecular patterns (PAMPs). *Immunological Reviews* **230**, 172–187 (2009).

41. Seropian, I. M. *et al.* Galectin-1 Controls Cardiac Inflammation and Ventricular Remodeling during Acute Myocardial Infarction. *The American Journal of Pathology* **182**, 29–40 (2013).

42. Midwood, K. *et al.* Tenascin-C is an endogenous activator of Toll-like receptor 4 that is essential for maintaining inflammation in arthritic joint disease. *Nat Med* **15**, 774–780 (2009).

43. Liao, K.-C. & Mogridge, J. Activation of the Nlrp1b Inflammasome by Reduction of Cytosolic ATP. *Infect Immun* **81**, 570–579 (2013).

44. Mezzaroma, E. *et al.* The inflammasome promotes adverse cardiac remodeling following acute myocardial infarction in the mouse. *Proc. Natl. Acad. Sci. U.S.A.* **108**, 19725–19730 (2011).

45. Liu-Bryan, R., Scott, P., Sydlaske, A., Rose, D. M. & Terkeltaub, R. Innate immunity conferred by toll-like receptors 2 and 4 and myeloid differentiation factor 88 expression is pivotal to monosodium urate monohydrate crystal–induced inflammation. *Arthritis & Rheumatism* **52**, 2936–2946 (2005).

46. Martinon, F., Pétrilli, V., Mayor, A., Tardivel, A. & Tschopp, J. Gout-associated uric acid crystals activate the NALP3 inflammasome. *Nature* **440**, 237–241 (2006).

47. Xie, L. *et al.* Exogenous administration of mitochondrial DNA promotes ischemia reperfusion injury via TLR9-p38 MAPK pathway. *Regulatory Toxicology and Pharmacology* **89**, 148–154 (2017).

48. Oka, T. *et al.* Mitochondrial DNA that escapes from autophagy causes inflammation and heart failure. *Nature* **485**, 251–255 (2012).

49. Zhou, R., Yazdi, A. S., Menu, P. & Tschopp, J. A role for mitochondria in NLRP3 inflammasome activation. *Nature* **469**, 221–225 (2011).

50. Onódi, Z. *et al.* AIM2-driven inflammasome activation in heart failure. *Cardiovascular Research* cvab202 (2021) doi:10.1093/cvr/cvab202.

51. Shimada, K. *et al.* Oxidized Mitochondrial DNA Activates the NLRP3 Inflammasome during Apoptosis. *Immunity* **36**, 401–414 (2012).

52. Karikó, K., Ni, H., Capodici, J., Lamphier, M. & Weissman, D. mRNA Is an Endogenous Ligand for Toll-like Receptor 3. *Journal of Biological Chemistry* **279**, 12542–12550 (2004).

53. Scheibner, K. A. *et al.* Hyaluronan Fragments Act as an Endogenous Danger Signal by Engaging TLR2. *The Journal of Immunology* **177**, 1272–1281 (2006).

54. Dobaczewski, M., Gonzalez-Quesada, C. & Frangogiannis, N. G. The extracellular matrix as a modulator of the inflammatory and reparative response following myocardial infarction. *Journal of Molecular and Cellular Cardiology* **48**, 504–511 (2010).

55. Zuo, W., Sun, R., Ji, Z. & Ma, G. Macrophage-driven cardiac inflammation and healing: insights from homeostasis and myocardial infarction. *Cell Mol Biol Lett* **28**, 81 (2023).

56. Li, T. *et al.* Cardiac repair after myocardial infarction: A two-sided role of inflammation-mediated. *Front Cardiovasc Med* **9**, 1077290 (2022).
57. Sutton, M. G. St. J. & Sharpe, N. Left Ventricular Remodeling After Myocardial Infarction: Pathophysiology and Therapy. *Circulation* **101**, 2981–2988 (2000).
58. Hill, J. A. & Olson, E. N. Cardiac Plasticity. *N Engl J Med* **358**, 1370–1380 (2008).
59. Christia, P. *et al.* Systematic Characterization of Myocardial Inflammation, Repair, and Remodeling in a Mouse Model of Reperfused Myocardial Infarction. *J Histochem Cytochem.* **61**, 555–570 (2013).
60. Hinz, B. & Lagares, D. Evasion of apoptosis by myofibroblasts: a hallmark of fibrotic diseases. *Nat Rev Rheumatol* **16**, 11–31 (2020).
61. Heidenreich, P. A. *et al.* 2022 AHA/ACC/HFSA Guideline for the Management of Heart Failure: A Report of the American College of Cardiology/American Heart Association Joint Committee on Clinical Practice Guidelines. *Circulation* **145**, (2022).
62. Dunlay, S. M., Roger, V. L. & Redfield, M. M. Epidemiology of heart failure with preserved ejection fraction. *Nat Rev Cardiol* **14**, 591–602 (2017).
63. McDonagh, T. A. *et al.* 2021 ESC Guidelines for the diagnosis and treatment of acute and chronic heart failure. *European Heart Journal* **42**, 3599–3726 (2021).
64. Chioncel, O. *et al.* Epidemiology and one-year outcomes in patients with chronic heart failure and preserved, mid-range and reduced ejection fraction: an analysis of the ESC Heart Failure Long-Term Registry. *European J of Heart Fail* **19**, 1574–1585 (2017).
65. Simmonds, S. J., Cuijpers, I., Heymans, S. & Jones, E. A. V. Cellular and Molecular Differences between HFpEF and HFrEF: A Step Ahead in an Improved Pathological Understanding. *Cells* **9**, 242 (2020).
66. Murphy, S. P., Ibrahim, N. E. & Januzzi, J. L. Heart Failure With Reduced Ejection Fraction: A Review. *JAMA* **324**, 488 (2020).
67. Heidenreich, P. A. *et al.* 2022 AHA/ACC/HFSA Guideline for the Management of Heart Failure. *Journal of the American College of Cardiology* **79**, e263–e421 (2022).
68. Vásquez-Trincado, C. *et al.* Mitochondrial dynamics, mitophagy and cardiovascular disease. *The Journal of Physiology* **594**, 509–525 (2016).

69. Bertero, E. & Maack, C. Metabolic remodelling in heart failure. *Nat Rev Cardiol* **15**, 457–470 (2018).

70. Bravo-San Pedro, J. M., Kroemer, G. & Galluzzi, L. Autophagy and Mitophagy in Cardiovascular Disease. *Circulation Research* **120**, 1812–1824 (2017).

71. Morciano, G. *et al.* Mitophagy in Cardiovascular Diseases. *JCM* **9**, 892 (2020).

72. Aubert, G., Vega, R. B. & Kelly, D. P. Perturbations in the gene regulatory pathways controlling mitochondrial energy production in the failing heart. *Biochimica et Biophysica Acta (BBA) - Molecular Cell Research* **1833**, 840–847 (2013).

73. Liu, M., Liu, H. & Dudley, S. C. Reactive Oxygen Species Originating From Mitochondria Regulate the Cardiac Sodium Channel. *Circulation Research* **107**, 967–974 (2010).

74. Aguiar, C. J. *et al.* Succinate causes pathological cardiomyocyte hypertrophy through GPR91 activation. *Cell Commun Signal* **12**, 78 (2014).

75. Von Lueder, T. G. *et al.* Neurohormonal Blockade in Heart Failure. *Cardiac Failure Review* **03**, 19 (2017).

76. Lopaschuk, G. D., Ussher, J. R., Folmes, C. D. L., Jaswal, J. S. & Stanley, W. C. Myocardial Fatty Acid Metabolism in Health and Disease. *Physiological Reviews* **90**, 207–258 (2010).

77. Gorski, P. A., Ceholski, D. K. & Hajjar, R. J. Altered Myocardial Calcium Cycling and Energetics in Heart Failure—A Rational Approach for Disease Treatment. *Cell Metabolism* **21**, 183–194 (2015).

78. The SOLVD Investigators*. Effect of Enalapril on Survival in Patients with Reduced Left Ventricular Ejection Fractions and Congestive Heart Failure. *N Engl J Med* **325**, 293–302 (1991).

79. Allard, M. F., Schonekess, B. O., Henning, S. L., English, D. R. & Lopaschuk, G. D. Contribution of oxidative metabolism and glycolysis to ATP production in hypertrophied hearts. *American Journal of Physiology-Heart and Circulatory Physiology* **267**, H742–H750 (1994).

80. Chaanine, A. H. *et al.* Mitochondrial Integrity and Function in the Progression of Early Pressure Overload–Induced Left Ventricular Remodeling. *JAHA* **6**, e005869 (2017).
81. Tsutsui, H., Kinugawa, S. & Matsushima, S. Oxidative stress and heart failure. *American Journal of Physiology-Heart and Circulatory Physiology* **301**, H2181–H2190 (2011).
82. Murphy, M. P. How mitochondria produce reactive oxygen species. *Biochemical Journal* **417**, 1–13 (2009).
83. Zorov, D. B., Filburn, C. R., Klotz, L.-O., Zweier, J. L. & Sollott, S. J. Reactive Oxygen Species (Ros-Induced) Ros Release. *The Journal of Experimental Medicine* **192**, 1001–1014 (2000).
84. Denton, R. M., Richards, D. A. & Chin, J. G. Calcium ions and the regulation of NAD+-linked isocitrate dehydrogenase from the mitochondria of rat heart and other tissues. *Biochemical Journal* **176**, 899–906 (1978).
85. Hopper, R. K. *et al.* Mitochondrial Matrix Phosphoproteome: Effect of Extra Mitochondrial Calcium. *Biochemistry* **45**, 2524–2536 (2006).
86. Duchen, M. R. Mitochondria and calcium: from cell signalling to cell death. *The Journal of Physiology* **529**, 57–68 (2000).
87. Xu, X. *et al.* Pyrroloquinoline quinone can prevent chronic heart failure by regulating mitochondrial function. *Cardiovasc Diagn Ther* **10**, 453–469 (2020).
88. De Stefani, D., Raffaello, A., Teardo, E., Szabò, I. & Rizzuto, R. A forty-kilodalton protein of the inner membrane is the mitochondrial calcium uniporter. *Nature* **476**, 336–340 (2011).
89. Bernardi, P. & Di Lisa, F. The mitochondrial permeability transition pore: Molecular nature and role as a target in cardioprotection. *Journal of Molecular and Cellular Cardiology* **78**, 100–106 (2015).
90. Ide, T. *et al.* Mitochondrial DNA Damage and Dysfunction Associated With Oxidative Stress in Failing Hearts After Myocardial Infarction. *Circulation Research* **88**, 529–535 (2001).

91. Halestrap, A. P. & Pasdois, P. The role of the mitochondrial permeability transition pore in heart disease. *Biochimica et Biophysica Acta (BBA) - Bioenergetics* **1787**, 1402–1415 (2009).

92. Zhu, P. *et al.* Ripk3 promotes ER stress-induced necroptosis in cardiac IR injury: A mechanism involving calcium overload/XO/ROS/mPTP pathway. *Redox Biology* **16**, 157–168 (2018).

93. Nakayama, H. & Otsu, K. Mitochondrial DNA as an inflammatory mediator in cardiovascular diseases. *Biochemical Journal* **475**, 839–852 (2018).

94. Morciano, G. *et al.* Comprehensive Analysis of Mitochondrial Dynamics Alterations in Heart Diseases. *IJMS* **24**, 3414 (2023).

95. Hernandez-Resendiz, S. *et al.* Targeting mitochondrial shape: at the heart of cardioprotection. *Basic Res Cardiol* **118**, 49 (2023).

96. Chen, H. *et al.* Titration of mitochondrial fusion rescues *Mff* -deficient cardiomyopathy. *Journal of Cell Biology* **211**, 795–805 (2015).

97. Ong, S.-B. *et al.* Inhibiting Mitochondrial Fission Protects the Heart Against Ischemia/Reperfusion Injury. *Circulation* **121**, 2012–2022 (2010).

98. Burman, J. L. *et al.* Mitochondrial fission facilitates the selective mitophagy of protein aggregates. *Journal of Cell Biology* **216**, 3231–3247 (2017).

99. Chen, Y., Liu, Y. & Dorn, G. W. Mitochondrial Fusion is Essential for Organelle Function and Cardiac Homeostasis. *Circulation Research* **109**, 1327–1331 (2011).

100. Davidson, S. M. *et al.* Multitarget Strategies to Reduce Myocardial Ischemia/Reperfusion Injury. *Journal of the American College of Cardiology* **73**, 89–99 (2019).

101. Davidson, S. M. *et al.* Mitochondrial and mitochondrial-independent pathways of myocardial cell death during ischaemia and reperfusion injury. *J Cellular Molecular Medi* **24**, 3795–3806 (2020).

102. Karamanlidis, G. *et al.* Defective DNA Replication Impairs Mitochondrial Biogenesis In Human Failing Hearts. *Circulation Research* **106**, 1541–1548 (2010).

103. Wu, Z. *et al.* Mechanisms Controlling Mitochondrial Biogenesis and Respiration through the Thermogenic Coactivator PGC-1. *Cell* **98**, 115–124 (1999).

104. Finck, B. N. & Kelly, D. P. Peroxisome Proliferator–Activated Receptor γ Coactivator-1 (PGC-1) Regulatory Cascade in Cardiac Physiology and Disease. *Circulation* **115**, 2540–2548 (2007).

105. Billia, F. *et al.* PTEN-inducible kinase 1 (PINK1)/Park6 is indispensable for normal heart function. *Proc. Natl. Acad. Sci. U.S.A.* **108**, 9572–9577 (2011).

106. Hoshino, A. *et al.* Cytosolic p53 inhibits Parkin-mediated mitophagy and promotes mitochondrial dysfunction in the mouse heart. *Nat Commun* **4**, 2308 (2013).

107. Anttila, V. *et al.* Synthetic mRNA Encoding VEGF-A in Patients Undergoing Coronary Artery Bypass Grafting: Design of a Phase 2a Clinical Trial. *Molecular Therapy - Methods & Clinical Development* **18**, 464–472 (2020).

108. Post, M. Therapeutic angiogenesis in cardiology using protein formulations. *Cardiovascular Research* **49**, 522–531 (2001).

109. Braile, M. *et al.* VEGF-A in Cardiomyocytes and Heart Diseases. *IJMS* **21**, 5294 (2020).

110. Gallo, G., Volpe, M. & Savoia, C. Endothelial Dysfunction in Hypertension: Current Concepts and Clinical Implications. *Front. Med.* **8**, 798958 (2022).

111. Shibuya, M. Vascular Endothelial Growth Factor (VEGF) and Its Receptor (VEGFR) Signaling in Angiogenesis: A Crucial Target for Anti- and Pro-Angiogenic Therapies. *Genes & Cancer* **2**, 1097–1105 (2011).

112. Zhang, C. *et al.* Sirtuin 3 deficiency aggravates angiotensin II-induced hypertensive cardiac injury by the impairment of lymphangiogenesis. *J Cellular Molecular Medi* **25**, 7760–7771 (2021).

113. Khurana, R., Simons, M., Martin, J. F. & Zachary, I. C. Role of Angiogenesis in Cardiovascular Disease: A Critical Appraisal. *Circulation* **112**, 1813–1824 (2005).

114. Gao, S. *et al.* FABP5 Deficiency Impairs Mitochondrial Function and Aggravates Pathological Cardiac Remodeling and Dysfunction. *Cardiovasc Toxicol* **21**, 619–629 (2021).

115. Szalai, G., Csordás, G., Hantash, B. M., Thomas, A. P. & Hajnóczky, G. Calcium Signal Transmission between Ryanodine Receptors and Mitochondria. *Journal of Biological Chemistry* **275**, 15305–15313 (2000).

116. Eisner, V., Csordás, G. & Hajnóczky, G. Interactions between sarco-endoplasmic reticulum and mitochondria in cardiac and skeletal muscle – pivotal roles in Ca2+ and reactive oxygen species signaling. *Journal of Cell Science* jcs.093609 (2013) doi:10.1242/jcs.093609.

117. Baughman, J. M. *et al.* Integrative genomics identifies MCU as an essential component of the mitochondrial calcium uniporter. *Nature* **476**, 341–345 (2011).

118. Bononi, A. *et al.* Identification of PTEN at the ER and MAMs and its regulation of Ca2+ signaling and apoptosis in a protein phosphatase-dependent manner. *Cell Death Differ* **20**, 1631–1643 (2013).

119. Hamasaki, M. *et al.* Autophagosomes form at ER–mitochondria contact sites. *Nature* **495**, 389–393 (2013).

120. Boengler, K., Bornbaum, J., Schlüter, K.-D. & Schulz, R. P66shc and its role in ischemic cardiovascular diseases. *Basic Res Cardiol* **114**, 29 (2019).

121. Brookes, P. S., Yoon, Y., Robotham, J. L., Anders, M. W. & Sheu, S.-S. Calcium, ATP, and ROS: a mitochondrial love-hate triangle. *American Journal of Physiology-Cell Physiology* **287**, C817–C833 (2004).

122. Robert, V. Beat-to-beat oscillations of mitochondrial [Ca2+] in cardiac cells. *The EMBO Journal* **20**, 4998–5007 (2001).

123. Liu, D., Zeng, X., Li, X., Mehta, J. L. & Wang, X. Role of NLRP3 inflammasome in the pathogenesis of cardiovascular diseases. *Basic Res Cardiol* **113**, 5 (2018).

124. Friedman, J. R. *et al.* ER Tubules Mark Sites of Mitochondrial Division. *Science* **334**, 358–362 (2011).

125. De Brito, O. M. & Scorrano, L. Mitofusin 2 tethers endoplasmic reticulum to mitochondria. *Nature* **456**, 605–610 (2008).

126. Chen, Y., Shi, Y., Wu, J. & Qi, N. MAVS: A Two-Sided CARD Mediating Antiviral Innate Immune Signaling and Regulating Immune Homeostasis. *Front. Microbiol.* **12**, 744348 (2021).

127. Meylan, E. *et al.* Cardif is an adaptor protein in the RIG-I antiviral pathway and is targeted by hepatitis C virus. *Nature* **437**, 1167–1172 (2005).

128. Seth, R. B., Sun, L., Ea, C.-K. & Chen, Z. J. Identification and Characterization of MAVS, a Mitochondrial Antiviral Signaling Protein that Activates NF-κB and IRF3. *Cell* **122**, 669–682 (2005).

129. Vazquez, C. & Horner, S. M. MAVS Coordination of Antiviral Innate Immunity. *J Virol* **89**, 6974–6977 (2015).

130. Ren, Z. *et al.* Regulation of MAVS Expression and Signaling Function in the Antiviral Innate Immune Response. *Front. Immunol.* **11**, 1030 (2020).

131. West, A. P., Shadel, G. S. & Ghosh, S. Mitochondria in innate immune responses. *Nat Rev Immunol* **11**, 389–402 (2011).

132. Wu, B. & Hur, S. How RIG-I like receptors activate MAVS. *Current Opinion in Virology* **12**, 91–98 (2015).

133. Hou, F. *et al.* MAVS Forms Functional Prion-like Aggregates to Activate and Propagate Antiviral Innate Immune Response. *Cell* **146**, 448–461 (2011).

134. Liu, S. *et al.* MAVS recruits multiple ubiquitin E3 ligases to activate antiviral signaling cascades. *eLife* **2**, e00785 (2013).

135. Liu, S. *et al.* Phosphorylation of innate immune adaptor proteins MAVS, STING, and TRIF induces IRF3 activation. *Science* **347**, aaa2630 (2015).

136. Liu, B. *et al.* The ubiquitin E3 ligase TRIM31 promotes aggregation and activation of the signaling adaptor MAVS through Lys63-linked polyubiquitination. *Nat Immunol* **18**, 214–224 (2017).

137. Zhou, R., Zhang, Q. & Xu, P. TBK1, a central kinase in innate immune sensing of nucleic acids and beyond. *ABBS* **52**, 757–767 (2020).

138. Subramanian, N., Natarajan, K., Clatworthy, M. R., Wang, Z. & Germain, R. N. The Adaptor MAVS Promotes NLRP3 Mitochondrial Localization and Inflammasome Activation. *Cell* **153**, 348–361 (2013).

139. Park, S. *et al.* The Mitochondrial Antiviral Protein MAVS Associates with NLRP3 and Regulates Its Inflammasome Activity. *The Journal of Immunology* **191**, 4358–4366 (2013).

140. Allam, R. *et al.* Mitochondrial apoptosis is dispensable for NLRP 3 inflammasome activation but non-apoptotic caspase-8 is required for inflammasome priming. *EMBO Reports* **15**, 982–990 (2014).

141. Nakahira, K. *et al.* Autophagy proteins regulate innate immune responses by inhibiting the release of mitochondrial DNA mediated by the NALP3 inflammasome. *Nat Immunol* **12**, 222–230 (2011).

142. Hu, Y. *et al.* Zika virus antagonizes interferon response in patients and disrupts RIG-I–MAVS interaction through its CARD-TM domains. *Cell Biosci* **9**, 46 (2019).

143. Uhlén, M. *et al.* Tissue-based map of the human proteome. *Science* **347**, 1260419 (2015).

144. Lin, H.-B. *et al.* Innate Immune Nod1/RIP2 Signaling Is Essential for Cardiac Hypertrophy but Requires Mitochondrial Antiviral Signaling Protein for Signal Transductions and Energy Balance. *Circulation* **142**, 2240–2258 (2020).

145. Wang, Q. *et al.* Reduced Immunity Regulator MAVS Contributes to Non-Hypertrophic Cardiac Dysfunction by Disturbing Energy Metabolism and Mitochondrial Homeostasis. *Front. Immunol.* **13**, 919038 (2022).

146. Kang, Z. *et al.* Myocardial mitochondrial antiviral signaling protein promotes heart Ischemia-reperfusion injury via RIG-I signaling in mice. *Nat Commun* **16**, 5101 (2025).

147. Perlman, R. L. Mouse models of human disease: An evolutionary perspective. *Evol Med Public Health* **2016**, 170–176 (2016).

148. Bryda, E. C. The Mighty Mouse: the impact of rodents on advances in biomedical research. *Mo Med* **110**, 207–211 (2013).

149. Bolli, R., Patel, B. S., Jeroudi, M. O., Lai, E. K. & McCay, P. B. Demonstration of free radical generation in ‘stunned’ myocardium of intact dogs with the use of the spin trap alpha-phenyl N-tert-butyl nitrone. *J. Clin. Invest.* **82**, 476–485 (1988).

150. Johns, T. N. P. & Olson, B. J. EXPERIMENTAL MYOCARDIAL INFARCTION. I. A. METHOD OF CORONARY OCCLUSION IN SMALL ANIMALS: *Annals of Surgery* **140**, 675–682 (1954).

151. Salimova, E. *et al.* Variable outcomes of human heart attack recapitulated in genetically diverse mice. *npj Regen Med* **4**, 5 (2019).

152. Nossuli, T. O. *et al.* Brief murine myocardial I/R induces chemokines in a TNF-α-independent manner: role of oxygen radicals. *American Journal of Physiology-Heart and Circulatory Physiology* **281**, H2549–H2558 (2001).

153. De Villiers, C. & Riley, P. R. Mouse models of myocardial infarction: comparing permanent ligation and ischaemia-reperfusion. *Disease Models & Mechanisms* **13**, dmm046565 (2020).

154. Zong, Y. *et al.* Mitochondrial dysfunction: mechanisms and advances in therapy. *Sig Transduct Target Ther* **9**, 124 (2024).

155. Bonora, M. *et al.* Targeting mitochondria for cardiovascular disorders: therapeutic potential and obstacles. *Nat Rev Cardiol* **16**, 33–55 (2019).

156. Brown, D. A. *et al.* Mitochondrial function as a therapeutic target in heart failure. *Nat Rev Cardiol* **14**, 238–250 (2017).

157. Chen, W., Zhao, H. & Li, Y. Mitochondrial dynamics in health and disease: mechanisms and potential targets. *Sig Transduct Target Ther* **8**, 333 (2023).

158. Selvarajah, B., Azuelos, I., Anastasiou, D. & Chambers, R. C. Fibrometabolism—An emerging therapeutic frontier in pulmonary fibrosis. *Sci. Signal.* **14**, eaay1027 (2021).

159. Del Gaudio, F. *et al.* Left ventricular hypertrophy and metabolic resetting in the Notch3-deficient adult mouse heart. *Sci Rep* **13**, 15022 (2023).

160. Wu, J., Dai, F., Li, C. & Zou, Y. Gender Differences in Cardiac Hypertrophy. *J. of Cardiovasc. Trans. Res.* **13**, 73–84 (2020).

161. Kessler, E. L., Rivaud, M. R., Vos, M. A. & Van Veen, T. A. B. Sex-specific influence on cardiac structural remodeling and therapy in cardiovascular disease. *Biol Sex Differ* **10**, 7 (2019).

162. Patten, R. D. Models of gender differences in cardiovascular disease. *Drug Discovery Today: Disease Models* **4**, 227–232 (2007).

163. Mazza, M. *et al.* Beyond One-Size-Fits-All: Personalized Medicine and Future Directions in Sex-Based Psychopharmacological Treatment. *Future Pharmacology* **4**, 541–563 (2024).

164. Sullivan, K. *et al.* Sex-Specific Differences in Heart Failure: Pathophysiology, Risk Factors, Management, and Outcomes. *Canadian Journal of Cardiology* **37**, 560–571 (2021).

165. Wang, X. *et al.* Sex Differences in Clinical Characteristics and Outcomes After Myocardial Infarction With Low Ejection Fraction: Insights From PARADISE-MI. *JAHA* **12**, e028942 (2023).

166. Villalba-Orero, M., Garcia-Pavia, P. & Lara-Pezzi, E. Non-invasive assessment of HFpEF in mouse models: current gaps and future directions. *BMC Med* **20**, 349 (2022).

167. Alwi, I. Diagnosis and management of cardiogenic pulmonary edema. *Acta Med Indones* **42**, 176–184 (2010).

168. Kemp, C. D. & Conte, J. V. The pathophysiology of heart failure. *Cardiovascular Pathology* **21**, 365–371 (2012).

169. J.W. Lee, D. & Aw, T.-C. Natriuretic Peptides in Clinical Practice: A Current Review. *J Immunological Sci* **7**, 28–34 (2023).

170. Clerico, A. *et al.* Circulating levels of cardiac natriuretic peptides (ANP and BNP) measured by highly sensitive and specific immunoradiometric assays in normal subjects and in patients with different degrees of heart failure. *J Endocrinol Invest* **21**, 170–179 (1998).

171. Januzzi, J. L. *et al.* NT-proBNP testing for diagnosis and short-term prognosis in acute destabilized heart failure: an international pooled analysis of 1256 patients. *European Heart Journal* **27**, 330–337 (2006).

172. Maisel, A. S. *et al.* Rapid Measurement of B-Type Natriuretic Peptide in the Emergency Diagnosis of Heart Failure. *N Engl J Med* **347**, 161–167 (2002).

173. Zile, M. R. *et al.* Transition From Chronic Compensated to Acute Decompensated Heart Failure: Pathophysiological Insights Obtained From Continuous Monitoring of Intracardiac Pressures. *Circulation* **118**, 1433–1441 (2008).

174. Shioura, K. M., Geenen, D. L. & Goldspink, P. H. Sex-related changes in cardiac function following myocardial infarction in mice. *Am J Physiol Regul Integr Comp Physiol* **295**, R528-534 (2008).

175. Radakrishnan, A. *et al.* Underpinnings of Heart Failure With Preserved Ejection Fraction in Women - From Prevention to Improving Function. A Co-publication With the American Journal of Preventive Cardiology and the Journal of Cardiac Failure. *J Card Fail* S1071-9164(25)00037–5 (2025) doi:10.1016/j.cardfail.2025.01.008.

176. Sotomi, Y. *et al.* Sex Differences in Heart Failure With Preserved Ejection Fraction. *J Am Heart Assoc* **10**, e018574 (2021).

177. Cao, Y. *et al.* Sex differences in heart mitochondria regulate diastolic dysfunction. *Nat Commun* **13**, 3850 (2022).

178. Colom, B., Oliver, J., Roca, P. & Garciapalmer, F. Caloric restriction and gender modulate cardiac muscle mitochondrial H2O2 production and oxidative damage. *Cardiovascular Research* **74**, 456–465 (2007).

179. Ostadal, B., Netuka, I., Maly, J., Besik, J. & Ostadalova, I. Gender Differences in Cardiac Ischemic Injury and Protection—Experimental Aspects. *Exp Biol Med (Maywood)* **234**, 1011–1019 (2009).

180. Ostadal, B. *et al.* Developmental and sex differences in cardiac tolerance to ischemia–reperfusion injury: the role of mitochondria. *Can. J. Physiol. Pharmacol.* **97**, 808–814 (2019).

181. Chen, C. *et al.* Apoptosis and autophagy contribute to gender difference in cardiac ischemia–reperfusion induced injury in rats. *Life Sciences* **93**, 265–270 (2013).

182. Luk, H., Jiwan, N. C., Appell, C. R., Levitt, D. E. & Vingren, J. L. Sex-specific mitochondrial dynamics and mitophagy response to muscle damage. *Physiological Reports* **10**, e15230 (2022).

183. Li, X. *et al.* Mitochondrial dysfunction in fibrotic diseases. *Cell Death Discov.* **6**, 80 (2020).

184. Zhao, X., Kwan, J. Y. Y., Yip, K., Liu, P. P. & Liu, F.-F. Targeting metabolic dysregulation for fibrosis therapy. *Nat Rev Drug Discov* **19**, 57–75 (2020).

185. Yang, Y. *et al.* Role of Mitophagy in Cardiovascular Disease. *Aging and disease* **11**, 419 (2020).

186. He, Q. *et al.* MAVS integrates glucose metabolism and RIG-I-like receptor signaling. *Nat Commun* **14**, 5343 (2023).

187. Sun, X. *et al.* MAVS maintains mitochondrial homeostasis via autophagy. *Cell Discov* **2**, 16024 (2016).

188. Vives-Bauza, C. *et al.* PINK1-dependent recruitment of Parkin to mitochondria in mitophagy. *Proc. Natl. Acad. Sci. U.S.A.* **107**, 378–383 (2010).

189. Jin, S. M. & Youle, R. J. PINK1- and Parkin-mediated mitophagy at a glance. *Journal of Cell Science* **125**, 795–799 (2012).

190. Lazarou, M. *et al.* The ubiquitin kinase PINK1 recruits autophagy receptors to induce mitophagy. *Nature* **524**, 309–314 (2015).

191. Shiba-Fukushima, K. *et al.* PINK1-mediated phosphorylation of the Parkin ubiquitin-like domain primes mitochondrial translocation of Parkin and regulates mitophagy. *Sci Rep* **2**, 1002 (2012).

192. Youle, R. J. & Narendra, D. P. Mechanisms of mitophagy. *Nat Rev Mol Cell Biol* **12**, 9–14 (2011).

193. Bu, L. *et al.* The Ubiquitin E3 Ligase Parkin Inhibits Innate Antiviral Immunity Through K48-Linked Polyubiquitination of RIG-I and MDA5. *Front. Immunol.* **11**, 1926 (2020).

194. Gautier, C. A., Kitada, T. & Shen, J. Loss of PINK1 causes mitochondrial functional defects and increased sensitivity to oxidative stress. *Proc. Natl. Acad. Sci. U.S.A.* **105**, 11364–11369 (2008).

195. Haque, M. E. *et al.* Cytoplasmic Pink1 activity protects neurons from dopaminergic neurotoxin MPTP. *Proc. Natl. Acad. Sci. U.S.A.* **105**, 1716–1721 (2008).

196. Huang, E. *et al.* PINK1-mediated phosphorylation of LETM1 regulates mitochondrial calcium transport and protects neurons against mitochondrial stress. *Nat Commun* **8**, 1399 (2017).

197. Joselin, A. P. *et al.* ROS-dependent regulation of Parkin and DJ-1 localization during oxidative stress in neurons. *Human Molecular Genetics* **21**, 4888–4903 (2012).

198. Siddall, H. K. *et al.* Loss of PINK1 Increases the Heart's Vulnerability to Ischemia-Reperfusion Injury. *PLoS ONE* **8**, e62400 (2013).

199. Kim, S.-H. *et al.* PINK1 Inhibits Multimeric Aggregation and Signaling of MAVS and MAVS-Dependent Lung Pathology. *Am J Respir Cell Mol Biol* **64**, 592–603 (2021).

200. Zevini, A., Olagnier, D. & Hiscott, J. Crosstalk between Cytoplasmic RIG-I and STING Sensing Pathways. *Trends in Immunology* **38**, 194–205 (2017).

201. Ishikawa, H. & Barber, G. N. STING is an endoplasmic reticulum adaptor that facilitates innate immune signalling. *Nature* **455**, 674–678 (2008).

202. Zhong, B. *et al.* The Adaptor Protein MITA Links Virus-Sensing Receptors to IRF3 Transcription Factor Activation. *Immunity* **29**, 538–550 (2008).

203. Luo, W. *et al.* Critical Role of the cGAS-STING Pathway in Doxorubicin-Induced Cardiotoxicity. *Circulation Research* **132**, (2023).

204. Oduro, P. K. *et al.* The cGAS–STING signaling in cardiovascular and metabolic diseases: Future novel target option for pharmacotherapy. *Acta Pharmaceutica Sinica B* **12**, 50–75 (2022).

205. Koentges, C., Bode, C. & Bugger, H. SIRT3 in Cardiac Physiology and Disease. *Front. Cardiovasc. Med.* **3**, (2016).

206. Guo, Z. *et al.* NEU1 Regulates Mitochondrial Energy Metabolism and Oxidative Stress Post-myocardial Infarction in Mice via the SIRT1/PGC-1 Alpha Axis. *Front. Cardiovasc. Med.* **9**, 821317 (2022).

207. Zhang, X. *et al.* MicroRNA-195 Regulates Metabolism in Failing Myocardium Via Alterations in Sirtuin 3 Expression and Mitochondrial Protein Acetylation. *Circulation* **137**, 2052–2067 (2018).

208. Kong, X. *et al.* Sirtuin 3, a New Target of PGC-1α, Plays an Important Role in the Suppression of ROS and Mitochondrial Biogenesis. *PLoS ONE* **5**, e11707 (2010).

209. Wen, J. *et al.* Protective effects of higenamine combined with [6]-gingerol against doxorubicin-induced mitochondrial dysfunction and toxicity in H9c2 cells and potential mechanisms. *Biomedicine & Pharmacotherapy* **115**, 108881 (2019).

210. Sun, D. & Yang, F. Metformin improves cardiac function in mice with heart failure after myocardial infarction by regulating mitochondrial energy metabolism. *Biochemical and Biophysical Research Communications* **486**, 329–335 (2017).

211. Jia, D., Hou, L., Lv, Y., Xi, L. & Tian, Z. Postinfarction exercise training alleviates cardiac dysfunction and adverse remodeling via mitochondrial biogenesis and SIRT1/PGC-1α/PI3K/Akt signaling. *Journal Cellular Physiology* **234**, 23705–23718 (2019).

212. Liu, X. *et al.* Dual modifying of MAVS at lysine 7 by SIRT3-catalyzed deacetylation and SIRT5-catalyzed desuccinylation orchestrates antiviral innate immunity. *Proc. Natl. Acad. Sci. U.S.A.* **121**, e2314201121 (2024).

213. Cai, X., Xu, H. & Chen, Z. J. Prion-Like Polymerization in Immunity and Inflammation. *Cold Spring Harb Perspect Biol* **9**, a023580 (2017).

214. Toldo, S. *et al.* Inhibition of the NLRP3 inflammasome limits the inflammatory injury following myocardial ischemia–reperfusion in the mouse. *International Journal of Cardiology* **209**, 215–220 (2016).

215. Sandanger, Ø. *et al.* The NLRP3 inflammasome is up-regulated in cardiac fibroblasts and mediates myocardial ischaemia–reperfusion injury. *Cardiovascular Research* **99**, 164–174 (2013).

216. Van Hout, G. P. J. *et al.* The selective NLRP3-inflammasome inhibitor MCC950 reduces infarct size and preserves cardiac function in a pig model of myocardial infarction. *Eur Heart J* ehw247 (2016) doi:10.1093/eurheartj/ehw247.

217. Xu, H. *et al.* TAX1BP1 protects against myocardial infarction-associated cardiac anomalies through inhibition of inflammasomes in a RNF34/MAVS/NLRP3-dependent manner. *Science Bulletin* **66**, 1669–1683 (2021).

218. Li, H., Zhang, S., Li, F. & Qin, L. NLRX1 attenuates apoptosis and inflammatory responses in myocardial ischemia by inhibiting MAVS-dependent NLRP3 inflammasome activation. *Molecular Immunology* **76**, 90–97 (2016).

219. Liu, S. *et al.* The E3 ubiquitin ligase MARCH2 protects against myocardial ischemia-reperfusion injury through inhibiting pyroptosis via negative regulation of PGAM5/MAVS/NLRP3 axis. *Cell Discov* **10**, 24 (2024).

220. Sun, Q. *et al.* The Specific and Essential Role of MAVS in Antiviral Innate Immune Responses. *Immunity* **24**, 633–642 (2006).

221. Liu, S. *et al.* Phosphorylation of innate immune adaptor proteins MAVS, STING, and TRIF induces IRF3 activation. *Science* **347**, aaa2630 (2015).

222. Lam, J. *et al.* A Universal Approach to Analyzing Transmission Electron Microscopy with ImageJ. *Cells* **10**, 2177 (2021).

223. Haque, A., Engel, J., Teichmann, S. A. & Lönnberg, T. A practical guide to single-cell RNA-sequencing for biomedical research and clinical applications. *Genome Med* **9**, 75 (2017).

224. Onódi, Z. *et al.* Systematic transcriptomic and phenotypic characterization of human and murine cardiac myocyte cell lines and primary cardiomyocytes reveals serious limitations and low resemblances to adult cardiac phenotype. *Journal of Molecular and Cellular Cardiology* **165**, 19–30 (2022).

225. Dana, H. *et al.* Molecular Mechanisms and Biological Functions of siRNA. *Int J Biomed Sci* **13**, 48–57 (2017).

226. Karakikes, I., Ameen, M., Termglinchan, V. & Wu, J. C. Human induced pluripotent stem cell-derived cardiomyocytes: insights into molecular, cellular, and functional phenotypes. *Circ Res* **117**, 80–88 (2015).

227. Walsh, M. A., Musci, R. V., Jacobs, R. A. & Hamilton, K. L. A practical perspective on how to develop, implement, execute, and reproduce high-resolution respirometry experiments: The physiologist's guide to an Oroboros O2k. *The FASEB Journal* **37**, e23280 (2023).

7 APPENDIX A: SUPPLEMENTAL DATA

7.1.1 Two Angiotensin II treatment regimens induce MAVS activation in AC16 cells

Two ANG II treatment regimens, 200nM for 24hrs and 1μM for 2hrs were able to induce MAVS activation. The 24hr experiment produced absolute increases in MAVS expression while maintaining mitochondrial abundance, as indicated by mitotraker CMXRos (**Figure S1A/C**). By extension, MAVS expression, normalized to mitochondrial abundance, is increased 24 hours post 200nM ANG II treatment (**Figure S1A/C**). The 2-hrs ANG II treatment regime resulted in increased MAVS activation and reduced mitochondrial abundance (**Figure S1B/D**). Both absolute and normalized MAVS expression levels were increased after 2-hrs of 1μM ANG II treatment (**Figure S1B/D**).

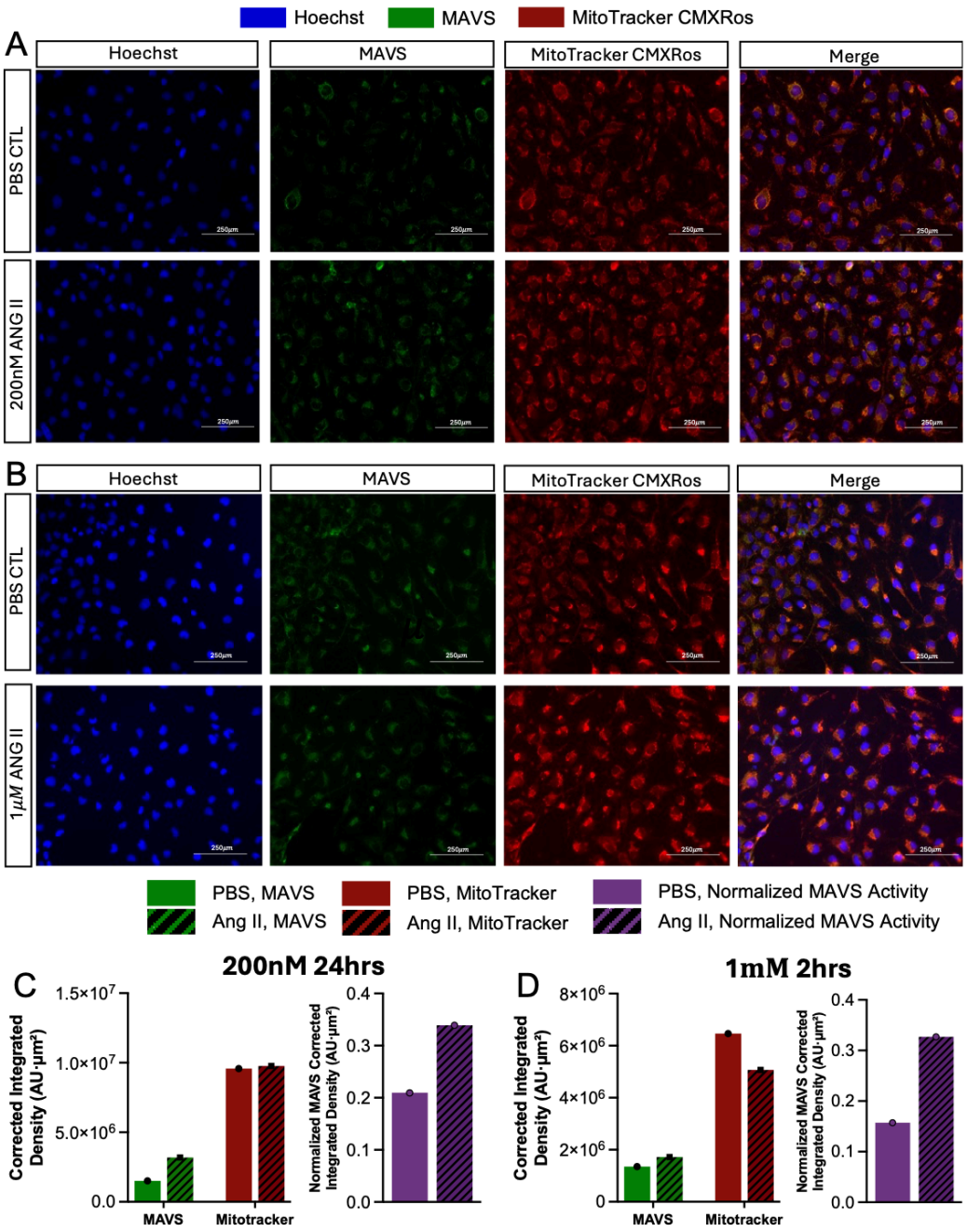

Figure 7.7.1 Two Angiotensin II treatment regimens induce MAVS activation in AC16 cells. (A,C) Fluorescent images and Corrected Integrated Density (AU*μm^2) of AC16 cells treated with 200nm Ang II for 24hrs compared to PBS CTL (**B, D**). Fluorescent images and Corrected Integrated Density (AU*μm^2) of AC16 cells treated with 1μm Ang II for 2hrs compared to PBS CTL. Hoechst (blue), MAVS (green), MitoTracker CMXRos (red), and merge. Scale bars, 250μm.

7.1.2 24-hour treatment with 200nm Angiotensin II induces MAVS activation in AC16 cells

Confocal images of single AC16 cells display decreased absolute MAVS and mitochondrial expression following 24-hour treatment with 200nm ANG II. However, following normalization, MAVS expression levels are elevated relative to mitochondrial abundance (**Figure S2**).

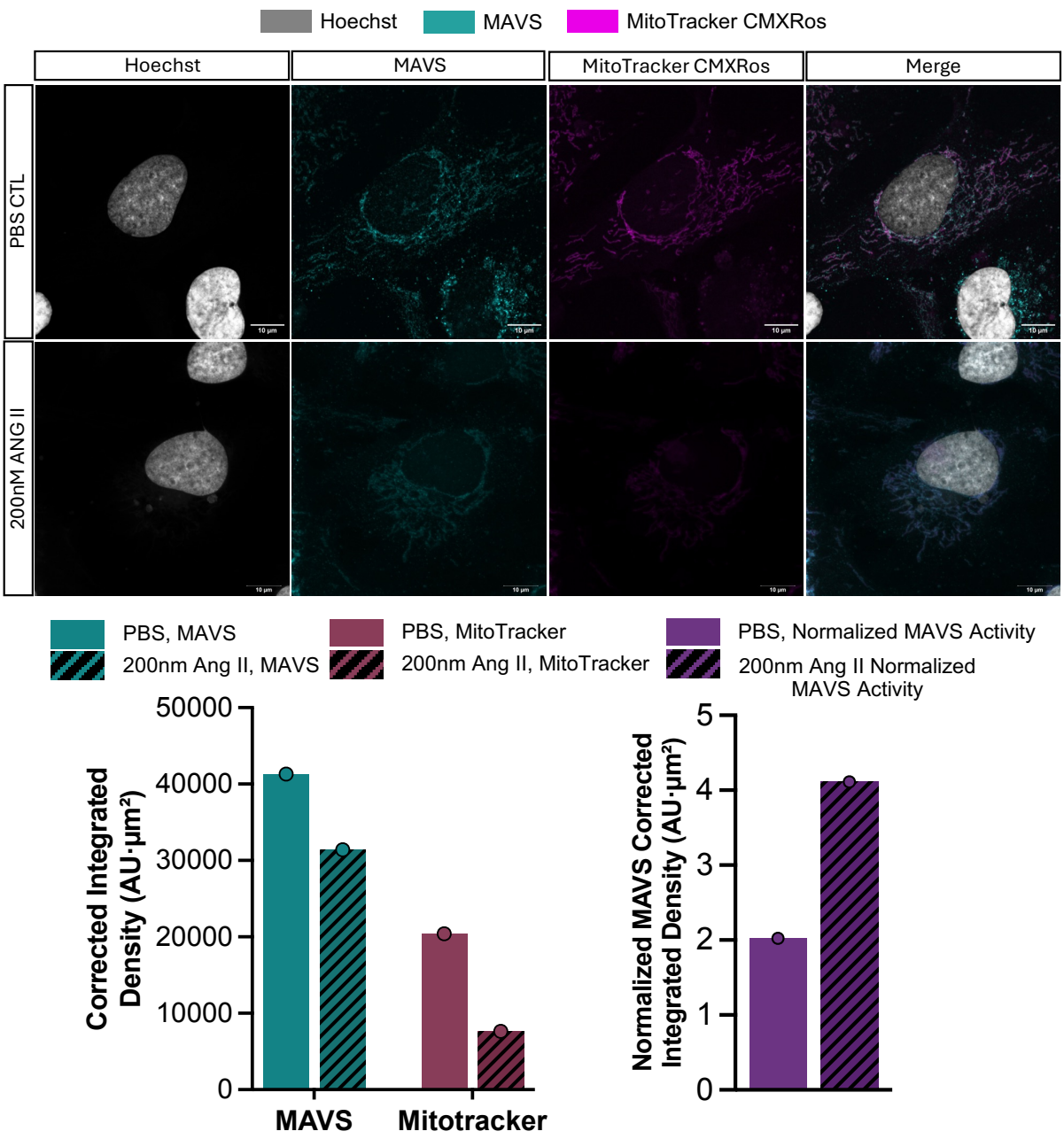

Figure 7.2 200nm 24hrs Ang II treatment induces MAVS activation in AC16 cells. AC16 cells treated with 200nm ANG II for 24hours compared to PBS CTL. Hoechst (grey), MAVS (cyan), MitoTracker CMXRos (purple), and merge. Magnification 60x, scale bars, 10μm.

7.1.3 MAVS antibody is most effective in detecting MAVS in mitochondrial isolates from human AC16 cells

As indicated by a strong VDAC signal, mitochondrial isolation from mouse tissue is successful. However, MAVS antibody (PA5-17256, 1:50) was ineffective in detecting MAVS in these mouse mitochondrial isolates (**Figure S3A**). In AC16 human cells, MAVS and VDAC were both undetectable in whole cell lysates, but both were clearly detectable in mitochondrial isolates (**Figure S3B/C**). MAVS was most readily detected in mitochondrial isolates from human AC16 cells (**Figure S3D**). Although insignificant, preliminary results suggest that a 24-hour treatment with 200nm ANG II increases MAVS expression in AC16 cells (**Figure S3E**). MAVS siRNA knockdown was unsuccessful (**Figure S3D/E**).

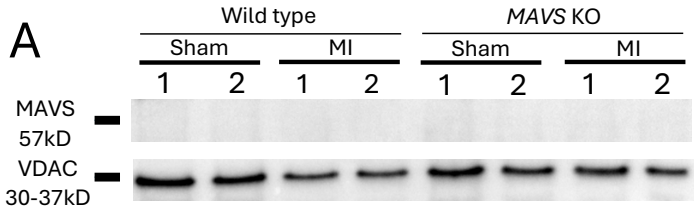
A
Wild type
MAVS KO
Sham
MI
Sham
MI
1 2 1 2 1 2 1 2
MAVS
57kD
VDAC
30-37kD

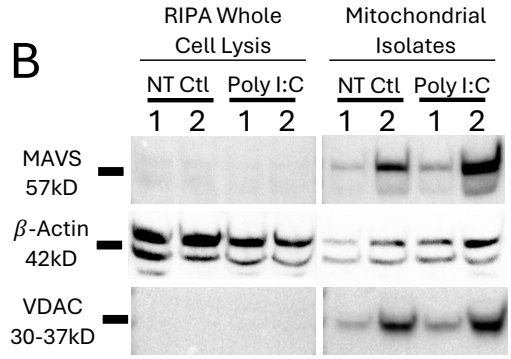
B
RIPA Whole Cell Lysis
Mitochondrial Isolates
NT Ctl
Poly I:C
NT Ctl
Poly I:C
1 2 1 2 1 2 1 2
MAVS
57kD
β-Actin
42kD
VDAC
30-37kD

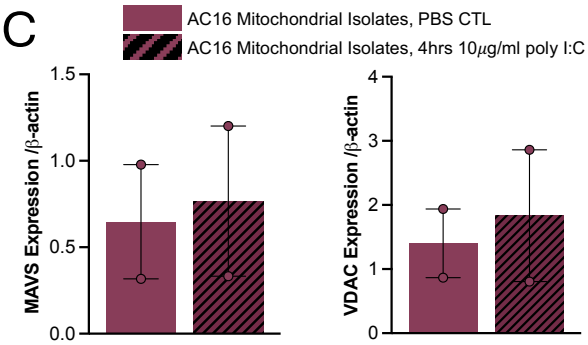
C
AC16 Mitochondrial Isolates, PBS CTL
AC16 Mitochondrial Isolates, 4hrs 10μg/ml poly I:C
MAVS Expression /β-actin
1.5
1.0
0.5
0.0
VDAC Expression /β-actin
4
3
2
1
0

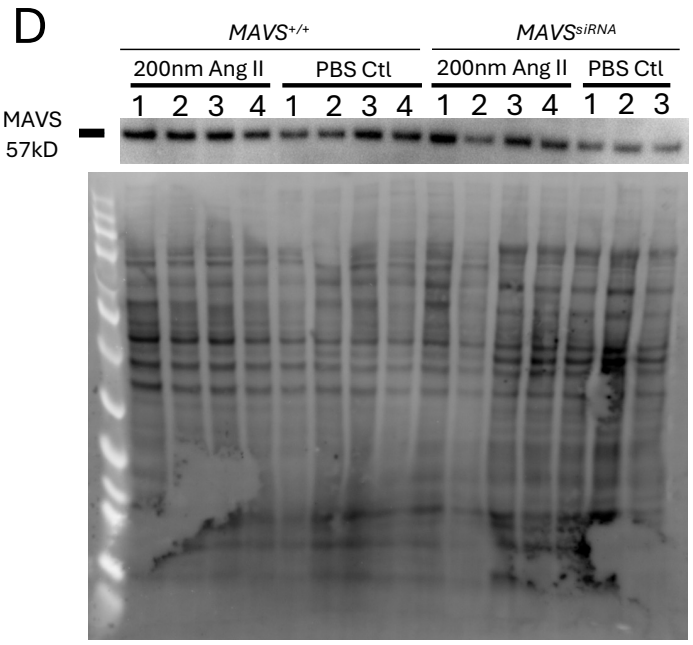
D
MAVS+/+
MAVSsiRNA
200nm Ang II
PBS Ctl
200nm Ang II
PBS Ctl
1 2 3 4 1 2 3 4 1 2 3 4 1 2 3
MAVS
57kD

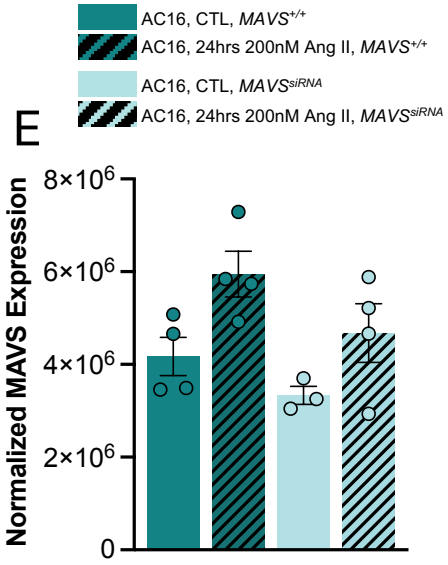
E
AC16, CTL, MAVS+/+
AC16, 24hrs 200nM Ang II, MAVS+/+
AC16, CTL, MAVSsiRNA
AC16, 24hrs 200nM Ang II, MAVSsiRNA
Normalized MAVS Expression
8×10^6
6×10^6
4×10^6
2×10^6
0

Figure 7.3 MAVS antibody is most effective in detecting MAVS in mitochondrial isolates from human AC16 cells. (**A**) successful mitochondrial isolation from mouse heart tissues, MAVS undetectable (**B/C**), MAVS successfully detected in mitochondrial isolates but not in RIPA whole cell lysis collected from human AC16 cells. No significant changes in MAVS activation with 4-hour treatment with 10μg/ml poly I:C. (**D/E**) AC16 cells were transfected with *Mavs* siRNA or siRNA scramble control and treated with 200nm Ang II or PBS control for 24 hours. No notable significant differences. All values are presented as mean ± s.e.m.; n refers to the sample size. $P < 0.05$ was considered statistically significant. P values were calculated using ANOVA with Bonferroni correction.

7.1.4 Verification of Mavs$^{-/-}$ mouse by PCR genotyping and q-RT-PCR

q-RT-PCR confirmed there is no *Mavs* mRNA expression in *Mavs*$^{-/-}$ mice ($p<0.0494$) (**Figure S4**).

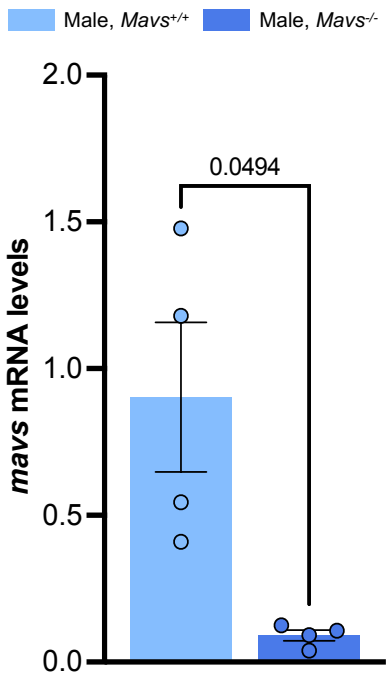

Figure 7.4 Mavs knockout model validation. No *Mavs* mRNA expression detected in *Mavs*$^{-/-}$ mice ($p<0.0494$). All values are presented as mean ± s.e.m.; n refers to the sample size. $P < 0.05$ was considered statistically significant. P values were calculated using ANOVA with Bonferroni correction.

7.1.5 No significant differences in body weight between mouse cohorts

Male WT sham, WT MI, *Mavs*$^{-/-}$ sham, and *Mavs*$^{-/-}$ MI cohorts have approximately the same body weights pre- and post-procedures (**Figure S5A**). Likewise, female WT sham, WT MI, *Mavs*$^{-/-}$ sham, and *Mavs*$^{-/-}$ MI cohorts have approximately the same body weights pre- and post-procedures (**Figure S5B**).

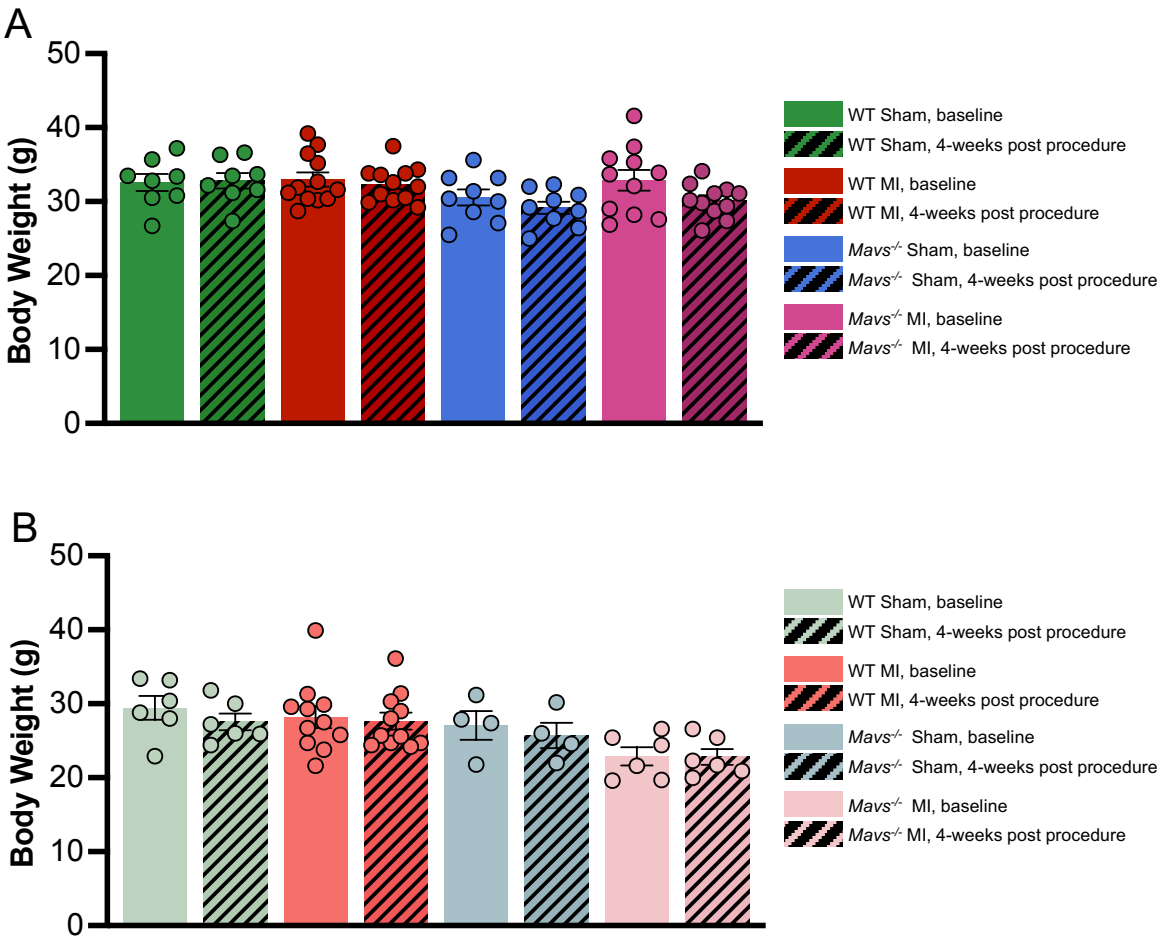

Figure 7.5 No significant differences in body weights between groups pre and 4 weeks post MI. (A) Male body weight (g) before surgery and 4 weeks post MI (B) Female body weight (g) before surgery and 4 weeks post MI. All values are presented as mean ± s.e.m.; n refers to the sample size. $P < 0.05$ was considered statistically significant. P values were calculated using ANOVA with Bonferroni correction.

7.1.6 Summary of all cardiac function measures acquired from echocardiography

No significant differences were observed in cardiac function measures between cohorts acquired from echocardiography 4 weeks post-procedures. Cardiac functional measures include: male heart rate (beats per minute (BPM)) (**Figure A**); male area (mm^2) (**Figure B**); male area;s (mm^2) (**Figure C**); male area;d (mm^2) (**Figure D**); male volume (μL) (**Figure E**); male volume;s (μL) (**Figure F**); male volume;d (μL) (**Figure G**); male stroke volume (μL) (**Figure H**); male fractional shortening (%) (**Figure I**); male cardiac output (mL/min) (**Figure J**); female heart rate (BPM) (**Figure K**); female area (mm^2) (**Figure L**); female area;s (mm^2) (**Figure M**); female area;d (mm^2) (**Figure N**); female volume (μL (**Figure O**); female volume;s (μL) (**Figure P**); female volume;d (μL) (**Figure Q**); female stroke volume (μL) (**Figure R**); female fractional shortening (%) (**Figure S**); female cardiac output (mL/min) (**Figure T**).

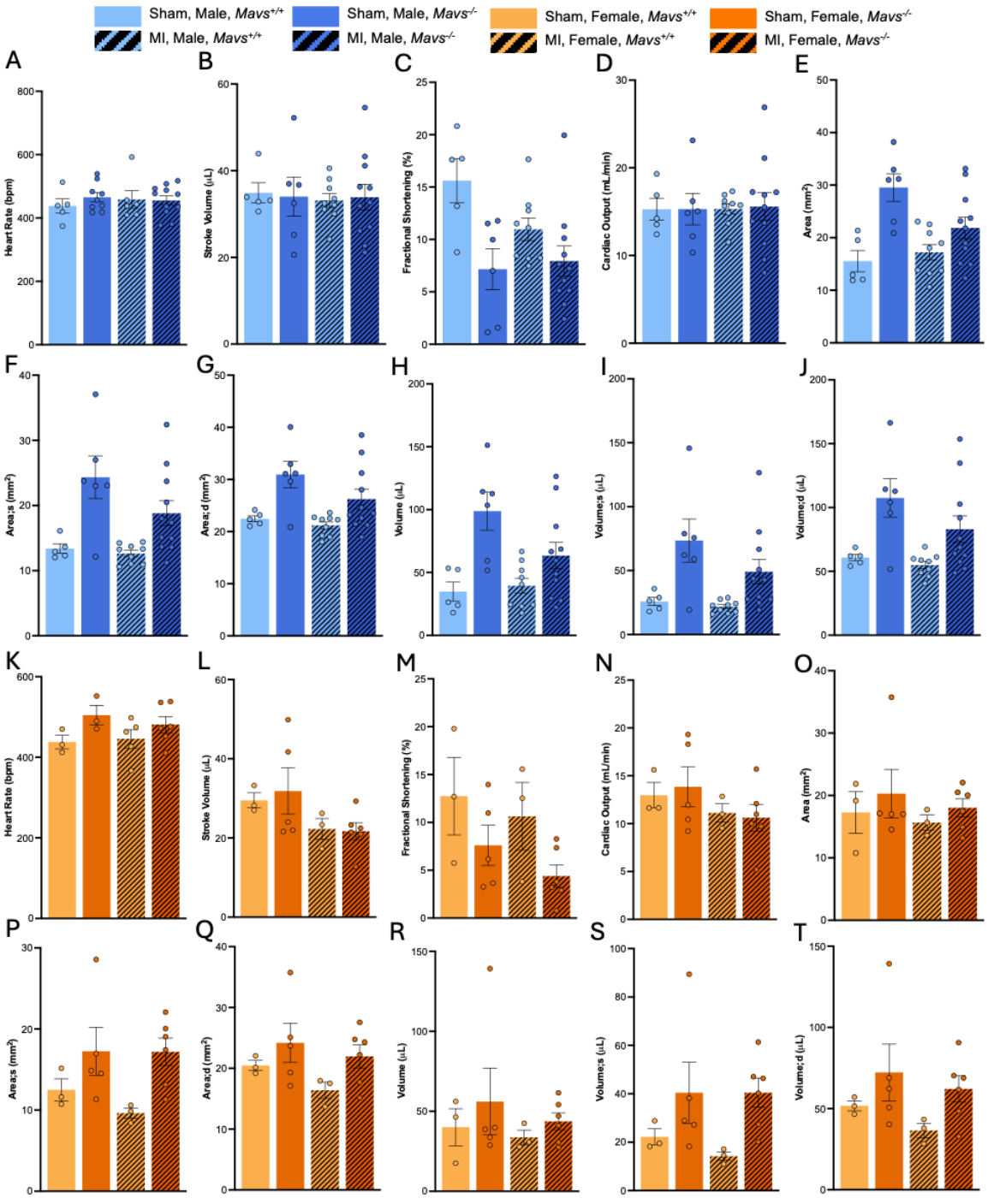
Sham, Male, Mavs+/+
MI, Male, Mavs+/+
Sham, Male, Mavs-/-
MI, Male, Mavs-/-
Sham, Female, Mavs+/+
MI, Female, Mavs+/+
Sham, Female, Mavs-/-
MI, Female, Mavs-/-
A
Heart Rate (bpm)
B
Stroke Volume (μL)
C
Fractional Shortening (%)
D
Cardiac Output (mL/min)
E
Area (mm²)
F
Area;s (mm²)
G
Area;d (mm²)
H
Volume (μL)
I
Volume;s (μL)
J
Volume;d (μL)
K
Heart Rate (bpm)
L
Stroke Volume (μL)
M
Fractional Shortening (%)
N
Cardiac Output (mL/min)
O
Area (mm²)
P
Area;s (mm²)
Q
Area;d (mm²)
R
Volume (μL)
S
Volume;s (μL)
T
Volume;d (μL)

Figure 7.6 Cardiac measure calculated from echocardiography, males and female mice 4-week post MI. Male heart rate (BPM) (**Figure A**); male area (mm2) (**Figure B**); male area;s (mm2) (**Figure C**); male area;d (mm2) (**Figure D**); male volume (μL) (**Figure E**); male volume;s (μL) (**Figure F**); male volume;d (μL) (**Figure G**); male stroke volume (μL) (**Figure H**); male fractional shortening (%) (**Figure I**); male cardiac output (mL/min) (**Figure J**); female heart rate (BPM) (**Figure K**); female area (mm2) (**Figure L**); female area;s (mm2) (**Figure M**); female area;d (mm2) (**Figure N**); female volume (μL (**Figure O**); female volume;s (μL) (**Figure P**); female volume;d (μL) (**Figure Q**); female stroke volume (μL) (**Figure R**); female fractional shortening (%) (**Figure S**); female cardiac output (mL/min) (**Figure T**). All values are presented as mean ± s.e.m.; n refers to the sample size. $P < 0.05$ was considered statistically significant. P values were calculated using ANOVA with Bonferroni correction.

7.1.7 RT-qPCR Primer Sequences

Table S1: Primer Sequences (5' to 3') used for RT-qPCR

Primer Pairs Used for RT-qPCR	
Mouse *Bnp*	
gaggtcactcctatcctctgg	gccatttcctccgacttttctc
Mouse *Anp*	
gcttccaggccatattggag	gggggcatgacctcatctt
Mouse *Myh7*	
actgtcaacacttaagagggtca	ttggatgatttgatcttccaggg
Mouse *Il-6*	
cgagcccaccaggaacgaaagtc	ctggctggaagtctcttgcggag
Mouse *Ctgf*	
caaagcagctgcaaatacca	ggccaaatgtgtcttccagt
Mouse *Hprt*	
gctgacctgctggattacat	ttggggctgtactgcttaac
Mouse *B-actin*	
catgtacgttgctatccac	ctccttaatgtcagggacga
Mouse *Igfbp7*	
Bio-Rad PrimerPCR SYBR Green Assay:	qMmuCID0018853
Mouse *Col3a*	
Bio-Rad PrimerPCR SYBR Green Assay:	qMmuCIP0029022
Mouse *Mavs*	
ggccagatgcctgcttctaa	gtagaaacccacccatcccc
Mouse *Tgfβ*	
caacaaccccttgccaaag	tcccccaagcagttgacagt
Mouse *Pgc1α*	
agaaccccccttcccttcag	ccaacttgactgttgtggagag